PRELIMINARY NON-DESTRUCTIVE ASSESSMENT OF MOISTURE CONTENT, HYDRATION AND DIELECTRIC PROPERTIES OF PORTLAND CEMENT CONCRETE

A Thesis

by

IVAN AVELAR LEZAMA

Submitted to the Office of Graduate Studies of
Texas A&M University
in partial fulfillment of the requirements for the degree of

MASTER OF SCIENCE

December 2005

Major Subject: Civil Engineering

PRELIMINARY NON-DESTRUCTIVE ASSESSMENT OF MOISTURE CONTENT, HYDRATION AND DIELECTRIC PROPERTIES OF PORTLAND CEMENT CONCRETE

A Thesis

by

IVAN AVELAR LEZAMA

Submitted to the Office of Graduate Studies of
Texas A&M University
in partial fulfillment of the requirements for the degree of

MASTER OF SCIENCE

Approved by:

Chair of Committee,	Dan G. Zollinger
Committee Members,	Mohammed Haque
	Robert L. Lytton
Head of Department,	David Rosowski

December 2005

Major Subject: Civil Engineering

ABSTRACT

Preliminary Non-destructive Assessment of Moisture Content, Hydration and Dielectric Properties of Portland Cement Concrete. (December 2005)
Ivan Avelar Lezama, B.S., The University of Texas at El Paso
Chair of Advisory Committee: Dr. Dan G. Zollinger

Moisture availability is a focal point in the structural development of young concrete. Under low humidity and hot weather conditions, concrete loses moisture rapidly as it hardens, and it is very difficult, if not impossible, to minimize this loss even though proper curing procedures are used. Early losses in moisture content jumpstart premature surface self-dissecation, increase surface paste porosity, prevent concrete from achieving the mechanical properties for which it was originally designed, and facilitate the development of surface distresses such as spalling. Curing effectiveness and structural assessment of young concrete is generally done through conventional destructive or invasive testing. However, there is no fully established non-destructive testing protocol to assess moisture content and its effects on concrete properties quantitatively in an on-site, fast, and non-invasive way. The possibility and feasibility of establishing a testing protocol with such attributes is explored.

Previous research on pavement bases has used dielectric measurements to relate moisture content to their structural performance. Due to the high dielectric value of water as compared to any other material used in construction, it is possible to relate high volumetric water content to high dielectric readings. In this study, compressive strength tests combined with dielectric and mass measurements are used to investigate how dielectric properties change with hydration. The results of this study suggest that it may be possible to approximate the volumetric moisture content in concrete by measuring the dielectric value of concrete as it hardens.

DEDICATION

To God, to whom I credit many blessings and lessons in the two years of this program.

To my family, whose continuous support and love has empowered me to continue my studies, and who have endured many months of this distant relationship.

And to every single one of my friends, to whom I miss dearly.

ACKNOWLEDGEMENTS

My deepest gratitude to Dr. Zollinger and my committee. Thanks also to Dr. Lytton for his guidance and support in the crucial analysis stages of this research.

TABLE OF CONTENTS

Page

LIST OF TABLES

LIST OF FIGURES

FIGURE Page

CHAPTER I
INTRODUCTION

Non-destructive testing (NDT) targeted towards the assessment and evaluation of construction material properties is not a new subject, but its popularity has been growing in giant steps among transportation and state highway agencies in recent years. The reason for such popularity resides in the fact that many of these NDT methods are relatively quick and inexpensive. Most of those NDT methods involve the use of probes and equipment that can take advantage of the various degrees of sensitivity to temperature or electromagnetic responses of the material in question. However, some of those methods require invasive probing or embedding of sensors that can disrupt construction procedures. A very recent generation of surface probes that measure the dielectric properties of construction materials do not have those limitations. Measurements obtained from granular materials with these new probes have been shown to provide important clues about the relative amounts of moisture, a very important part of cement hydration. Unfortunately, limited in-depth analysis has been done on the significance and role of moisture availability as a major factor of the dielectric properties of concrete, and how it correlates to hydration and to mechanical properties.

The first phenomenon affected by moisture availability is cement hydration. Cement hydration produces a chemical compound that is intrinsically complicated in nature. Its structure has been accepted to consist on four different phases with different proportions shared among hydrated cement and water in various forms (Breugel 1991; Neville 1995). The second characteristic of concrete greatly affected by moisture is its dielectric properties from which technologists can take advantage, because the change of volumetric water availability in concrete as it hardens causes concrete to change its dielectric properties.

This thesis follows the style and format of the *Journal of Materials in Civil Engineering.*

The tracking of moisture loss changes and the corresponding effect on dielectric and hydration properties provides some evidence that important concrete properties through NDT during early curing periods can be assessed through quick and on-site testing.

Therefore, the present study focuses on the evaluation and discussion of the potential that dielectric measurements have on the approximation and possible prediction of conventional concrete properties such as moisture content and curing quality, or even hydration and strength. It is not the scope of this effort, however, to establish a protocol or to establish new curing requirements or procedures. The scope is to present a baseline study of dielectric measurements in concrete for future, more advanced research. Therefore, it is of interest to:

- Identify key time-dependent changes in water availability and vapor pressure and their effect on cement hydration and early-age concrete properties
- Perform a quantitative analysis of measurements relative to the development of characterization relationships of concrete early-age properties that vary as a function of hydration
- Recommend key items to follow-up in future research and investigation

To satisfy such objectives, the study will be presented in the following main divisions that describe the development and results of the research effort. Background information about previous dielectric testing on concrete will be presented in Chapter II. Theoretical considerations as presented in Chapter III provide the basic research effort framework, while the laboratory data collection testing and strategies that provide the basic raw data for analysis are described in Chapter IV. Chapter V presents the quantitative analysis of the obtained data, discuss any potentially fundamental behavior, and propose characterizing models when deemed applicable or statistically reliable. Finally, Chapter VI presents the general conclusions obtained from the results of this project and recommends future research and the necessary focus to be given.

CHAPTER II
BACKGROUND

The purpose of this chapter is to present how hydration and moisture loss affect the dielectric properties of young Portland Cement Concrete (PCC), and to set the basis for a quantitative assessment, analysis and prediction of the changes that take place as concrete hardens. The investigative approach is to be based upon non-destructive testing (NDT) and the use of dielectric properties as indicators, or even potential predictors, of moisture and hydration-related factors. It is the intent of this chapter to offer a summary of the theory as it was later applied to the experimental investigation.

RELEVANCE OF MOISTURE CONTROL IN CONCRETE BEHAVIOR

Moisture availability and loss are, in practical terms, the driving forces in many of the concrete properties during its fresh, hardening, and hardened stages, yet is not in many instances given enough credit or blame for common successes or failures of concrete under service. In this study, the quantification and monitoring of moisture availability and loss presents a unique opportunity to identify the main factors affecting the dielectric properties of concrete, and to describe the moisture and dielectric changes that occur during hydration.

Moisture control is a critical part of all curing practices, and the quality of curing usually determines the performance of the finished structure (Somayaji 2001). Many premature failure mechanisms of PCC structures ultimately derive from deficiencies in construction methods or curing procedures, especially for those structures with large surface area-to-volume ratios that are exposed to the atmosphere like road and highway pavements. Moisture availability and management must therefore be taken often into consideration for construction methodologies and objectives. In fact, careful and effective curing practices applied during the hardening stage immediately following setting greatly improve the strength development and performance of concrete in the long term

(Mindess et al. 2003). In concrete terminology, curing involves procedures that maintain proper moisture and temperature conditions to ensure the concrete attains the desired performance properties such as strength, water tightness, and durability under freeze-thaw cycles (Somayaji 2001; Mamlouk and Zaniewski 1999). Curing is focused primarily to prevent excessive moisture loss, and to minimize the negative effects of shrinkage and creep stresses occurring during the hardening stages of hydration (Mindess et al. 2003). In turn, the progress and development of hydration is influenced by the initial water-cement ratio and the curing effectiveness. The degree of hydration is perhaps the main factor affecting the resulting micro- and macro-structural behaviors of hardened concrete. Therefore, there exists a common determining factor for most concrete properties: water. Moisture availability, moisture loss, and moisture distribution and history as it develops with time (Wang 2000) is thus a crucial piece of information worthy of further investigation and consideration for the improvement of concrete performance and curing practices.

MOISTURE LOSS: BLEEDING AND EVAPORATION

Bleeding and evaporation represent an important piece of the investigation reported herein. Mass quantification of these two stages of moisture loss can help complement observations made in other areas of concrete behavior such as creep and shrinkage. Due to the flowing nature of bleeding and moisture loss, changes in mass quantities may also help identify when major changes in microstructure and porosity occur.

Bleeding is common to most concrete mixtures. A portion of the mixed water gets displaced from the concrete mass and rises to the surface, and is subsequently lost by evaporation to the atmosphere (Somayaji 2001). Bleeding is accentuated by over-vibrating the concrete during placement, or by allowing high water-cement ratios, low cement contents, or high aggregate fineness moduli (Neville 1995; Somayaji 2001), and bleeding rates are higher for pastes with water-cement ratios above 0.38 (Neville 1995). Bleeding and evaporation translate into actual volumetric changes in the hydrated paste,

which causes shrinkage- and creep-related movements (Mindess et al. 2003). In conventional concrete mixture proportioning (without the consideration of water-reduction admixtures), water-cementitious materials ratios above 0.38 are necessary to maintain a desired level of workability and to maintain the cement paste moisture-saturated (Powers 1947), although this approach causes the formation of porous concrete surfaces (Cano-Barrita et al. 2004; Parrot 1991). In a concrete mixture, the water-cementitious materials ratio is defined as follows:

$$w_0 = \frac{w_{net}}{c} \tag{1}$$

where:

w_0 = water-cementitious materials (or water-binders) ratio

w_{net} = net water mass (corrected for absorption and moisture on aggregates), kg

c = cementious mass, kg

In this study, the applicable terminology needs to be defined for complete clarity. "Moisture" used henceforth will refer to either the vapor or liquid phase of the H_2O molecule, residing in either the ambient air or inside the concrete matrix at any hardening stage. "Water", on the other hand, will only be used to refer to the liquid form of the same molecule, which can only applicable to the fresh stages of concrete, including bleeding water. Nevertheless, it is emphatically stressed that either thermodynamic phase of water can exist in concrete, and sometimes even more that two states of bonding of water can co-exist in micro-capillary settings as either adsorbed layers, surface tension layers, or viscous (bulk) state layers (Guthrie and Scullion 2000).

In terms of moisture loss, bleeding and evaporation can occur simultaneously. Bleeding starts at the moment of placement of the concrete and ends approximately at setting time (Neville 1995) for common concrete mixes, while the bleed water deposited on top of the concrete evaporates at a rate depending on the thermodynamic balance of water-air interfaces in terms of saturation pressures affected by the ambient temperature and

relative humidity (Çengel and Turner 2001). This implies that evaporation of the bleed water is usually accentuated by w_0 values above 0.38 and accelerated by high concrete and/or ambient temperatures, low relative humidities, and windy conditions (Cano-Barrita et al. 2004; Jang et al. 2005). If the rate of evaporation of the bleed water exceeds the bleeding rate, the surface of the concrete dries and the free (capillary) water in concrete starts evaporating (Cano-Barrita et al. 2004) at a rate influenced by the hydration process and the porosity microstructure development (Powers 1947).

Water/moisture loss has been expressed in different quantitative ways, but no consistent form was identifiable from the available literature. The American Association for Testing and Materials Standard (ASTM) C232 requires bleeding measurements to be expressed in terms of mass by area of concrete surface (in kg/m^2) or as a mass fraction (percent) of net water (unitless ratio). It has also been expressed as a rate in terms of mass by fresh concrete weight or design concrete volume. Few quantitative measurements of vapor moisture generation and loss have been mentioned, and even fewer consistencies can be found when it comes to units of measurement, but the most practical ways to express such quantity appears to be those proposed by ASTM C232.

Previous quantitative measurements of bleeding and moisture loss were recorded in the development of ASTM C232, and non-destructive testing and research investigating detection and quantification of moisture content using radar or electromagnetic probing techniques have been conducted in unstabilized pavement bases or hardened concrete, where the moisture content can be considered to be a performance indicator (Al-Qadi et al. 1995; Scullion and Saaranketo 1996). Those radar or probing techniques seem to provide information that can generally be correlated to performance factors with high reliability. The basic methodology of these non-destructive methods will be discussed in detail in the last section of this chapter.

ROLE OF MOISTURE DISTRIBUTION AND RELATIVE HUMIDITY IN CONCRETE

Moisture distribution is usually expressed in terms of relative humidity. By thermodynamic principles, relative humidity is defined in terms of relative gas pressures as (Çengel and Turner 2001):

$$p = p_v + p_a \tag{2}$$

$$H = \frac{p_v}{p_s} \tag{3}$$

where:

p	=	Total ideal gas pressure, kPa
p_v	=	Partial pressure due to water vapor, kPa
p_a	=	Partial pressure in the air, kPa
H	=	Relative humidity, fraction or percentage
p_s	=	Saturation pressure of water at a specific temperature, kPa; at 40°C it corresponds to 7.38 kPa (as used in this study).

The distribution of moisture in hardening concrete is never uniform (presents a variable volumetric proportion with depth from surface), and it changes with time (Parrot 1991) due to the evaporation of free moisture available in the capillary voids from the concrete matrix at the surface. If the humidity in the air is lower than the concrete humidity, a moisture gradient is created, which forces moisture movement and loss through the interface. In other words, if a vapor pressure differential exists between the concrete and the environment, moisture will be lost through the available pores and capillaries (Powers 1947). In hardened concrete pavement slabs, moisture ditribution is sometimes a cause of slab warping due to moisture gradients developed by surface drying (Jannoo et al.1999). Hence, higher moisture concentrations and relative humidity occur in the inner parts of the concrete, since the outer parts in contact to the atmosphere loose moisture much more rapidly due to bleeding and evaporation. Previous research on hardened, water/moisture-cured concrete provided an insight on the water sorption-desorption behavior of concrete, which indicates the appearance of a porous,

penetration-susceptible "surface zone" displaying low relative humidities as compared to measurements made inside the concrete (Parrot 1991; Parrot 1992). Magnetic Resonance Imaging (MRI) measurements have been used to confirm this phenomenon (Cano-Barrita et al. 2004).

Relative humidity, in both ambient air and concrete, has a tremendous effect on the cement hydration process. Changes in concrete relative humidity values themselves are potential indicators of changes in microstructure and water availability, and they even dictate hydration rates (Powers 1947). When coupled with quantitative analyses of moisture availability, relative humidity measurements can offer a clear picture of self-dissecation characteristics of the hydrating paste (Parrot 1992), as will be elaborated further in this study.

Despite the recognized importance of moisture distribution and relative humidity in concrete technology, most relevant studies have failed to describe the natural self-dissecation characteristics of hardening young concrete. Self-dissecation is inherently hydration-rate dependent, occurs only once during the fresh, setting, and early hardening stages, and requires careful water-availability measurements from the mass and volumetric standpoints. Ultimately, the self-dissecation phenomena responds to vapor pressure, for hydration has been shown to stop if the ambient relative humidity drops below 80 percent or if pressure drop rates are zero, and pastes with water-cement ratios above 0.32 are able to maintain higher internal concrete humidity for longer periods of time (Powers 1947).

When combined with quantitative measurements of moisture loss, relative humidity measurements can yield important descriptive information about diffusivity, porosity and permeability (Parrot 1991). Research involving oven-drying practices narrow the focus to hardened concrete permeability rather than actual moisture history and distribution that are useful for design, construction, and curing practices. The present

study offers this missing perspective and the associated implications interpreted from the experimental results as reported in chapter III.

CEMENT HYDRATION

Cement hydration is defined as the exothermic chemical reaction between water and Portland cement (Mamlouk and Zaniewski 1999; Mindess et al. 2003; Neville 1995). This reaction produces the glue that binds all aggregate particles, and greatly contributes to the development of the mechanical properties of concrete. It is through this process that microstructure and porosity develop (Van Beek and Hilshorst 1999), which in turn affect the macroscopic mechanical properties. Therefore, much of the characterization of concrete properties can be correlated to the hydration process, development, and history. In fact, hydration development has been commonly approximated by measuring some of its characteristic behavior through heat and strength development (Khan et al. 1995). In this study, the measurement of the degree of hydration provides a clue about the development of concrete porosity and microstructure, and the necessary tools to establish a time-dependent volumetric analysis that is crucial to approximate the electric properties of concrete.

However, hydration is a very complex phenomenon. Among the circumstances contributing to the complexity of hydration is the existence of multiple, dependent and simultaneous reactions that take place for each of the chemical components of cement as reactants (Breugel 1991; Mindess et al. 2003; Neville 1995). The influence of heat availability, moisture availability and changes in pH are also significant during all three stages of hydration which implies that in many cases hydration is never 100 % thermodynamically efficient, for hydration requires ideal vapor pressure and temperature conditions (Mindess et al. 2003; Neville 1995).

Several stages of hydration have been proposed and identified. Five stages are generally defined as initial hydrolysis, induction, acceleration, deceleration, and steady state

(Mindess et al. 2003). In a more general and macroscopic approach, up to three stages are identified, and are defined as early, middle, and late (Breugel 1991; Neville 1995). It is in the early stage where high rates of bleeding and high moisture loss rates occur, whereas it is during the middle stage that the phenomenon known as setting (initial and final) takes place. Strength development occurs in the late stage, which can be used to determine the degree of hydration. Therefore, setting and strength development comprise an important piece in the analysis of this study.

Literature suggests that the main factors that control the rate, development and characterization of the hydration process are cement type and chemistry, cement fineness, water-cement ratio, ambient conditions, prescence of pozzolans or liquid admixtures, and curing effectiveness (Mindess et al. 2003; Neville 1995). For the purposes of this study, it was necessary to keep many of these factors constant, such as the type and chemistry of cement, and ambient conditions, as outlined in Chapter IV. It was also decided not to use liquid admixtures or pozzolans to avoid extraneous effects on moisture availability and measurements on hydration rates. Water-cement ratio and ambient conditions are of particular interest in this studysince these two factors greatly affect hydration and help describe the links between moisture loss, microstructure change, porosity, and self-dissecation.

Self dissecation occurs when the water available in liquid form in the capillaries is lost through bleeding and evaporation, leaving the capillaries empty. Hydration products can only form in water solution available in saturated capillary pores, and thus self-dissecation causes hydration to slow down and to practically stop, unless excess water is continuously available, which the hydrating cement paste can use during curing (Powers 1947; Taylor 1997). Then the underlined purpose of curing, in practical terms, is to keep the concrete as saturated as possible until the originally water-filled space has become filled with hydration products or space is no longer available, although thorough curing rarely guarantees complete hydration (Powers 1947).

The influence of the water-cementitious ratio in hydration can be expressed in several ways. It has been proposed that the minimum ratio to ensure full hydration of cement is between 0.36 (Mindess et al. 2003) and 0.38 (Taylor 1997). In chemically balanced terms, the ultimate amount of water that can ever be used for hydration has been identified to be only between 23 (Taylor 1997) and 25 (Powers 1947) percent of the mass of cement. In terms of water retention, it is known that cement can retain up to 50 percent of its mass via surface tension, but only up to half of that amount may ever be used for hydration, leaving the concrete susceptible to moisture loss. In that regard, 0.42 is recognized as the lowest water-cement ratio needed to avoid self-dissecation (Mindess et al. 2003), although sealed pastes below a limiting ratio value of 0.44 have shown signs of self-dissecation (Powers 1947).

From the discussion above, the best possible measure of hydration is then how much of the available capillary space is filled with hydrated cement products, but this measurement is impossible to accurately quantify. The hydration development is measured on the basis of more practical means via the degree of hydration. The basic concept for the degree of hydration follows the form (Breugel 1991; Van Beek and Hilshorst 1999):

$$\alpha(t)=\frac{\text{amount of cement that has reacted at time t}}{\text{total amount of cement at time t=0}} \tag{4}$$

or,

$$\alpha(t)=\frac{\text{amount of non-evaporable water a time t}}{\text{ultimate amount of non-evaporable water}} \tag{5}$$

However, neither ratio can be directly measured, so indirect methods are needed based on a ratio of two quantities, where the numerator is generally a time-dependent quantity, with the denominator being the ultimate value that the numerator can attain. The most accepted indicators of the degree of hydration are ratios of $Ca(OH)_2$ volumes, shrinkage, specific surface area, heat, and compressive strength (Breugel 1991). The last two can

be tested very easily and quickly, so strength tests were chosen in the methodology of this study.

The term non-evaporable water mentioned above is sometimes used loosely in cement hydration research. There is no clear agreement on what this mass fraction includes, and its place in the hydrated cement structure. For the objectives of this study, the following definitions will be used. *Chemically*-bound water, many times called *gel* or *non-evaporable* water, is considered to consist on the mass fraction of the available water that has reacted with cement and now forms part of the hydrated cement paste (HCP) structure (Mindess et al. 2003; Neville 1995). *Physically*-bound water is defined as the minuscule mass portion of the available water that is practically "trapped" or adsorbed onto or in between the Calcium-Silicate-Hydrate (CSH) layers of the hydrated cement paste. The binding mechanism of the physically-bound water is primarily Van-der Walls forces (Breugel 1991). This water portion can be evaporated at concrete humidities lower than 40 percent, but these humidity levels are only reached in oven drying conditions (Parrot 1991), not under realistically extreme hot-dry climatic conditions. Therefore, these two water states will henceforth referred to as *non-evaporable* water. The use of this term is intuitive and it is assumed not to affect the final outcome of the data analysis.

Free (capillary) water, on the other hand, is the portion of the water present in the capillary pores of the CSH structure. Much of this water proportion is assumed to behave like bulk (viscous) water, although it is possible that the water layers close to the CSH structure are either adsorbed or exerting surface tension and pore pressure (Mindess et al. 2003), similar to saturated soil-aggregate systems (Guthrie and Scullion 2000). As stated in the previous chapter, the complete saturation of capillary pores favors continuous hydration of the cement, until space is no longer available for hydration products (Powers 1947). In common concrete practice, a great percentage of this water is unavoidably lost during bleeding and evaporation. This loss creates new

porosity added to the initial air void content, and the addition of the two can be defined as total porosity (Mindess et al. 2003).

Finally, in this study, volumetric approximations need to be obtained for the analysis of the material dielectric properties warranting the use of basic volumetric concepts surrounding hydration processes. In simple terms, hydration of cement produces new compounds that require more volume than the initial mix proportion quantities. The total volume of a hydrated paste is dependent on the degree of hydration, and is the linear summation of the constituent products. As will be subsequently elaborated in the following chapter, a fully hydrated paste occupies the original volume of cement plus 1.4 times the dry volume of the hydrated cement at each stage of hydration (Powers 1947; Neville 1995).

DIELECTRIC PROPERTIES OF CONCRETE

A dielectric is any non-metallic material that cannot conduct electricity efficiently. Insulators and any poorly or semi-conducting material can be considered dielectrics (Anderson 1964), and portland cement concrete can be considered a dielectric because it meets these requirements. When an electric field or a current passes through a dielectric medium, the divergence, shape, and intensity of the outcoming electrical and generated magnetic fields can be measured to determine the electromagnetic properties of the medium. The electric property of the medium is known as permittivity, and the magnetic property of the medium is known as permeability. Research has shown that concrete has a negligible magnetic permeability, so the magnetic properties are usually assumed to be negligible (Rhim and Büyüköztürk 1998). Unless ferromagnetic or metallic materials are used in concrete as aggregates, there is no need to account the magnetic permeability of concrete.

However, the study of the dielectric properties of materials is not a simple task, for it is dependent on the way they are measured. The electric parameter of interest for dielectric

mediums is the permittivity. Permittivity is the proportionality constant that describes, as the name implies, how well an electric field travels through a medium. For static electric fields such as the ones generated by point charges and direct current (DC), the permittivity of free space (vacuum) can be found to be part of the common electric flux density equation (TransTech 2003):

$$\vec{D}=\varepsilon_0\vec{E}+\vec{P} \tag{6}$$

where:

$\vec{D}$	=	Electric flux density, C/m^2 (Coulombs/meter^2)
ε_0	=	Permittivity of free space, 8.85×10^{-12} F/m (Farads/meter)
$\vec{E}$	=	Electric field intensity or strength, V/m (Volts/meter)
$\vec{P}$	=	Induced polarization, C/m^2

If it is assumed that the medium or material through which the electric field passes through is linear and isotropic, then the polarization is proportional to the electric field intensity (TransTech 2003):

$$\vec{P}=\chi\varepsilon_0\vec{E} \tag{7}$$

where χ is the electrical susceptibility of the material, a measure of the proportion of the bound charge density to the free charge density (Anderson 1964), with values ranging only from zero to unity. Then, for an electric field passing through any other medium, the electric flux density becomes:

$$\vec{D}=\varepsilon_0\left(1-\chi\right)\vec{E} \tag{8}$$

so that

$$\vec{D}=\varepsilon_0\varepsilon_r\vec{E} \tag{9}$$

and,

$$\varepsilon_r=\frac{\varepsilon_{medium}}{\varepsilon_0}=(1-\chi) \tag{10}$$

where:

ε_r = Relative permittivity of medium, unitless; equal or larger than 1.00

ε_{medium} = Complex absolute permittivity of medium, F/m

When an alternating current (AC) passes through the medium, the permittivity is better represented as a complex number. The permittivity values are thus dependent of the frequency of the AC source (Al-Qadi et al. 1995; Guthrie and Scullion 2000). The complex permittivity is generally presented in the following form (Anderson 1964; Rhim and Büyüköztürk 1998; Van Beek and Hilshorst 1999).

$$\varepsilon^* = \varepsilon' - j\varepsilon'' \tag{11}$$

where:

ε^* = Complex permittivity of medium, F/m

ε' = Real term, dielectric constant of medium, F/m (Farads/meter)

j = $\sqrt{-1}$

ε'' = Imaginary or "loss" term, F/m

Yet in engineering practice it is generally more useful to present the permittivity relative to either the free space's or air's permittivity, so that (Anderson 1964):

$$\frac{\varepsilon^*}{\varepsilon_0} = \frac{\varepsilon'}{\varepsilon_0} - j\frac{\varepsilon''}{\varepsilon_0} \tag{12}$$

and since,

$$\varepsilon'' = \frac{\sigma_d}{\omega} \tag{13}$$

then,

$$\varepsilon^*_r = \varepsilon'_r - \varepsilon''_r \tag{14}$$

or ultimately,

$$\varepsilon^*_r = \varepsilon'_r - j\frac{\sigma_d}{\omega\varepsilon_0} \tag{15}$$

where:

σ_d	=	Dielectric conductivity, $\Omega^{-1}\cdot m^{-1}$ ($ohm^{-1}\cdot meter^{-1}$)
ω	=	Frequency of alternating current source, Hz
ε^*_r		(Relative) permittivity, unitless
ε'_r		(Relative) dielectric constant or dielectric value, unitless
ε''_r		(Relative) dielectric loss, unitless

Also in engineering practice, the term "relative" is commonly dropped from the definition. Henceforth, following common practice in this study, the real term of the complex permittivity is simply referred to as the dielectric constant, and the imaginary term is simply referred to as the dielectric loss. The dielectric loss is sometimes also presented as a factor of the dielectric constant in a term called the loss tangent (Al-Qadi et al. 1995; Anderson 1964; Rhim and Büyüköztürk 1998):

$$\tan\delta = \frac{\varepsilon''_r}{\varepsilon'_r} \tag{16}$$

where δ is graphically the angle between the two vectorial components (dielectric constant and loss) of the complex permittivity.

The dielectric constant can be thought of as a measure of the ability of a material to store charge or electrical energy for a given electrical field strength, whereas the dielectric loss (or the loss tangent) is a measure of the attenuation, dissipation or eventual unrecoverable loss of energy, and can help determine the depth of penetration of radar signals into concrete structures (Guthrie and Scullion 2000; Van Beek and Hilshorst 1999; Rhim and Büyüköztürk 1998; Zoughi et al. 1995). At frequencies lower than 1GHz, the dielectric constant for a pure material is fairly constant, and the loss is negligible (Rhim and Büyüköztürk 1998; TransTech 2003), and research suggests the use of a frequency between 1 and 40 MHz as the optimum range for good detection of permittivity values in soils, asphalt and concrete materials (Al-Qadi et al. 1995; Scullion and Saarenketo 1996).

Previous research also suggests that either parameter of the permittivity by itself seems to provide different detection capabilities. Resistivity measurements have shown to provide an insight into the heat of hydration, porosity and microstructure properties in concrete (Li et al. 2003; Xian-Yu et al. 2002), whereas dielectric constant measurements have successfully shown sensitivity to moisture content measurements in soil and aggregate construction materials (Scullion and Saarenketo 1996).

The statements above imply that one of the two options for the non-destuctive determination of hardening concrete properties can be to measure the dielectric conductivity. The dielectric conductivity, which is part of the dielectric loss, is related to resistivity through:

$$\sigma_d = \frac{1}{\rho} \tag{17}$$

where ρ is the resistivity of the medium (Ω/m). Due to the relative simplicity of resistivity measurements, they have been used to investigate the properties of concrete, and their sensitivity to cement hydration characteristics have paved the way towards the investigation of more thorough permittivity measurements as non-destructive testing tools. Resistivity measurements have been generally driven by the fact that conduction of electricity implies the concentration and movement of ions, and by the importance of hydration characterization and prevention of chloride attack phenomema (Khalaf and Wilson 1999; Li et.at. 2003). Resistivity testing on cement paste leads to the possible determination of the characteristic heat of hydration and is capable of approximating the volumetric porosity, for porosity is a controlling factor in conductivity of concrete and can be highly correlated to strength (Van Beek and Hilshorst 1999; Xian-Yu et. al 2002).

However, resistivity testing has serious setbacks. In order to measure resistivity (or both permittivity components at the same time), a capacitor plate-type arrangement is usually needed and hooked to a set of complicated equipment (Li et al. 2003; Xian-Yu et al.

2002) that cannot be used under field conditions. Also there exist problems with poor sensitivity and low statistical significance, since only one condition, one point and one location can be tested at each time. Embedding probes such as the time domain reflectometry (TDR) probe (Janoo et al. 1999) solve the sensitivity issue, but does not resolve the low statistical significance issues. It has also been documented that polarization and viscous conduction can be encountered if DC is used or even if the wrong AC frequency is chosen (Xian-Yu et al. 2002).

The only option left is therefore the measurement of the dielectric constant. Due to the energy and polar nature of water, water possesses one of the largest dielectric values that exist (Van Beek and Hilshorst 1999) as shown in Table 1. It is therefore heavily documented that dielectric constant measurements may be sensitive enough and be able to assess the amount of unbound water in aggregate construction materials, where high dielectric values imply high moisture contents (Guthrie and Scullion 2000). These measurements may eventually be successfully applied to concrete to obtain a clue of the free (capillary) moisture content during hardening, or a clue of the moisture sorption/desorption after hardening (Janoo et al. 1999). Furthermore, performance assessment guides have been implemented through the use of dielectric value measurements in soil-aggregate systems, for which high dielectric value ranges imply poor performance (Scullion and Saarenketo 1996).

Table 1. Dielectric Constant Range of Values at a Frequency of 40 MHz[a]

Common concrete material component	Dielectric constant
Air	1
Cement	3.6-4.0
Hydrated cement paste products	4.0-5.0
Gravel	5.8-6.5
Water	80-82

[a]Rhim and Büyüköztürk 1998; Zoughi et al. 1995)

Nevertheless, in order to limit the number of possible error-inducing testing factors during measurements of the dielectric constant of portland cement concrete, a non-embedding, a surface probe may be needed. The use of a surface probe is likely to eliminate the single-point issues faced with TDR (Time-Domain Reflectometry) probes, but may only be able to generate an electric field that penetrates a shallow depth into the tested material. Also, it is likely that repeated randomized testing at different locations of specimens for each testing round must be conducted for sake of statistical reliability. The dielectric value measurements in concrete are also likely to include systematic errors generated by the volumetric changes in the capillary moisture content and distribution, and random errors generated by differences in density and aggregate gradation (Frolov and Ivanovskii 1984).

Although the use of dielectric constant measurements in concrete as indicators of capillary water availability is not yet widely supported due to the potential limitations explained above, it may be possible to directly correlate specific dielectric value ranges to specific volumetric approximations. It is important to maintain caution with dielectric constant measurements, for the dielectric constant is not only dependent on the amount of water but also on the different stages of bonding of water in concrete at different curing times (Van Beek and Hilshorst 1999). Yet there is high potential for the detection and quantitative description of changes in moisture, relative humidity, and even hydration through dielectric testing, if proper complementary and conventional testing is conducted.

CHAPTER III
THEORETICAL CONSIDERATIONS

The purpose of this chapter is to present the theory used in the development of the research tasks. The intended purpose of the theory is to establish the analysis framework for the data collected in the experimental program of this study. Time-dependent volumetric equations commonly used for hydrated cement, linearization of concrete strength development for hydration approximations, and an empirically derived dielectric constant equation for composite materials are the three most prominent considerations to be used.

VOLUMETRIC APPROXIMATIONS AND HYDRATION OF CEMENT PASTE

The analysis of moisture availability requires the volumetric equations. As stated previously in this study, hydrated cement paste product, often referred to as HCP (Powers 1947; Neville 1995), consists of several phases that include both HCP and moisture, but excludes the unreacted cement. The Powers-Brownyard HCP model describes this product as a combination of reacted cement, gel water, free water and air voids (Taylor 1997), plus the unreacted cement. Figure 1 presents this arrangement visually. Within this arrangement, the structural hydration product, Calcium-Silicate-Hydrate (CSH) is assumed to consist of all phases except the unreacted cement. Although the actual structure of CSH is not entirely well established, its currently adopted structure is the Feldman-Sereda model (Neville 1995), as shown in Figure 2.

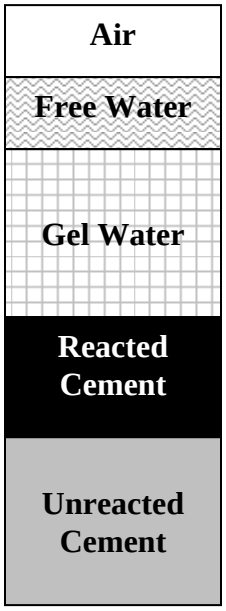

Figure 1 – Powers-Brownyard Model for a Hydrated Cement Paste with Degree of Hydration Lower than 100%. (Taylor 1997)

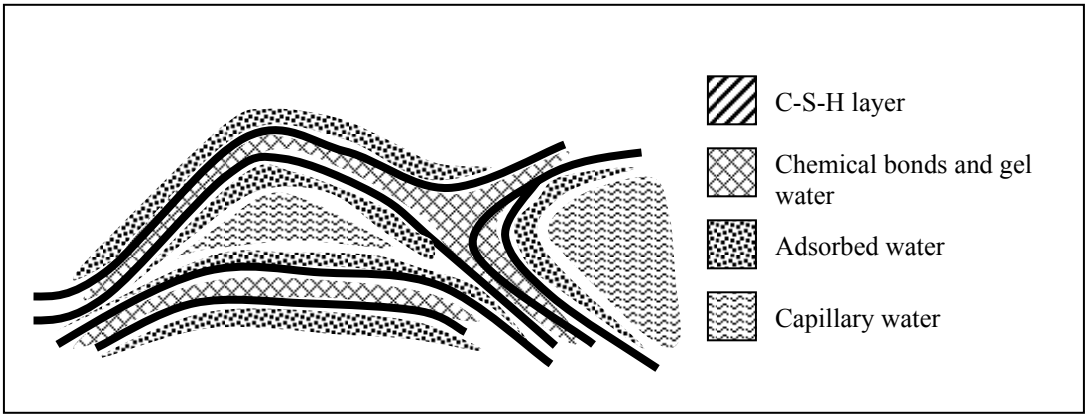

Figure 2 – Feldman-Sereda Model for C-S-H Structure (Neville 1995)

Despite the individual usefulness of these models in establishing a basic volumetric relationship, more detail is needed for this study in the description of water states and phases in the HCP. Although the main focus of previous hydration-related analyses has been the cement products, water availability will play a major role in this study. In order to satisfy the stated objectives, it is necessary to focus the attention on water availability. For this purpose, a slightly modified, Dutch model that incorporates both known models will be adopted. In this Dutch model, water will be considered to be present in the HCP in three different forms: chemically-bound water, physically-bound water, and free (capillary) water (Breugel 1991).

Based on the definitions collected from the three HCP models, the model used in this study is visually represented in Figure 3. This model incorporates the commonly accepted components and arrangement in order to construct the basic mass-volumetric relationships to be used in the quantitative analysis of the experimental results. The general definition of the volumetric model consists on the quantification of the individual volume components as a fraction of the actual fresh concrete volume. This approach is necessary for the quantitative measurements to be applicable to the dielectric properties model. It is also necessary that any volumetric model needs to satisfy the thermodynamic principle of mass-conservation (Çengel and Turner 2001):

$$\dot{m}_{pcc} = \dot{m}_{in} - \dot{m}_{out} \tag{18}$$

where:

$\dot{m}_{pcc}$ = Total mass rate of change of concrete, kg/hr

$\dot{m}_{in}$ = Inflow mass rate, kg/hr

$\dot{m}_{out}$ = Outflow mass rate, kg/hr

In concrete research, the only likely type of mass inflow or outflow is moisture, since the other components of concrete (aggregate or cement) cannot "escape" the system. As previously stated, if the humidity level in the ambient air is lower than the humidity level in the concrete, a concrete-air moisture gradient will develop (Parrot 1991). Thus, this principle implies that if low levels of moisture (or no moisture at all) are available in the air, a resulting mass loss will occur. Weight measurements are needed to quantify any moisture loss (or unlikely gain) that occurs during the curing length of the experimental program. The application of this principle translates into the following basic water mass relationship that can be derived from the adopted volumetric model:

$$w_{net} = w_n(t) + w_{free\_tot}(t) \tag{19}$$

and

$$w_{free\_tot} = w_{free}(t) + w_{free\_lost}(t) \tag{20}$$

where:

w_{net}	=	Net water mass (mix design-based, corrected for absorption and moisture on aggregates), kg
$w_n(t)$	=	Time-dependent non-evaporable water mass, kg
$w_{free\_tot}(t)$	=	Total free (capillary) water mass in concrete, kg
$w_{free}(t)$	=	Time-dependent free (capillary) water mass left in concrete capillary voids, kg
$w_{free\_lost}(t)$	=	Free (capillary) water mass lost to the atmosphere, kg

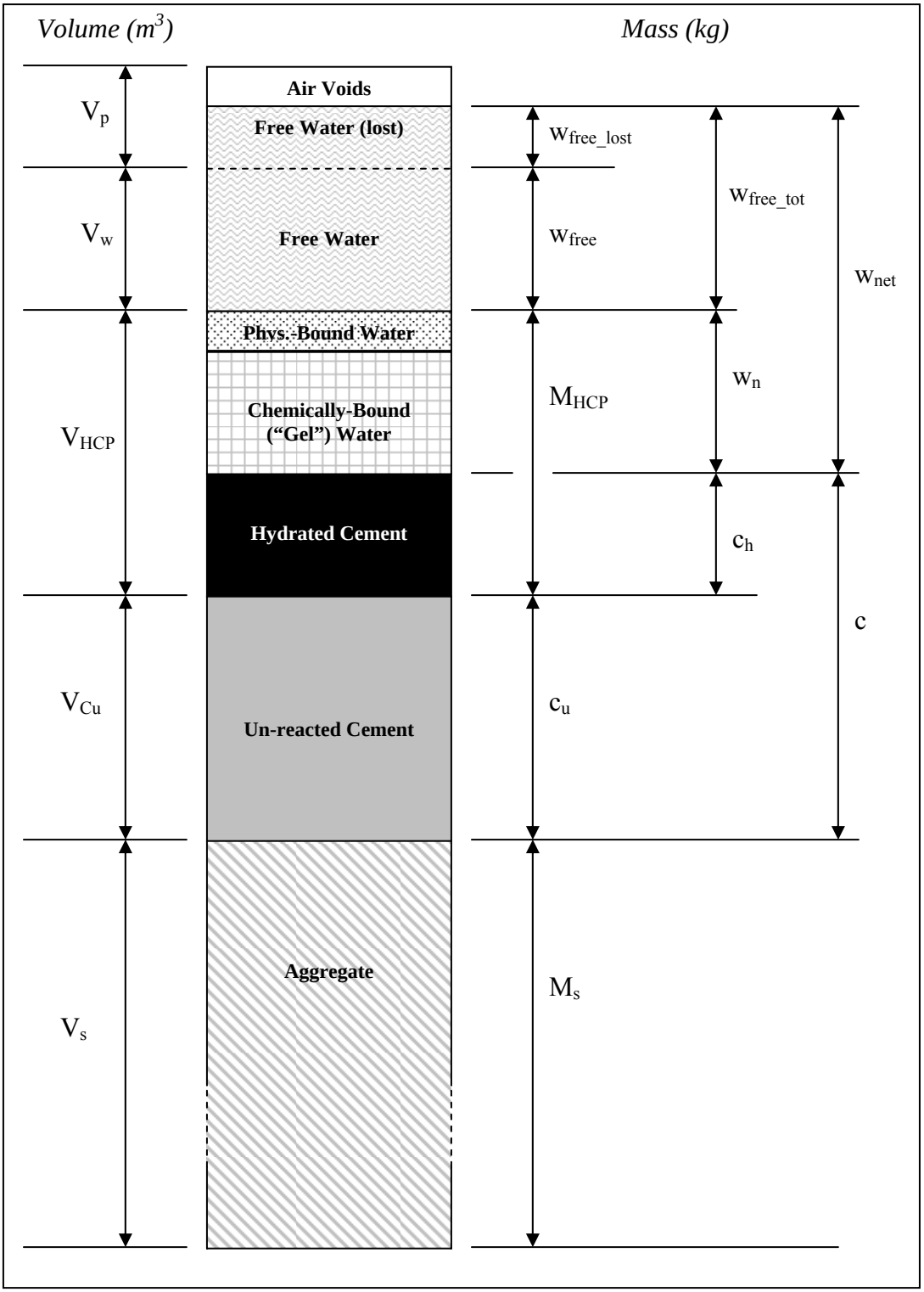

Figure 3 – Modified Breugel Mass/Volumetric Model for Portland Cement Concrete (Adopted for This Study)

It should be noticed that the correct quantification of the free (capillary) moisture mass will depend on a good approximation of the non-evaporable water mass. The lost (evaporated) part of the capillary moisture is easily determinable, following the conservation of mass principle, for it can be assumed that the only mass outflow crossing the boundary of the concrete system is the moisture lost through bleeding and evaporation, and the only mass inflow comes from the moisture available in the surrounding air (Wang 2000), as shown in Figure 4. Under harsh conditions (high temperatures and low relative humidities, the moisture outflow rate will be much larger than the inflow rate (i.e., $\dot{m}_{out} >>> \dot{m}_{in}$). For any ambient condition, it can be induced that any change in total concrete mass is exactly equivalent to the change in free (capillary) water content:

$$\Delta_{t_i}^{t_i+(\Delta t)_i} m_{pcc} = \Delta_{t_i}^{t_i+(\Delta t)_i} w_{free\_tot} \tag{21}$$

where:

$\Delta_{t_i}^{t_i+(\Delta t)_i} m_{pcc}$ = i^{th} change in concrete mass from time t_i to $t_i+(\Delta t)_i$, kg

$\Delta_{t_i}^{t_i+(\Delta t)_i} w_{free\_tot}$ = i^{th} change in free (capillary) moisture mass from time t_i to $t_i+(\Delta t)_i$, kg

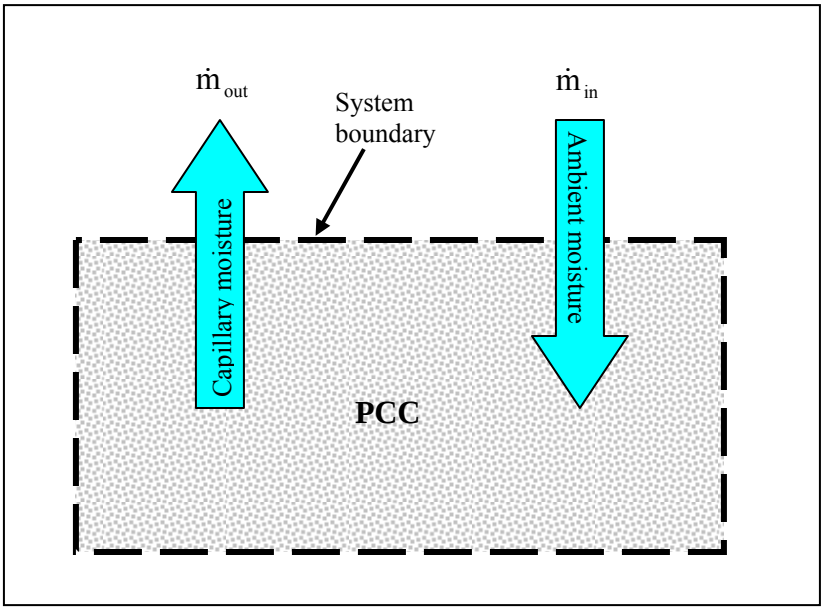

Figure 4 – Cross-boundary Mass Flow in Concrete

Concrete does not maintain the same volume throughout its hardening process. Although indirectly, the concrete volumetric change can be approximated through the joint use of the mass conservation principle and the adopted volumetric model. For the determination of basic volumetric quantities, it is necessary to establish a baseline from which to reference all the following calculations, and that baseline will be set at the fresh concrete mass/volumetric properties. Therefore, the volumetric content of a concrete component is simply defined as:

$$\theta_i = \frac{V_i}{Y} \tag{22}$$

where:

θ_i = Volumetric content of component

V_i = Absolute volume of component, m^3

Y = Fresh concrete yield, m^3

Thus, the volumetric aggregate content can be simply defined as:

$$\theta_s = \frac{V_s}{Y} \tag{23}$$

where:

θ_s = Constant volumetric content of aggregates

V_s = Solid-bulk volume of aggregates, m^3

The relationship between fresh concrete yield and solid volume of aggregates is given by:

$$V_s = Y - \sum V_i \tag{24}$$

where:

ΣV_i = Sum of absolute volume of air, cement and net water, m^3

The hydration process involves the remaining phases of the volumetric model, thus a consistent definition for the degree of hydration is important. The two main equivalent definitions of the degree of hydration are given as (Breugel 1991; Mindess et al. 2003; Taylor 1997

$$\alpha(t) = \frac{c_h(t)}{c}, \text{ and} \tag{25}$$

$$\alpha(t) = \frac{f'_c(t)}{f'_{c-ult}} \tag{26}$$

where:

$\alpha(t)$ = Time-dependent degree of hydration, 0.0 to 1.0

$c_h(t)$ = Time-dependent hydrated cement mass, kg

c = Mass of cement from mix design

$f'_c(t)$ = Concrete compressive strength, MPa

$f'_{c\text{-}ult}$ = Ultimate compressive strength, MPa

It can be seen from the adopted volumetric model that the mass of the unhydrated cement is, at all times, simply:

$$c = c_u(t) + c_h(t) \tag{27}$$

where:

$c_u(t)$ = Time-dependent mass of unhydrated cement

Hence, equations (25) and (27) can be combined to determine the mass of the unhydrated cement as (Mindess et al. 2003; Taylor 1997):

$$c_u(t) = \left(1 - \alpha(t)\right)c \tag{28}$$

The quantification of unhydrated cement is more useful for this study in volumetric terms. To transform this quantity, it is necessary to use the definition of specific gravity (Somayaji 2001):

$$G_{pc} = \frac{M_{pc}}{V_{pc}\rho_w} \tag{29}$$

where:

G_{pc} = Mean specific gravity of Portland cement, 3.15

M_{pc} = Mass of Portland cement sample, kg

V_{pc} = Volume of Portland cement sample, m^3

ρ_w = Mean density of water, 1,000 kg/m^3

Since unhydrated cement has the same mass/volumetric properties (specific gravity) as dry bulk cement, equation (28) can be transformed into:

$$\theta_{Cu}(t) = \left[1 - \alpha(t)\right]\theta_c \tag{30}$$

where:

$\theta_{Cu}(t)$ = Time-dependent volumetric content of unhydrated cement

θ_c = Volumetric content of cement from mix design

Hydrated cement quantification requires longer and more indirect calculations. The volumes of the unhydrated cement (V_{Cu}) and hydrated cement products (V_{HCP}), including chemically and physically bound water can only be approximated together through (Powers 1947; Neville 1995):

$$\theta_{Cu+HCP}(t) = \theta_{Cu}(t) + f_v \theta_c \alpha(t) \tag{31}$$

where:

$\theta_{Cu+HCP}(t)$ = Time-dependent volumetric content of both unhydrated and hydrated cement (including gel and trapped water)

$\theta_{Cu}(t)$ = Time-dependent volumetric content of unhydrated cement

f_v = Volumetric factor, 1.0 to 1.4

It is important to remark that the volumetric content of the hydrated cement products (HCP) consists on both volumetric contents of the non-evaporable water (gel and trapped water) and the hydrated cement. However, the volumetric content of HCP can be presented as simply:

$$\theta_{HCP}(t) = \theta_{Cu+HCP}(t) - \theta_{Cu}(t) \tag{32}$$

or as a linear relationship of the form (Figure 5):

$$\theta_{HCP}(t) = (1 + f_v)\theta_C[\alpha(t)] \tag{33}$$

The quantification of water in its three different forms also requires indirect calculations and initial guesses. From the default definition of volumetric content, the free water available in concrete can be quantified as:

$$\theta_w(t) = \frac{V_w(t)}{Y} \tag{34}$$

where:

$\theta_w(t)$ = Time-dependent volumetric content of free water

$V_w(t)$ = Time-dependent volume of free water, m^3

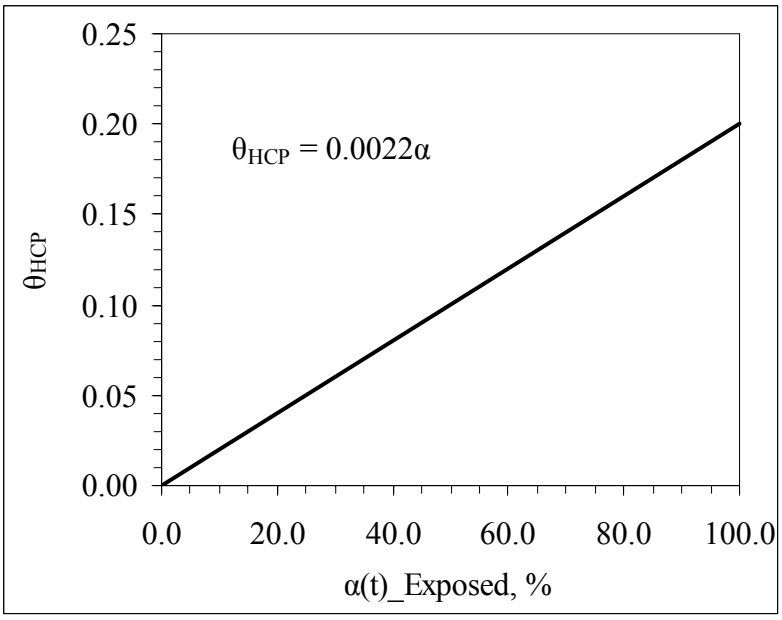

Figure 5 –Dependence of Volumetric Content of HCP on Hydration [All Treatments]

However, the volume of free water cannot be measured directly, and can only be approximated indirectly by calculating the free water as a mass fraction of net water. This is possible since the mass/volumetric properties of net and free water are assumed to be the same (Taylor 1997).

$$V_w(t) = \left(\frac{w_{free}(t)}{w_{net}} \right) V_{net} \tag{35}$$

where:

V_{net} = Net water volume, m^3

and

$$V_{net} = \frac{w_{net}}{\rho_w} \tag{36}$$

where:

ρ_w = Mean density of capillary water, 1,000 kg/m^3 (Taylor 1997)

The time-dependent mass of free (capillary) water cannot be measured directly either, but it can be calculated using the mass conservation principle:

$$w_{free}(t) = w_{net} - w_n(t) - w_{free\_lost}(t) \tag{37}$$

In order to determine the non-evaporable water mass, it is necessary to make the assumption that the non-evaporable water mass will have a limiting value at the ultimate degree of hydration, and it is defined as (Breugel 1991; Neville 1995):

$$\hat{w}_n = f_n c \tag{38}$$

where:

$\hat{w}_n$ = Ultimate water mass that can be reacted for hydration of cement, kg

f_n = Non-evaporable water mass factor, 0.20 to 0.30

It is important to emphasize that the non-evaporable water mass can still be quantifiable by total mass measurements and an initial guess for the f_n value. However, the complexity lies in the actual structure of the HCP, where the non-evaporable water volume is actually part of the hydrated cement product. Thus, in order to relate the non-evaporable mass to the rest of the volumetric relationships already described, a third definition of degree of hydration is needed. This additional form of the degree of hydration that is presented below is commonly accepted to determine the mass of gel water (Breugel, 1991), but as stated before for the purpose of this study, non-evaporable water will represent both gel and trapped water, not only gel water:

$$\alpha(t) = \frac{w_n(t)}{\hat{w}_n} \tag{39}$$

where:

$w_n(t)$ = Time-dependent non-evaporable water mass, kg

The remaining volumetric component is porosity as constituted by air-filled, empty pores and spaces. At the time of placement (t=0), it is assumed that the total porosity

will consist on the air void content of fresh concrete. As cement hydrates, the porosity will increase with the space left behind by moisture loss and decrease with the expanding hydrated cement products. From the adopted volumetric model, it can be concluded that this component is simply:

$$\theta_p(t) = 1 - \theta_s - \theta_w(t) - \theta_{Cu}(t) - \theta_{HCP}(t) \quad (40)$$

where:

$\theta_p(t)$ = Time-dependent porosity volumetric content

DEGREE OF HYDRATION MODELING

It should be noted that the adopted volumetric analysis revolves around a correct determination of the degree of hydration and total concrete weight. Of all the available forms of this parameter, only two of the existing definitions for degree of hydration can be directly approximated using conventional tests: strength testing and temperature (heat evolution) monitoring (Mindess et al. 2003; Neville 1995):

$$\alpha(t) = \frac{Q(t)}{Q_{ult}} \quad (41)$$

$$\alpha(t) = \frac{f'_c(t)}{f'_{c-ult}} \quad (42)$$

where:

$Q(t)$ = Time-dependent adiabatic heat signature, J/g

$Q_{ult}(t)$ = Ultimate adiabatic heat signature, J/g

The adiabatic heat signature (AHS) represents the amount of exothermic heat energy liberated by the cement hydration per unit mass of concrete (Neville 1995). The ultimate, cumulative heat generated by this reaction is commonly correlated to the amount and chemistry of cement that has been consumed by the reaction, as approximated by accepted and well-established models (Mindess et al. 2003). The

strength method to be used in this study is a modified adaptation of the ASTM C1074 mortar test. The actual objective of this mortar test is the determination of a characteristic heat energy parameter of cement (activation energy). However, as Figure 6 shows, this method still allows for the easy determination of the ultimate concrete strength by using a linear regression analysis. The basic form of this linear regression is expressed as:

$$[f'_c(t)]^{-1} = \frac{1}{f'_c(t)} \tag{43}$$

and

$$[f'_c(t)]^{-1} = m * t^{-1} + [f'_{c-ult}]^{-1} \tag{44}$$

where:

$f'_c(t)$	=	Time-dependent compressive strength of concrete, MPa
m	=	Slope of regression line, days/MPa
$f'_{c\text{-}ult}$	=	Ultimate compressive strength and reciprocal of the intercept of the regression line, MPa

Setting time determination can also obtained as a complementary measurement for early age hydration. The initial and final setting times of the mortar fraction of the concrete mix are parameters believed to identify a sudden microstructure change, as hydration turns fresh workable concrete into a hardened, solid mass. A commonly accepted approach is the use of penetration pressure needles as specified by ASTM C192, in which fixed, predetermined values for initial and final setting pressure values are used. Penetration resistance (R_p) pressure values of 3.45 MPa (500 psi), and 27.58 MPa (4000 psi) are set for initial and final setting indication marks. The accepted form of penetration measurements in this test is presented as:

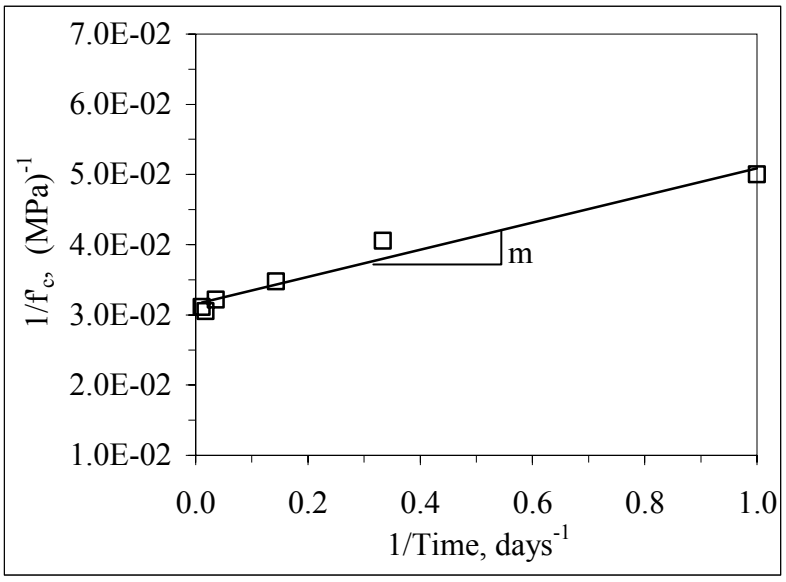

Figure 6 – Linearization and Linear Regression of Concrete Strength

$$R_p(t) = at^b \tag{45}$$

or,

$$\mathrm{Log}(t) = \frac{1}{b}\mathrm{Log}\left(\frac{R_p}{a}\right) \tag{46}$$

where:

$R_p(t)$	=	Time-dependent penetration resistance pressure of mortar, MPa
t	=	time, hrs or maturity
a	=	Statistically determined proportionality constant, MPa
b	=	Statistical regression value

COMPLEX REFRACTIVE INDEX MODEL (CRIM)

As stated in the previous chapter, the dielectric properties of a composite material are a combination of the dielectric properties of the individual components. These composite dielectric properties thus depend mainly on the averaged volumetric proportioning and relative micro-directionality of each of the components (Hashin 1982; Janoo et al. 1999; Khalaf and Wilson 1999). The complex refractive index model (CRIM) is assumed to follow what is known as a linear rule of mixtures, for which the total composite dielectric property is simply the addition of the volumetrically proportional dielectric properties of the individual components of a multy-phase composite material (Guthrie and Scullion 2000). Neglecting relative directionality of the arrangement of the material, the CRIM for the composite dielectric constant of any composite material can then be expressed in general as (Klemunes 1998; TransTech 2003):

$$\varepsilon^a = \sum_i^n \theta_i \varepsilon_i^a \tag{47}$$

where:

ε	=	Dielectric constant of concrete
a	=	Assumed power regression coefficient, 0.5 (for granular materials)
θ_i	=	Volumetric content of i^{th} component
ε_i	=	Dielectric constant of i^{th} component
n	=	Number of components

In other investigations, this model has been successfully used for unsaturated soil to predict water content and saturation values (Klemunes 1998). This model usually consists on two or three terms, since soil-water systems have at the most three mathematical terms (corresponding to air, water and solids). This is not the case for Portland cement concrete, where more than four different phases and components can be accounted for. To complicate matters, the dielectric constant of concrete cannot be fully described by the capillary water content (Van Beek and Hilshorst 1999). In order to use

the CRIM for Portland cement concrete, it might be necessary to consider a minimum of five components (adding the additional unhydrated cement and HCP phases). On the other hand, the dielectric properties of unsaturated soils are usually well fitted through the use of a 0.5-degree power model regression coefficient, possibly due to the granular nature of soils. Since Portland cement concrete is a composite granular material, this coefficient value may be well-suited for the concrete model construction. Therefore, in this study the applied CRIM for concrete should follow the form:

$$\varepsilon^{0.5} = \theta_p \varepsilon_p^{0.5} + \theta_w \varepsilon_w^{0.5} + \theta_{HCP} \varepsilon_{HCP}^{0.5} + \theta_c \varepsilon_c^{0.5} + \theta_s \varepsilon_s^{0.5} \quad (48)$$

where:

ε_p = Dielectric constant of porosity (air), 1

ε_w = Dielectric constant of free (capillary) water, 81

ε_{HCP} = Dielectric constant of hydrated cement product, 4 to 5

ε_c = Dielectric constant of Portland cement, 3.65

ε_s = Dielectric constant of aggregate, usually 5.8 for siliceous gravel and 20 for limestone

The average volumetric proportions, then, seem to be the only determining factors that can change the value of the composite dielectric constant. This approach presents an opportunity for the non-destructive determination of not only moisture content, but also approximated relative proportions of main hydration products.

CHAPTER IV
RESEARCH PROGRAM

The purpose of this chapter is to present the methodology followed for collecting moisture, hydration, and dielectric characteristic data on Portland Cement Concrete. The information collected from these measurements will serve as calibration data for the proposed models and to identify correlations that have not been extensively analyzed previous to this study.

EXPERIMENTAL DESIGN

The proposed experimental design was established with the main purpose to conduct testing and observations from a baseline reference point for future development and research. The environment in which the tests were conducted resembles marginal hot and dry weather conditions present in the southwest geographical areas of the United States. A 40°C (104°F) temperature and an ambient relative humidity of 40 percent were set for all tests runs. These conditions were chosen in order to fix the moisture mass flow in one direction: out of the concrete system boundary, since that simplifies the analysis performed in this study and can be interpreted as a "worst-case" or baseline scenario. Lower temperatures and higher humidity values would generate a two-way moisture mass flow that would be impossible to separate by direction quantitatively by mass measurements (see Chapter III).

The remaining elements of the baseline conditions have to do with the materials used. It was decided to use neither mineral nor chemical admixtures in order to prevent unintended influences on moisture content, moisture loss or hydration development. Furthermore, only siliceous gravel and sand were chosen to avoid paste-aggregate interface reaction that occurs in limestone concrete. All baseline weather conditions and concrete materials used in this study are shown in Table 2

Table 2. Experimental Baseline

Baseline Element	Design Value, Condition or Type
Environment	40°C (104°F), 40% relative humidity No wind or solar exposure
Cementitious Materials	ASTM C150 Type I Portland cement Cement Factor: 332 kg/m^3 (6 bags/yd^3) No mineral admixtures used
Aggregate	ASTM C33 Gradation; Max. Size = 38mm (1.5in) Coarse Aggregate Factor = 0.7, about 1,116 kg/m^3 (1,900 lbs/yd^3) Siliceous gravel and sand
Admixtures	No admixtures were used

The research tasks involved the measurement of eight important concrete characteristics through the tests outlined in Table 3. It is important to emphasize that moisture content/loss and strength measurements are the main factors to be considered in the testing methodology. Moisture loss was assumed to be dependent on the amount of area exposed and sensitive to shallow depths, especially in hot-dry weather conditions. Consequently, moisture loss specimens with shallow depth and wide dimensions were considered. Furthermore, a round shape was also necessary in order to minimize concrete-mold interface water concentration and to force the moisture loss to occur through the concrete matrix. These two dimension requirements describe a shallow cylindrical shape that needed to be manufactured specifically for this study. Besides, due to the large aggregate size used, a minimum depth dimension requirement was introduced, since it is common practice to fit the smallest dimension to at least three times the maximum aggregate size (Somayaji 2001). Figure 7 shows the conclusive design of the moisture specimens. On the other hand, the strength measurements required samples described by ASTM C31 (except for the curing requirements).

The experimental design test series could not be enclosed into a single factorial design due to the individually different characteristics of the seven types of tests. Table 4 better explains the factorial design used according to the test type.

Table 3. Test Program

Test	Test Name	Instrumentation	Parameter / Objective
1	ASTM C138 (Volumetrics)	Gravimetric bucket	Unit weight, air content
2	ASTM C143 (Slump)	Slump Cone	Slump
3	Modified ASTM C232 (Bleeding / Mass loss)	Weight scale	Total water content
4	Permittivity measurements	Adek™ Percometer	Dielectric Constant, Conductivity
5	ASTM C39 (Compression)	Tinius-Olsen Testing Machine	Compressive strength, degree of hydration
6	Calorimetry	Q-Drum™	Adiabatic heat signature, degree of hydration
7	Relative humidity	A-Tek™ Moisture meter	Relative humidity
8	ASTM C192 (Penetration)	Penetrometer	Setting time

Table 4. Factor Combinations

Exposure Level	Treatment	Tests Performed under Combination
Exposed	0.32	1, 2[a], 3, 4, 5, 7[a], 8[a]
Exposed	0.36	1, 2[a], 3, 4, 5, 7[a], 8[a]
Exposed	0.40	1, 2[a], 3, 4, 5, 7[a], 8[a]
Exposed	0.44	1, 2[a], 3, 4, 5, 7[a], 8[a]
Covered	0.32	1, 3, 4, 5, 6[a]
Covered	0.36	1, 3, 4, 5, 6[a]
Covered	0.40	1, 3, 4, 5, 6[a]
Covered	0.44	1, 3, 4, 5, 6[a]

[a]Restricted to this combination due to test characteristics and procedure

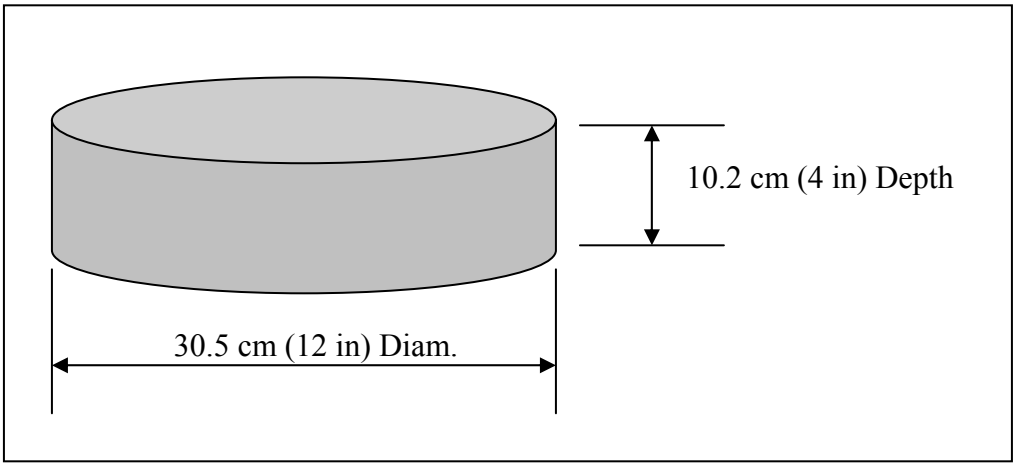

Figure 7 - Specimen for Moisture Loss and Permittivity Measurements

BLEEDING AND MOISTURE LOSS MEASUREMENTS

As previously stated, concrete looses some of its net mixing water as it hardens. This part of the investigation first determines the actual total water mass remaining in the concrete samples, and thus can indirectly determine the total amounts of moisture mass loss in its two stages: bleeding and post-bleeding. These measurements represent the water that will be lost during bleeding and post-bleeding, and provides an important piece of the information needed to determine actual time-dependent concrete water content in two of its forms: free (capillary) water, and non-evaporable water. Water quantification then, is the major factor and focus of these measurements.

Following the initial (fresh concrete) mass measurement of the samples, controlling bleeding measurements required careful procedures, and it was necessary to avoid any movement or vibration of the fresh specimen after casting. Although this last approach is contrary to ASTM C232 requirements, it was realized that the absence of vibration would provide a more fundamental look at the behavior and loss of post-casting bleeding

water. Disposable paper towels were immediately laid on the concrete surface after casting, and the high suction of paper towels allowed for the bled water to be trapped without carrying out cement particles. In order to prevent the absorbed bled water from evaporating during the bleeding period (of unknown duration), a lid with hardened silicon caulking on the rim was also placed immediately after the towels are laid. The bled water was thus collected in the towels every 15 or 30 minute intervals $(\Delta t)_i$, depending on the perceived bleeding rate. Having measured the dry mass of each towel previous to each measurement, the difference in towel mass after absorption is simply the amount of bled water for the specific time interval. The measurements were repeated several times until the difference in towel mass was negligible (lower than 1.0 grams). Following to the post-bleeding stage, the specimen was uncovered and the concrete was subjected to moisture loss. In order to quantify this loss, the entire specimen was measured at intervals $(\Delta t)_i$, that were progressively increasing in duration, since it is assumed that the loss rates would decrease with time as concrete hardens. Medium-high precision weight scales were used to monitor bleeding water mass quantities and changes in concrete mass. Figures 8 and 9 show the basic bleeding and moisture loss measurement setup.

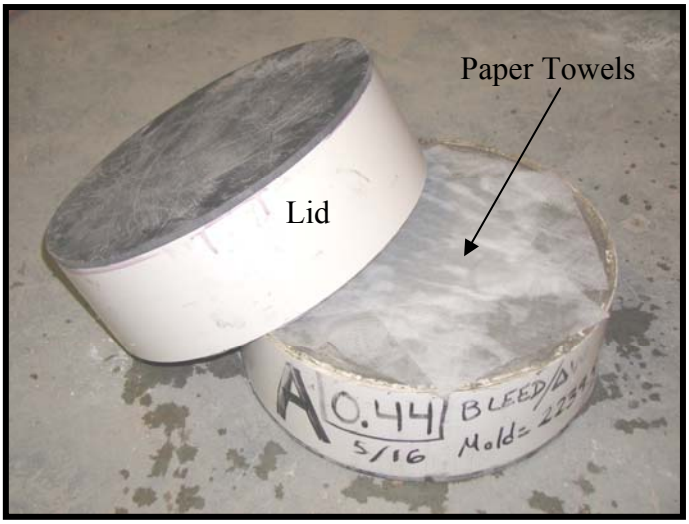

Figure 8 - Moisture Loss Measurements, Bleeding Stage

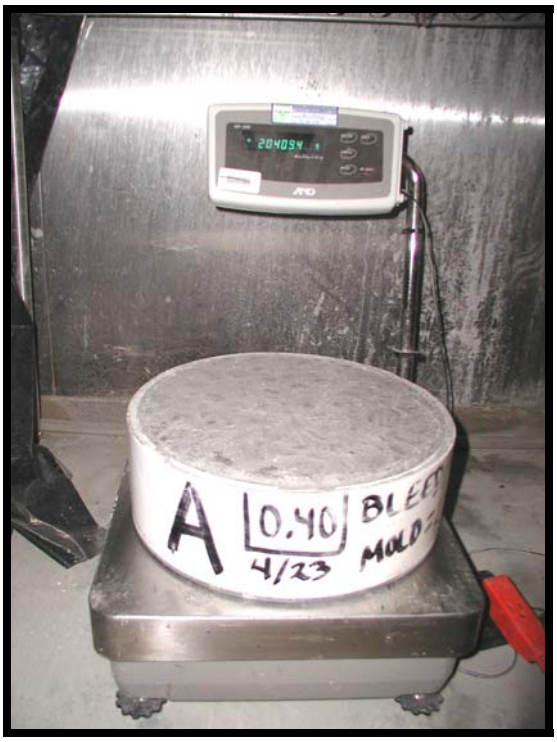

Figure 9 - Moisture Loss Measurements, Post-bleeding Stage

PERMITTIVITY MEASUREMENTS

Permittivity, as stated in Chapter II, can be very sensitive to water content, due to the high dielectric constant of water as compared to any other material at any signal frequency. The equipment used for both permittivity parameters (dielectric constant and conductivity) was the Adek™ Percometer (Figure 10), and was used only for surface measurements, as illustrated in Figure 11. In these measurements, an electric field ($\vec{E}$) is generated and received by the same device. Table 5 presents the general specifications of this equipment. During testing at each planned time for measurements, five random locations on the sample were tested and averaged, and thus one value was reported at each time.

Table 5. Adek™ Percometer Specifications

Parameter	Value
Dielectric constant measurement range	1.00 to 32.0
Electrical conductivity measurement range	0 to 9999 mS/cm
Precision	±0.1% to 1%
Operational temperature range	-40 to+80°C (-104 to 176°F)
Surface Probe size(diameter)	60 mm (2.36 in)

Figure 10 - Adek™ Percometer

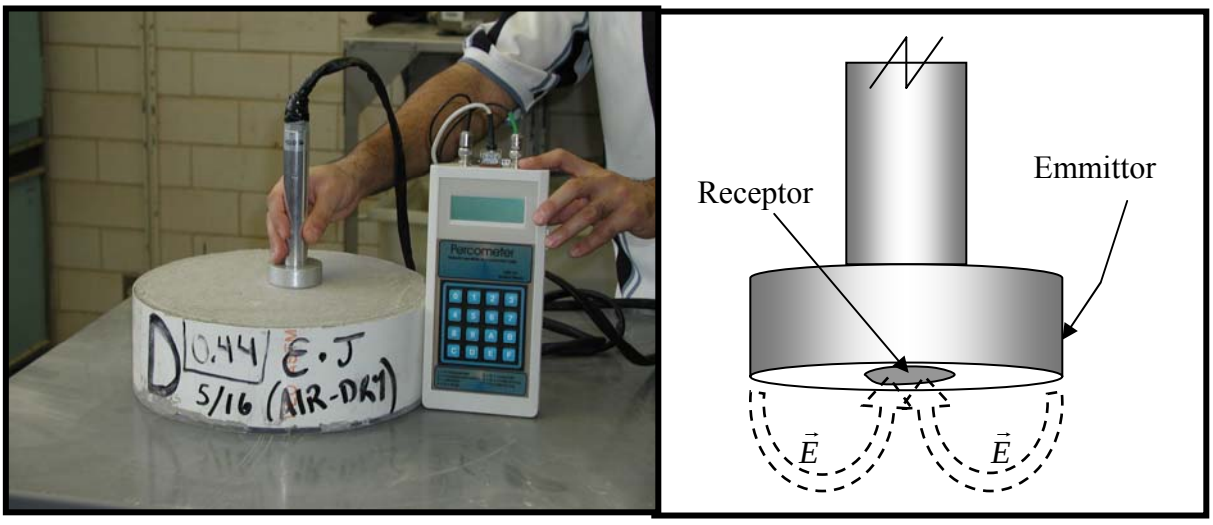

Figure 11 - Permittivity (Dielectric Constant and Conductivity) Measurement

Surface permittivity measurements may or may not be representative of the entire concrete sample volume considered in this study. Previous studies (Scullion and Saarenketo 1996) have been conducted on aggregate pavement base materials using dielectric value measurements on soil suction samples 30.5 cm (12 inches) deep. Despite electric field penetration distance of 20mm in average for soil suction samples, surface dielectric value ranges for soil-suction samples were accepted to be a good indication of the relative base material performance ranges. In the case of concrete, surface permittivity measurements will *not* be representative of the entire depth of the samples, but when it is compared against the predicted composite dielectric (CRIM) value, it is expected to identify volumetric differences between surface and inner layers.

It is believed that any systematic error that is introduced to the permittivity measurements because of unknown penetration limitations is consistent yet low compared to the random-effect variability originated by the measurement location and the amount of area of concrete exposure to the ambient conditions. To minimize the effect of systematic variability, the timing of dielectric measurements was set parallel to the moisture loss measurements and performed on the same batch in order to eliminate batch-related variability. Since moisture loss and dielectric property measurements were planned to be measured together, concrete samples were cast in the combinations shown in Figure 12.

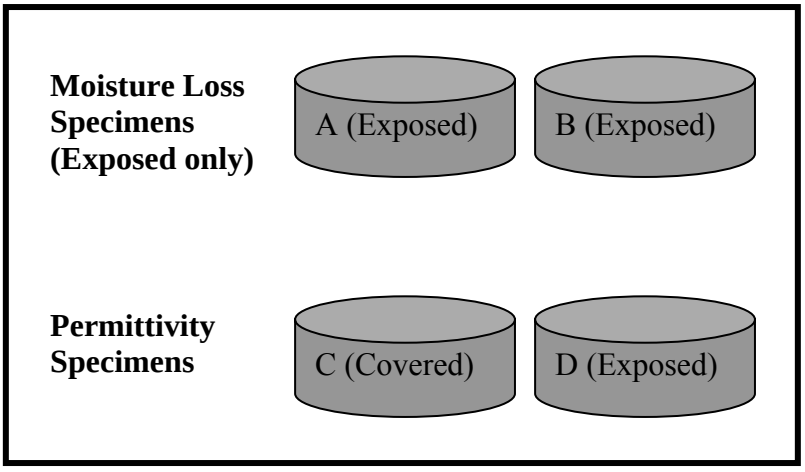

Figure 12 - Moisture Loss/Dielectric Measurements Sample Combination for One Treatment (One Water-Cement Ratio)

RELATIVE HUMIDITY MEASUREMENTS

Relative humidity as a dependent parameter on moisture content in concrete seems to provide a good indication of the self-dissecation phenomenon of cement hydration (see Chapter II). Thus, moisture availability (volumetric moisture content) may not be enough to identify how fast hydration is slowing down or coming to a stop. It is believed that as the moisture content decreases, the relative humidity inside concrete decreases, but its rate and modeling shape may not be easily identifiable for hardening concrete. The present study investigates and approximates the actual relative humidity and moisture content change as concrete hydrates that has not been considered in previous research (Parrot 1991).

Measurements of relative humidity require more advanced methods and equipment. In many instances, these methods and equipment simply require the use of a sensor probe to be embedded in the concrete sample at a desired depth, but steady-state environmental conditions were needed in order to simplify the data reduction process. Nonetheless, an A-Tek™ moisture meter with a sensor probe was used in this investigation (Figure 13)

and inserted at a depth of only 2.5 cm (about 1 inch) from the concrete surface. The size of the concrete samples was the same as for the moisture loss measurements because using the same sample type and size helps minimize unwanted variability, not to mention that moisture loss measurements are to be analyzed against humidity measurements as one of the primary concerns of the self-dissecation investigation.

Figure 13 - Concrete Relative Humidity Moisture Meter and Embedding Sensor Probe

As it will be shown in the following chapter, most of the relative humidity data obtained was strongly affected by minor changes in the tightly controlled environment. These minor changes might have been caused by sudden pressure and temperature drops (door opening/closing) or even possible voltage variation from the device. Due to these sensitivity issues, the collected information showed sudden data discontinuities. However, it was possible to identify a decreasing humidity values that were compatible with previous literature predicting trends, where it can be assumed that the initial relative humidity value of fresh concrete is between 80 and 100% (Wang 2000). Therefore, it is

reasonable to assume that the recorded humidity data can be "substituted" by using these trends in its place (Figure 14). This approach was necessary in order to eliminate known discontinuities and identify the approximated actual trends and behavior of self-dissecation.

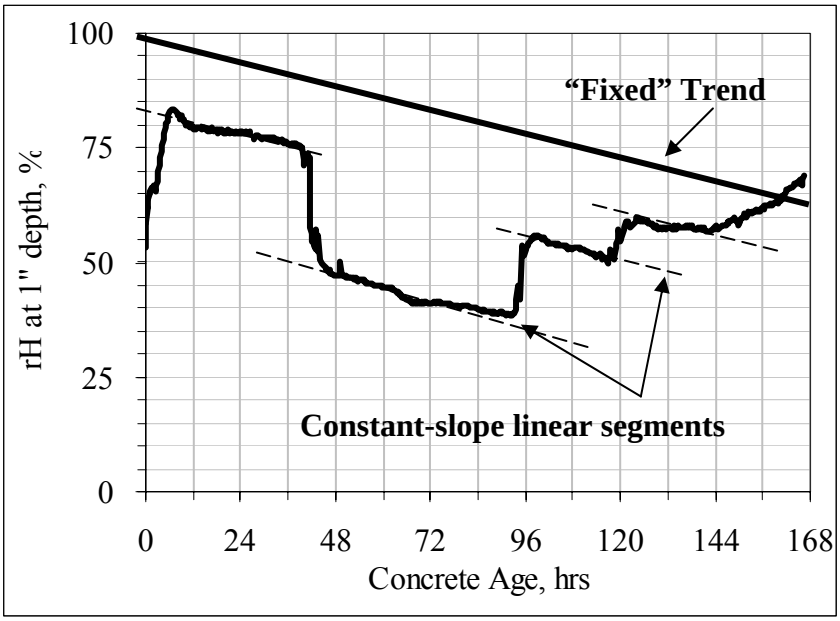

Figure 14 - Post-collection Relative Humidity Data Prediction

COMPRESSIVE STRENGTH AND HEAT EVOLUTION MEASUREMENTS

Although being the most practical performance measurement, the determination of compressive strength was only a stepping stone in this study. The compressive strength parameter can be translated to the actual degree of hydration through the use of the strength hydration model as described in Chapter III. The degree of hydration is of most interest in order to approximate the time-dependent volumetric quantities of the

unhydrated cement and the hydrated cement product (HCP), which in turn helps approximate the remaining volumetric quantities of the rest of the concrete components. Standard compressive strength samples 15.3 cm diameter by 30.5 cm high (6 inches diameter by 12 inches high) were cast according to ASTM C31, but followed the factorial design and the baseline requirements for curing in this study for the ages of 1, 3, 7, 28, 56, and 90 days. Figure 15 shows the samples made for a specific age testing of treatment 0.40, and the corresponding statistical sample sizes used for each exposure level.

Figure 15 - Compressive Strength Specimens

Adiabatic heat signature (AHS) measurements were also recorded in order to determine maximum possible degrees of hydration for each of the four treatments of the factorial design. These limiting values will in turn be an indication of the maximum amount of cement that can be hydrated and serve as a calibration factor against strength-based degree of hydration values. This calibration factor can then be used as one of the steps

performed in a proposed testing and assessment protocol. However, the AHS measurements only provide a backup check for the determination of the actual degree of hydration as determined by the exposed condition, and only if the strength-based degree of hydration definition turns out to be higher than the heat-based definition at a certain time, the application of the calibration factor would then be justified.

Given the nature of these measurements, a special sealed container (the Q-drum) is used to track the heat generation of concrete (Figure 16). This implies that the exposure level of the factorial design is not applicable to this test, and this test only responds to the different assigned factorial treatments.

Figure 16 - Q-Drum for AHS Measurements

FRESH CONCRETE GRAVIMETRIC TESTS

Porosity was defined in Chapter III as the addition of the air void content of fresh concrete and the capillary porosity resulting from moisture loss. Fresh concrete gravimetric tests (unit density tests) as described by ASTM C138 provide the first part of such information. By comparing the design, airless density to the fresh concrete density, it is possible to calculate the air content using simple calculations. Although simple in its determination, the fresh air content provides a crucial initial piece of volumetric information that is further used for the dielectric value modeling.

SETTING TIME DETERMINATION

As mentioned in Chapter II, setting represents the hydration stage in which hydrated grain particles start bonding across capillary voids. Final setting is thus believed to affect the rate of moisture loss between its bleeding and post-bleeding stage due to increasing micro-structure restrictions through which free water is not allowed to escape. However, it is important to emphasize that the time at which bleeding stops may not necessarily be the same as the setting time.

In order to measure setting time, only the mortar part of the concrete mix can be used. However, separation of mortar and coarse aggregate by sieving is a very slow procedure but yields a parameter of extreme importance in the testing methodology. To minimize delay, separate mortar mixes were prepared. By calculating the mortar proportions of each of the four concrete mixes and by correcting for absorbed or released moisture from aggregate, the resulting material resembled the actual proportions of the mortar part of the mixtures. With the use of a Penetrometer (Figure 17) on a mortar sample 15.3 cm diameter by 15.3 cm high (6 inches diameter by 6 inches high), penetration testing was conducted on only exposed specimens and according to ASTM C192, but the rest of the experimental design and baseline requirements applied.

Figure 17 - Penetrometer

CHAPTER V
RESEARCH FINDINGS

This chapter presents the summarized results of the research tasks performed according to the baseline conditions and experimental design. The summarized results on moisture loss and availability, hydration, and dielectric properties are presented first, as well as possible effects or dependence among parameters measured. Correlation analyses that were also conducted follow, and possible fundamental dielectric behavior is identified last. The full set of graphical relationships exposed in the following sections can be found in Appendices A and B.

SETTING AND DEGREE OF HYDRATION

It was observed in the results of this study that setting may play a role in the moisture loss rates, and changes to those rates may occur around the time final setting takes place. Figure 18 presents an example of the determination of the initial and final setting times for the 0.44 mix, where R_p is the penetration pressure. As previously stated in the experimental design, the initial and final penetration pressures are pre-determined according to ASTM C192. Table 6 summarizes the setting times recorded for the four treatments (water-cement ratios) values used.

It was found that the degree of hydration defined as a strength ratio was the best option to connect and relate all volumetric relationships, because it is the only conditioned parameter that best approximates the degree of hydration of the tested specimens. The reason behind choosing the strength method is also to maintain consistency in the analysis and to make all analysis compatible with the methodology and testing baseline previously discussed. Besides, this approach allows the comparison of results as affected by two different exposure levels (which can be thought of two different curing qualities, with covered samples having “better” curing quality than exposed samples), as will be shown later.

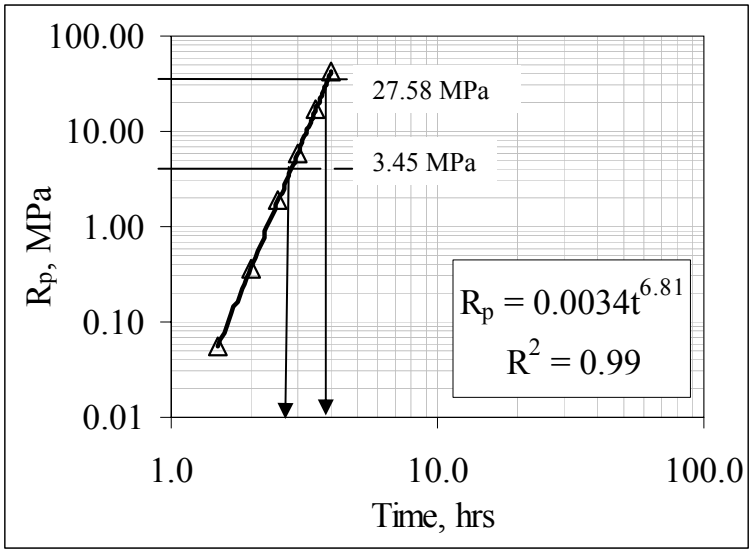

Figure 18 – Initial and Final Setting Time Determination [w_0=0.44]

Table 6. Bleeding Stop Time and Setting Times

w_0	Approximated Bleeding Stop Time (hrs)	Initial Setting time (hrs)	Final Setting Time (hrs)
0.32	No bleeding observed	0.91	2.94
0.36	0.50	1.48	3.15
0.40	1.50	2.08	3.14
0.44	2.00	2.76	3.75

In regards to the degree of hydration, it is clear that the exposure level affected the rate of hydration, as supported by theory. The effect of the exposure level is observed since the strength development in Figures A-5 and A-6 in Appendix A. Before the seventh day, the rate of hydration for the exposed level turned out to be slightly higher than for the covered level, as shown in Figure 19. After the seventh day, the exposed level seems to stabilize, whereas the covered level continues to increase. On the other hand, the hydration trend obtained from heat evolution data shows the highest rate of all, and stabilizes in a relatively shorter time, as also predicted by theory, since the conservation of heat is the most important catalyzing factor for the hydration process. This justifies the use of the strength method as the means to determine the degree of hydration, because the strength method is more realistic and conservative than the heat evolution method. The heat evolution method was therefore only used as a correction check, in case it yields lower values than the strength method.

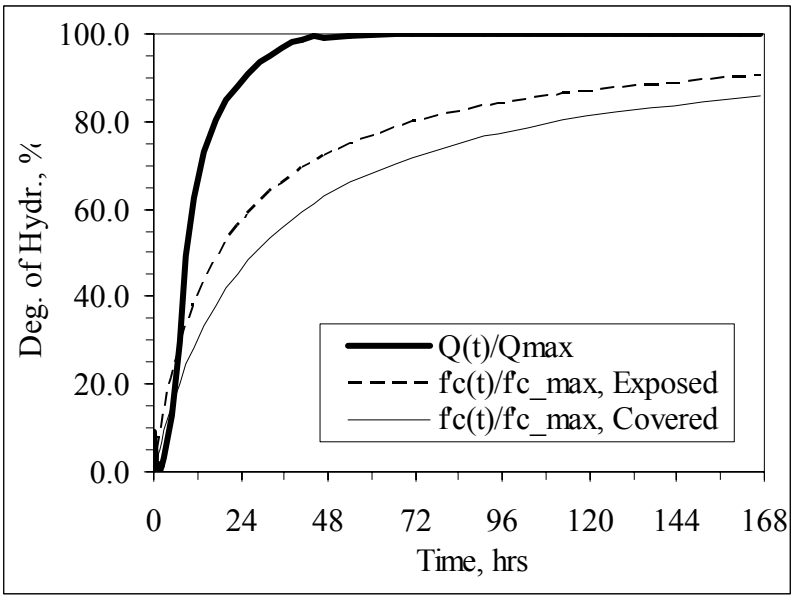

Figure 19 – Degree of Hydration According to Model Chosen and Exposure Level [w_0=0.44]

There was a very strong and clear relationship between the degree of hydration values at the exposed level, and the values at the covered level. As it can be seen in Figure 20, there exists a clear polynomial trend of the mathematical form shown below, with all trends showing a coefficient of determination (R^2) higher than 0.999, which indicates high level of fit:

$$\alpha(t)\_Cov = a\left(\alpha(t)\_Exp - b\right)^2 + c^2 \tag{49}$$

where:

$\alpha(t)\_Cov$	=	Time-dependent degree of hydration at the covered level, %
$\alpha(t)\_Exp$	=	Time-dependent degree of hydration at the exposed level, %
a, b, c	=	Regression coefficients (2^{nd} degree polynomial)

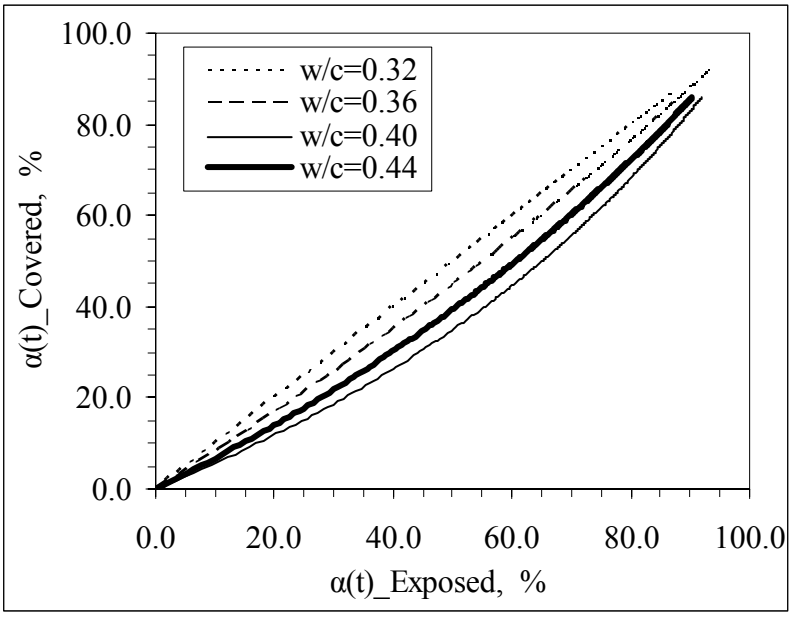

Figure 20 – Effect of Exposure Level on Degree of Hydration

MOISTURE LOSS AND AVAILABILITY

The moisture loss behavior was thought to exhibit a very simple trend, in which moisture loss rates were expected to be very high soon after casting, and to slow down smoothly after a few hours as concrete hardens. Experimental results supported those expectations and provided further detail into the pre-setting moisture loss behavior. Figures 21 and 22 show the actual moisture loss recorded in terms of area and as a fraction of net water, respectively, both forms required by ASTM C232. These trends reinforce the expectations and observations made during testing, but also introduce a new one. It was noticed that within the laboratory testing baseline conditions described previously, there is a limit on the value of water-cement ratio (w_0) for which a maximum loss history can occur. That is, the moisture loss curves show an increasing vertical "shift factor" as w_0 increases, except for the last w_0 value (0.44). This might be due to the relatively larger amount of net water that is initially available in the w_0=0.44 mixture which in comparison to the lower net water amounts on the other mixes, cannot be as quickly exhausted in the same timeframe.

A closer look made to the moisture loss results shows that bleeding loss rates and final setting times may affect the early loss history, as shown in detail in Figure 23. It was observed during laboratory testing that the early bleeding rates follow an approximately linear trend, but only applicable for the lowest w_0 values. In the case of higher w_0 values, the moisture loss results diverge a bit from linearity for the same timeframe. That is, an actual early acceleration in the moisture loss rates was observed during the bleeding stage.

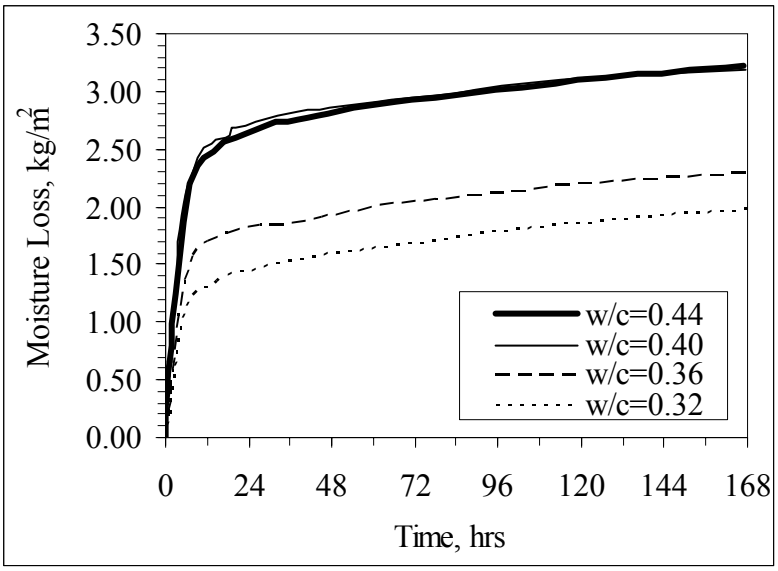

Figure 21 – Moisture Loss per Area

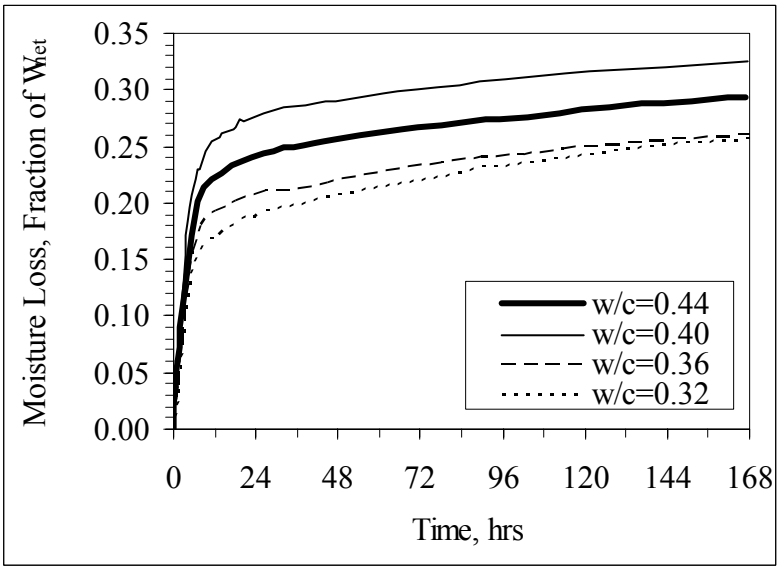

Figure 22 – Moisture Loss per Unit Mass of Net Water

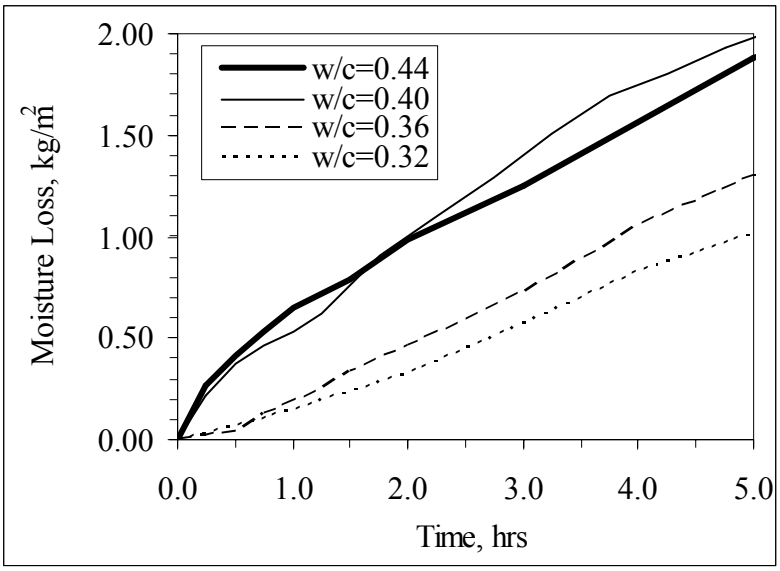

Figure 23 – Early Moisture Loss Detail

Figure 24 shows the relative position of the bleeding "exhaustion" limits on the total moisture loss history. These limits show a limited effect on the rate of change of moisture loss for the post-bleeding stage. It is more likely, however, that rate changes in moisture loss were actually caused by developing changes in microstructure due to setting. In fact, the final setting time (t_{set}) in particular seemed to have dictated the location of the inflection point on the moisture loss rate history as shown also in Figure 24, and this inflection point is obvious only through the use of a logarithmic scale for time. The bleeding stop times preceded both initial and final setting times, as listed previously in Table 6.

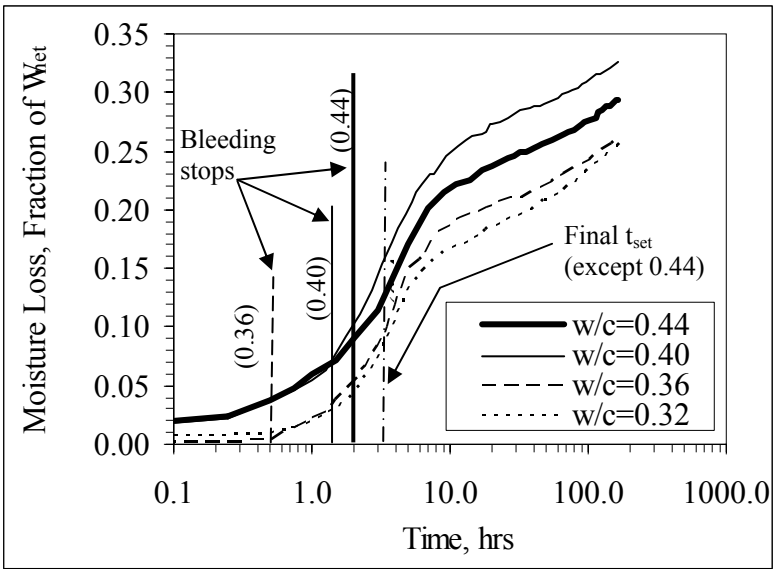

Figure 24 – Detail of Total Moisture Loss History

The careful quantification of lost free (capillary) moisture (w_{free_lost}) proved to have constituted the most important measurement of this study. Following these measurements, a very clear idea of the remaining portion of the initial net water can be approximated, as seen in Figure 25. This remaining moisture portion, according to the adopted volumetric model, can be broken into two smaller parts: the free moisture mass still available in capillaries (w_{free}), and the non-evaporable moisture mass used in the hydration process (w_n), which includes both the chemically-bound and physically-bound portions. However, at humidity levels below 40 percent (encountered only in oven-drying conditions) the physically bound portion would need to be added to the evaporable portion.

Under the mass conservation principle, all quantities must be accounted for until they add up to the initial net water value. It is impossible, however, to determine either free or non-evaporable portions without the use of an initial guess for the ultimate non-evaporable moisture ($\hat{w}_n$). As an initial guess, a value of 0.23 for the factor f_n was used

to approximate the $\hat{w}_n$ proportion. By using Equations 38 and 39 in Chapter III for $\hat{w}_n$ and the degree of hydration based on $\hat{w}_n$, the factor f_n value was iterated until the non-evaporable content converges with the total moisture content around the projected time of 100% hydration. By applying the volumetric model relationships to the testing results on moisture availability and loss, the remaining free moisture can be accounted for and quantified simply by subtracting the lost and non-evaporable moisture from the net (initial) water content. The main assumption of this approach is that hydration will advance by entirely consuming the available capillary moisture portion. Table 7 and Figures 25 and 26 summarize the moisture proportionality characteristics for the four different treatments at the end of the exposure time.

Table 7. Moisture Fractioning at 7th Day of Exposure

		Non-evaporable moisture		
Treatment (w_0)	Lost moisture mass fraction	Mass fraction	f_n factor used (from Equation. 38)	Free (capillary) moisture mass fraction
0.32	0.257	0.682	0.25	0.062
0.36	0.260	0.673	0.26	0.067
0.40	0.325	0.598	0.31	0.077
0.44	0.293	0.636	0.31	0.071

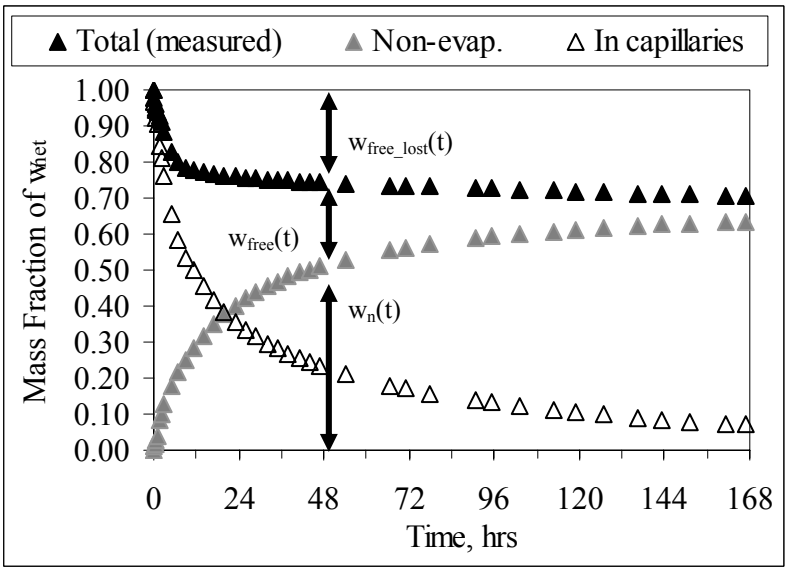

Figure 25 – Approximated Actual Moisture Mass Proportion and History [w_0=0.44]

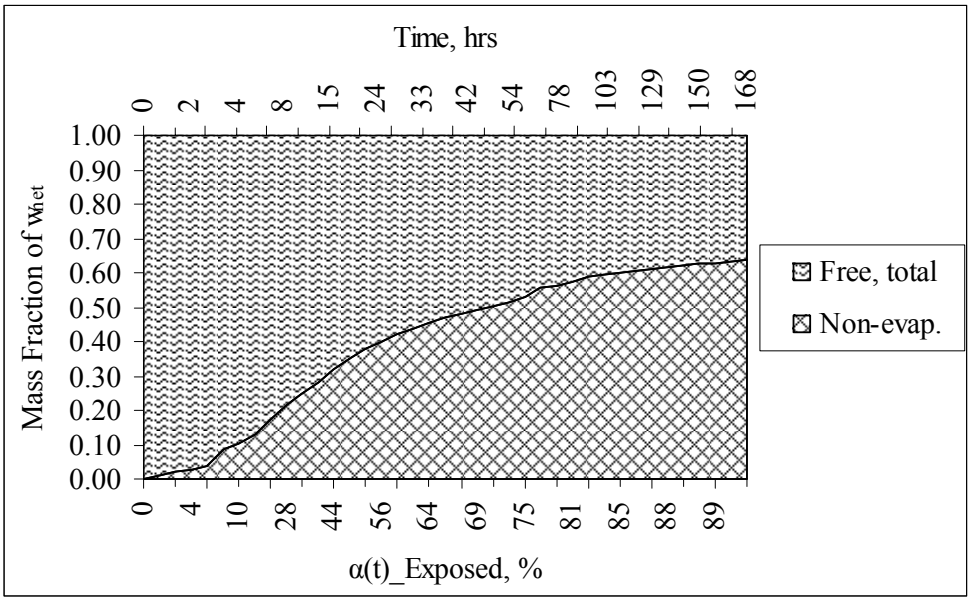

Figure 26 – Hypothetical Moisture Mass Proportion and History for Zero Moisture Loss [w_0=0.44]

VOLUMETRIC APPROXIMATIONS

Following the determination of moisture loss, non-evaporable moisture, and the approximation of the degree of hydration, the volumetric equations derived in Chapter III were applied in order to approximate the proportions of each of the five concrete components. The approximated relative volumetric percentages can then be presented as a volumetric phase diagram and inspected.

Shrinkage was not considered in the volumetric approximations. Shrinkage is most likely to raise the porosity proportion, but its contribution determination is not the scope of this study. Although the volumetric contribution from shrinkage may still be approximated by other means, porosity carries the lowest dielectric value as it is used in the prediction of the composite dielectric value. The relatively small contribution of shrinkage to porosity and the low dielectric value of porosity itself allows the composite dielectric value model to closely approximate the resulting volumetric porosity regardless of its origin or how many factors contributed to its change.

Volumetric free moisture and air (porosity) content is initially dependent on the treatment only, and can change its value dramatically with time due to moisture loss (in the case of exposed concrete) and hydration. The free (capillary) moisture proportion is quickly reduced by hydration or loss, or both, as shown in Figure 27. The approximated volumetric content of HCP was kept at a conservative rate of change by using a volume expansion factor (f_v) value of 1.1 for all treatments. HCP is shown to quickly develop and occupy a larger volume fraction as hydration advances, as literature suggests (Powers 1947). Although the actual volume fraction of HCP cannot be precisely measured, its approximated value will suffice for its use in the proposed dielectric value model.

In the case of covered concrete as shown in Figure 28, the volumetric free moisture and air (porosity) are assumed to change only due to hydration, not to moisture loss, for the covered specimens are assumed to loose no moisture. The volumetric expansion proportion of HCP is kept at the same value as for the exposed level (f_v=1.1) because the same cement type is used, but it shows a slower growth rate due to the slower degree of hydration rate.

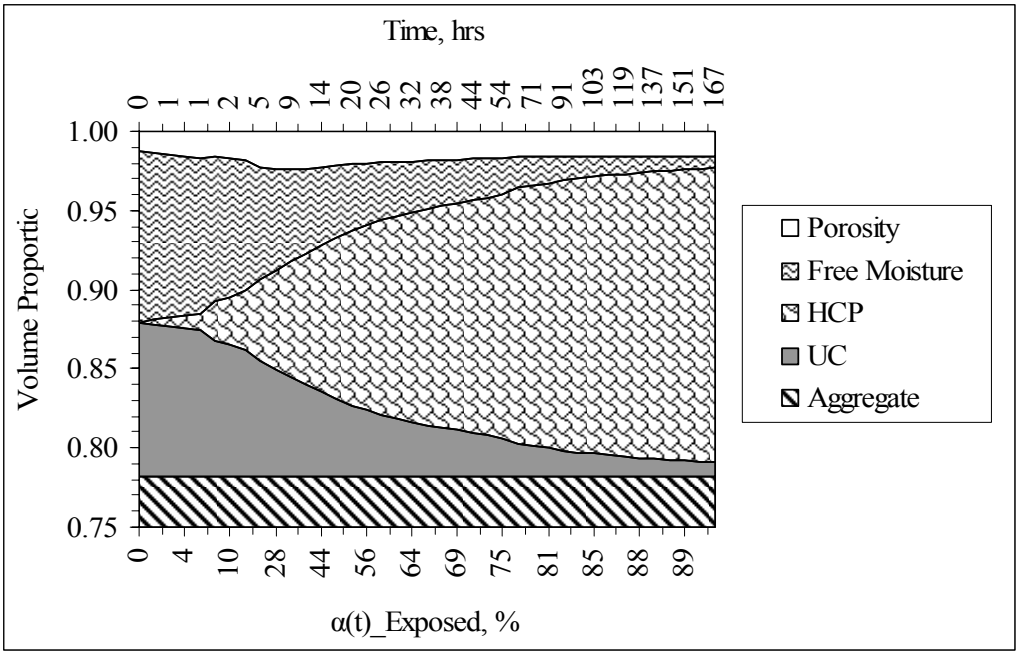

Figure 27 – Approximated Volumetric Proportions for Exposed Level [w_0=0.44]

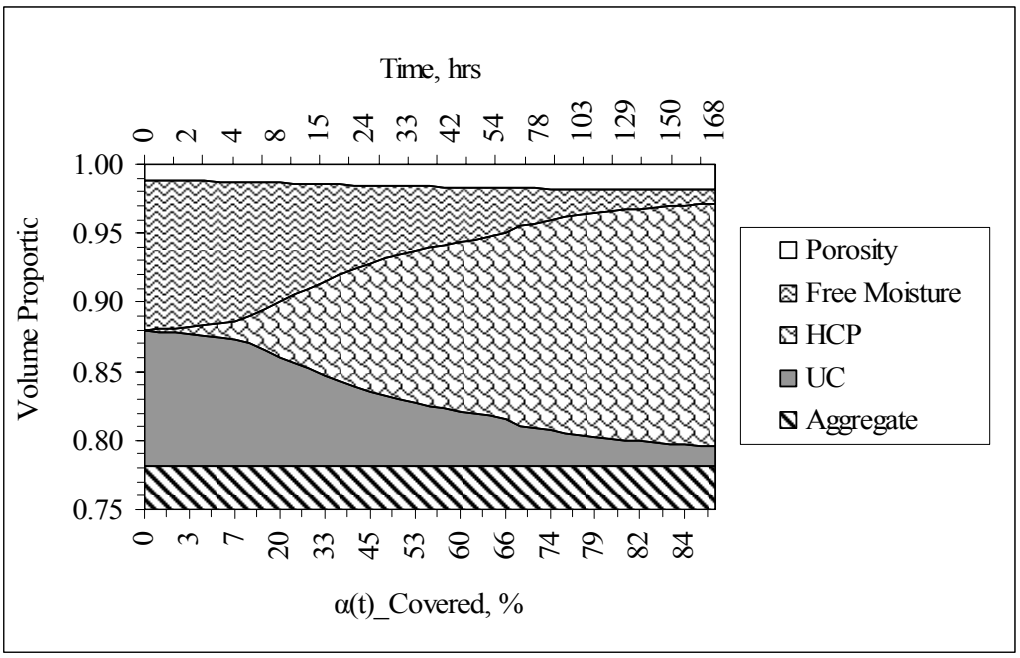

Figure 28 – Approximated Volumetric Proportions for Covered Level [w_0=0.44]

PERMITTIVITY PARAMETER BEHAVIOR

Previous to the measurements of both dielectric constant and conductivity, it was assumed that these two permittivity parameters would decrease smoothly with time as concrete hardened and as moisture is lost. However, during measurements of these parameters, smooth changes appeared to be the exception, not the rule, for dramatic changes in dielectric constant values and severely dramatic changes in conductivity were consistently observed at all ages. In fact, dielectric constant measurements could only be used partially in the subsequent analysis, and it was necessary to discard all conductivity measurements due to unreasonably variable values before setting time, soon after which the conductivity drops to zero and does not change afterwards. It is then emphasized that only dielectric constant measurements were considered in the in-depth analysis. Figure 29 illustrates the dielectric constant history for the w/cm=0.44 treatment.

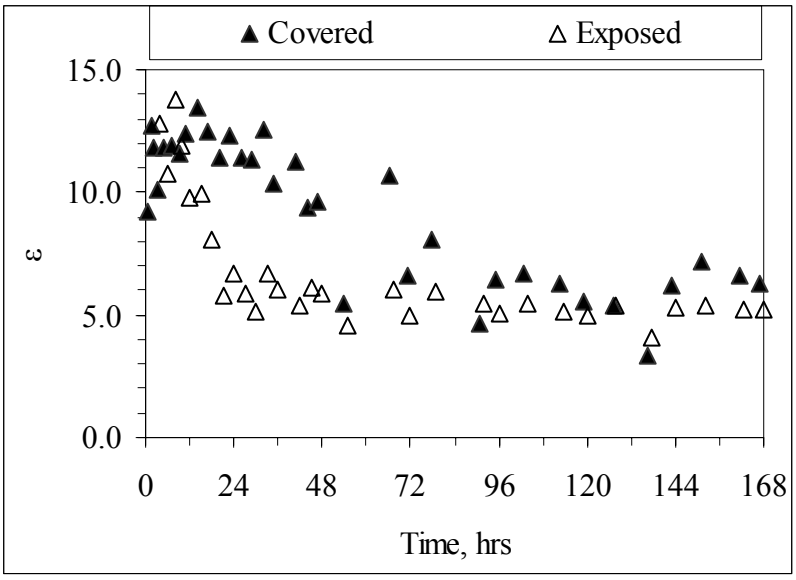

Figure 29 – Recorded History for Dielectric Constant [w_0=0.44]

The cause of the measurement variations may be due to several issues that were encountered during testing. The first source had to do with the randomization of the point measurement locations. As previously explained in Chapter IV, five point measurements were conducted at random locations on the surface of the specimens for each age. It is very likely that the variability in these measurements was mainly originated due to the discrete distribution of the aggregate, in which its large size of 38 mm (1.5 in) is also a main factor, because the surface probe is only 60 mm (2.4 in) in diameter. This implies that there will be some random cases in which the probe might be placed precisely over a relatively large aggregate grain, and this would certainly cause a biased permittivity measurement, because the volumetric distribution (and hence the dielectric value) of the tested point is highly influenced by the solid aggregate material.

The second source for the observed variability comprises several issues that arose during the early stages of hydration (up to the final setting time). Concrete that had not reached the final setting point tended to be too moist on the surface due to bleeding flow. High concentration of moisture on the concrete surface can force permittivity parameter values to fall outside of the probe's measuring range. These excess surface moisture effects were detected in the data trends, where large data clutters cause unreasonably high variability. Therefore, dielectric values previous to setting time were not considered in the analysis.

In spite of the high variability of the dielectric constant measurements, a certain degree of sensitivity to the exposure level was identified. Exposed samples tended to yield lower dielectric values than covered samples, and this trend can also be seen in Figure 29. This is due to the fact that covered samples (under "better" curing) can retain higher proportions of moisture for longer periods of time, and higher proportions of moisture imply higher dielectric constant values. The practical meaning of such behavior is that dielectric measurements may be able to discern two different levels of curing quality as long as they are performed *within the same concrete batch*. The statistical significance of these measured differences by means of a paired t-test is presented in Table 8 that shows significant differences for all treatments, except for the 0.40 treatment, in which each exposure test was batched separately. It is important to recognize, however, that it might be possible to encounter either discernible or indiscernible differences for any treatment replicate.

Table 8. Significance of the Difference in Dielectric Constant Measurements Between Exposure Levels

Treatment (w_0)	Statistical difference in dielectric constant (by Paired t-test)
0.32	Significant
0.36	Significant
0.40	Not significant (different batches)
0.44	Significant

EFFECTS OF RELATIVE HUMIDITY ON DIELECTRIC VALUE

As the moisture content in concrete decreases with time, the relative humidity can be expected to decrease. Previous research on moisture content–humidity measurements (Parrot 1992) was conducted on long-time water-cured concrete through oven drying and showed that moisture content (as a mass ratio of free moisture to cement) in hardened samples decreases rapidly, stabilizes, and drops to zero during a long timeframe. Oven drying in that study is able to control the amount of moisture present, facilitated by the fact that fully-hardened concrete has a constant porosity, microstructure and permeability characteristics. A study of that sort, therefore, refers more to sorption, desorption, and suction characteristics than moisture availability, where concrete serves the function of a dry sponge. Furthermore, the results of that literature example do not necessarily apply to hardening concrete as analyzed in this study. In this study and in hardening concrete, moisture availability was not controlled and is highly dependent on the ongoing hydration and microstructure change. It is also important to recognize that moisture content measurements can be much higher for hardening concrete than for fully-hardened concrete, given the fact that higher capillary volume fractions would be available in early-age concrete development stages.

It is possible, however, to track the history of relative humidity against the available moisture content as an indicator of self-dissecation. In actual observations, it is very likely that a sudden drop in the relative humidity within a very narrow range of moisture content might indicate that the moisture layers in the capillary pores have "thinned out" when the humidity approaches 80 percent, enough to be interpreted as the beginning of the self-dissecation process as proposed in literature, and Figure 30 may be a representative example of such behavior. These results indicate that under natural conditions, the moisture content cannot drop lower than a certain value after the relative humidity stabilizes at a certain level. Only oven-drying can take these relative humidity measurements over to lower humidity values, but this condition is unlikely to happen in common concrete construction, not even in the severe environmental conditions applied in this study. It is also important to notice that the stabilization of both free water content and relative humidity indicate cessation of vapor pressure change, a potential detection threshold for the beginning of self-dissecation (Powers 1947).

It was also possible to correlate dielectric properties to the relative humidity history. In such relationship, there are two limits: 100% for relative humidity, and the final dielectric value of the composite material (Figure 31). These two graphical limits are most likely asymptotic for practical purposes, so an asymptotic mathematical model can be fitted to the data with relatively small errors. This prediction model can be presented in the form:

$$\varepsilon = \varepsilon_{\infty} + \frac{a}{(100 - H)^{b}} \tag{50}$$

where:

ε	=	Dielectric constant of concrete at any time
ε_{∞}	=	Assumed or predicted final dielectric constant value
H	=	Predicted relative humidity of concrete, %
a	=	Regression coefficient (proportionality factor), %
b		Regression coefficient

To test the adequacy of this model, a statistical analysis of variance (ANOVA) was performed to test for the significance of regression between the asymptotic model and the predicted relative humidity. The test for significance of linear regression requires the use of the F-test with the f-statistic in the form $f_{\alpha,1,n-2}$, for which (1-α)% is confidence interval, and the null hypothesis is $H_0:\beta_1=0$, where β_1 is the linear coefficient of the regressor term (Çengel and Turner 2001). The statistical p-value is the smallest α at which the null hypothesis can be rejected. For all treatments, the p-value was practically zero, which implies that there is good confidence in the potential for the use of this model as a prediction tool for the surface relative humidity.

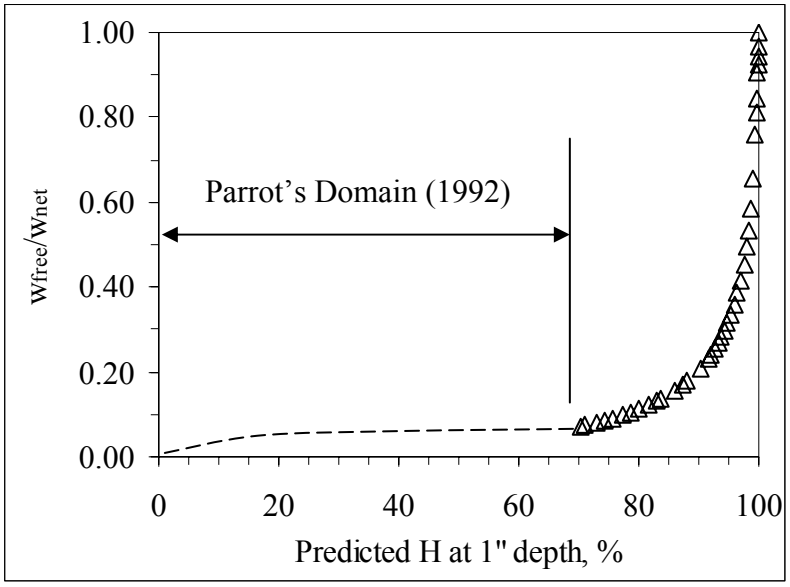

Figure 30 – Actual Free Moisture Mass Fraction for Relative Humidity Values [w_0=0.44]

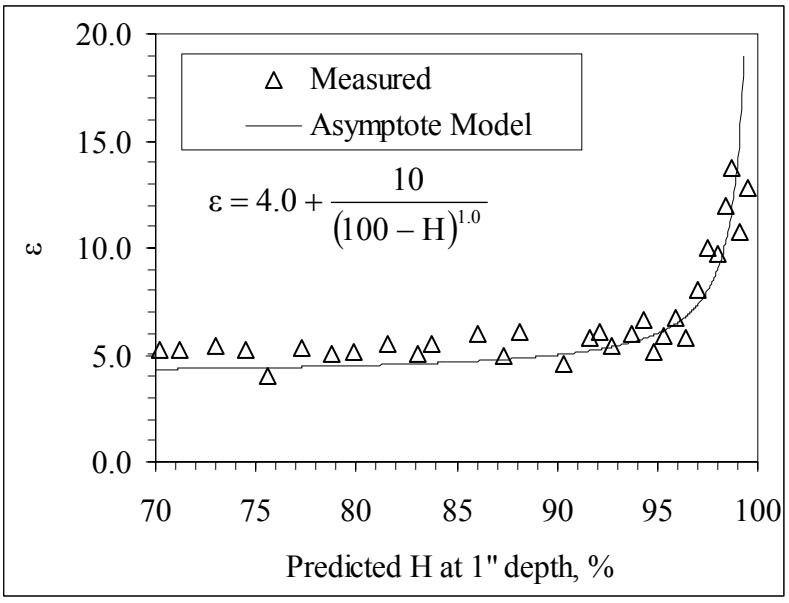

Figure 31 – Actual Dielectric Constant for Predicted Relative Humidity Values [w_0=0.44]

EFFECTS OF HYDRATION ON VOLUMETRIC FREE MOISTURE CONTENT

Theory suggests a direct link between the degree of hydration and the increasing amount of non-evaporable water, which can be predicted through the use of any of the volumetric relationships. As hydration advances, the non-evaporable moisture content should increase with a corresponding decrease in the free (capillary) moisture (Breugel 1991). The volumetric free moisture content is therefore partially but directly affected by the degree of hydration.

Data obtained from the exposed condition shows a semi-linearly decreasing trend as shown in Figure 32. This trend can be approximated by a standard linear model of the form:

$$y = mx + b \tag{51}$$

Based on Figure 33, the parameters of this linear model are described by:

$$\theta_w = m\alpha(t) + f\theta_{Wnet} \tag{52}$$

or in its most useful form by:

$$\theta_w = f\left[\frac{(w_0)(CF)}{\rho_w}\right]\left[1 - \frac{\alpha(t)}{\alpha_\infty}\right] \tag{53}$$

where:

θ_w	=	Volumetric free moisture content
f	=	Moisture loss factor, mass ratio of ultimate non-evaporable moisture to net water
w_0	=	Design water cement ratio
CF	=	Design cement factor, kg/m^3
ρ_w	=	Mean density of free (capillary) water, kg/m^3
$\alpha(t)$	=	Time-dependent degree of hydration
α_∞	=	Ultimate degree of hydration

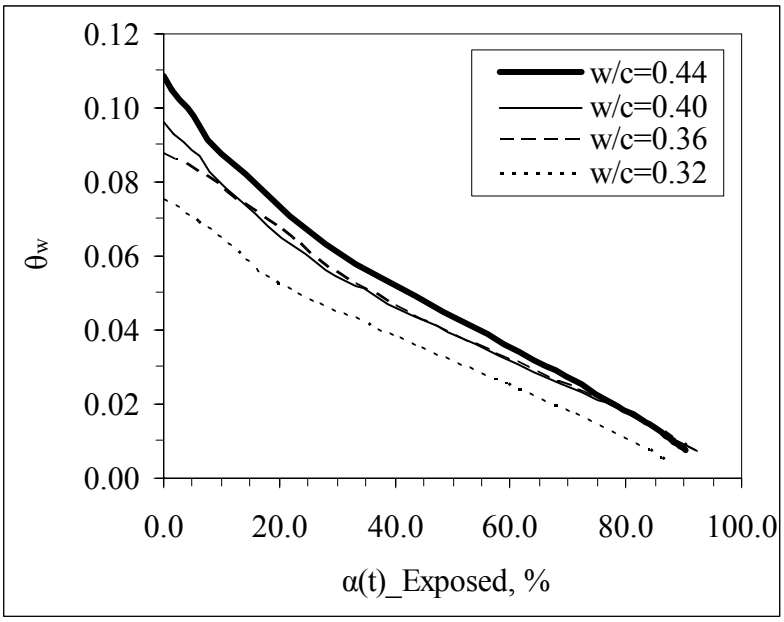

Figure 32 – Dependence of Volumetric Content of Free Moisture on Hydration (Exposed) [All Treatments]

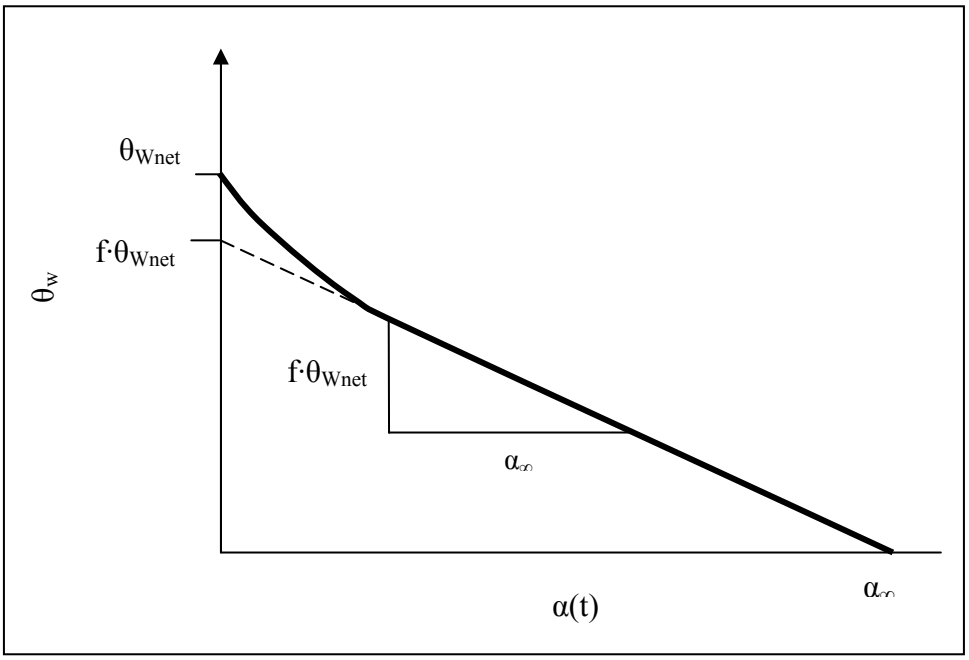

Figure 33 – Conceptual Volumetric Free Moisture Content Model

Conversely, the covered condition shows the free moisture content to exhibit an almost perfectly linear relationship, as shown in Figure 34. This was mainly due to the initial assumption of zero moisture loss, and the linear relationships that can be derived from the volumetric model equations. However, this level of linearity was not completely expected, for the degree of hydration cannot be controlled by the volumetric equations (it is derived from the linearized compressive strength regression, as shown in the methodology). The standard linear model for exposed condition seems to apply to the covered level condition as well, with the moisture loss factor (f) at a value of 1.0.

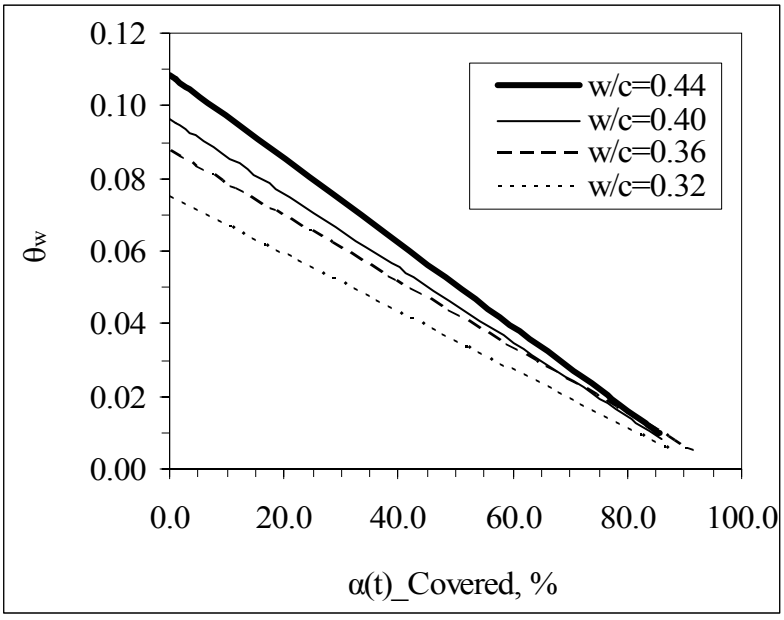

Figure 34 – Dependence of Volumetric Content of Free Moisture on Hydration (Covered) [All Treatments]

Therefore, the free moisture content model seems to depend primarily on three parameters: mixture design, rate of hydration, and curing quality. The portion of the net water used for hydration after accounting for any loss may be guessed, or precisely determined only from mass measurements and calibrated through the iteration of the non-evaporable mass factor f_n, the latter method being identical to the procedures followed in this study.

EFFECTS OF HYDRATION ON DIELECTRIC CONSTANT

The dielectric constant decreased as hydration advances. However, the shapes of the trends were neither predictable, nor their cause easily identifiable. Besides, curing quality (exposure level) also seems to influence the results.

In the exposed condition, concrete with the highest treatments (0.44 and 0.40) showed trends that decreased smoothly toward a final dielectric value. On the other hand, the lower treatments (0.36 and 0.32) on the exposed conditions show a more abrupt change in the behavior, where an apparent bilinear trend exists, although this was later found to be not true. In those lower treatments, the dielectric constant seems to abruptly stabilize close to the final (moisture-less) dielectric value (Figure 35). This is the first indication of the occurrence of two phenomena in concrete: 1) surface self-dissecation, and 2) the surface top layer actually had higher moisture contents than the average specimen during the first 24 or 36 hours, which would undoubtedly raise the dielectric value of that top layer, as will be confirmed later.

Conversely, in relatively well-sealed and covered environments, the relationship between the dielectric constant and the degree of hydration show slightly different trends. Affected by the degree of hydration measured by covered strength samples, the dielectric properties exhibit an almost linear relationship for the lowest treatments (0.32 and 0.36), where the final concrete dielectric value is the value of the linear trend at the ultimate degree of hydration for a particular treatment. On the other hand, this linear

trend seems to "buckle" upward for the highest treatments (0.40 and 0.40) as seen in Figure 36, which indicates that better curing maintains higher levels of moisture, which also in turn maintains high dielectric readings. These observations confirm with the observations made earlier for the detection of the differences in curing quality through dielectric readings. Refer to Figures B-9 to B-16 in Appendix B for the actual data plots of both exposure levels.

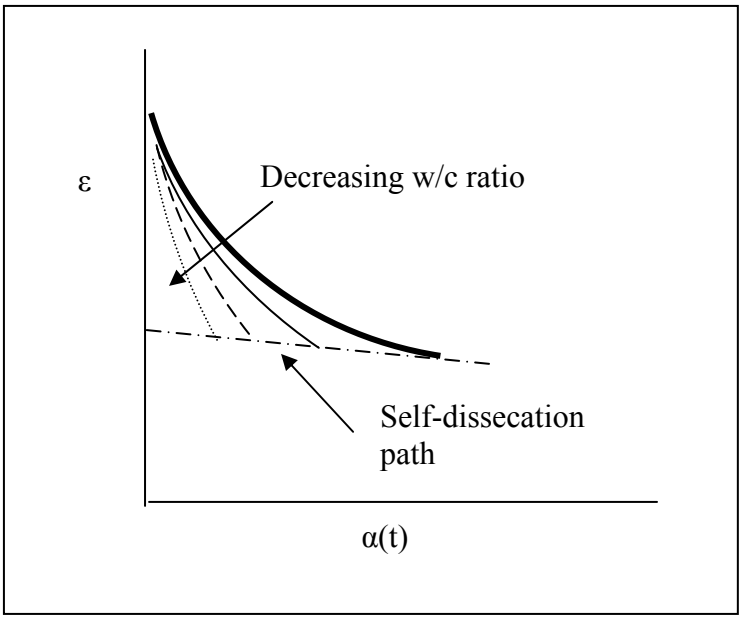

Figure 35 – Conceptual Dependence of Dielectric Value on Hydration (Exposed)

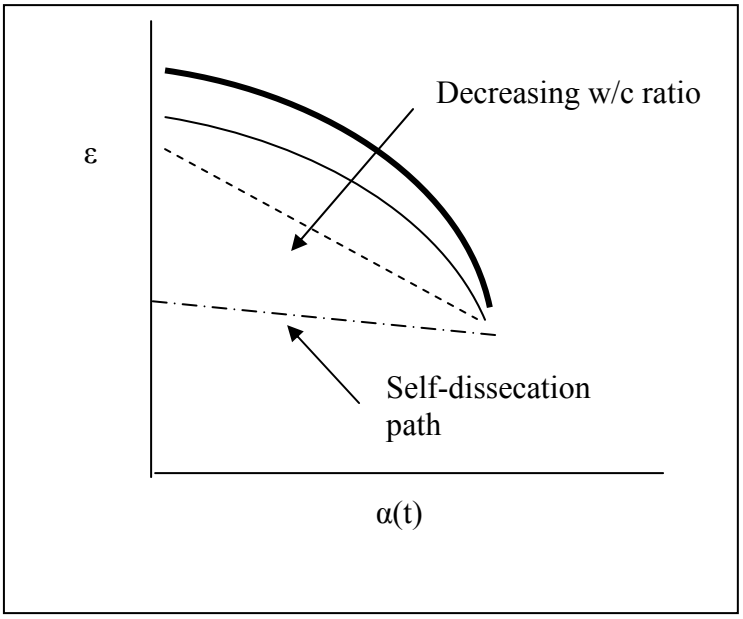

Figure 36 – Conceptual Dependence of Dielectric Value on Hydration (Covered)

EFFECTS OF VOLUMETRIC FREE MOISTURE CONTENT

The dielectric value of a composite material like concrete can be a combination of the individual dielectric value contributions from each of the components. It is this basic idea that suggests that the composite dielectric value of concrete can be approximated if the detailed volumetric proportions of the mix are known, or vice versa. In this study as in theory, it has been implied that the volumetric content of free moisture controls the dielectric value of the composite concrete material, for free moisture has the highest dielectric value of all of the other components. This implies that any drastic changes in moisture content should reflect drastic changes in the measured dielectric value of concrete.

The changes in dielectric constant as a function of the volumetric free moisture content were compared against the complex refractive index model (CRIM). By simply plotting the measured dielectric and CRIM values against the moisture content as shown in Figures 37 and 38, the CRIM seems to fail to properly predict higher values at earlier concrete ages. In the case of exposed concrete, the loss of excess moisture causes the dielectric value to follow a relatively smooth and decreasing trend toward a final dielectric value for the highest treatments (0.44 and 0.40), contrary to the broken pattern seen in the lowest treatments (0.36 and 0.32). In the case of covered concrete, no trends seem broken, but all measured dielectric values stay higher than the CRIM values for the majority of the testing. These trends can be seen in Figures B-17 through B-24 in Appendix B.

The explanation to such trends was not immediately obvious. It should be recalled that the CRIM value is based on the average-depth volumetric proportions, and that the CRIM closely approximates the measured surface dielectric value *only after the surface layer of the concrete has begun to self-dissecate*, because in practical terms, a self-dissecated concrete does not change volumetrically. Besides, the surface layer contains higher moisture contents than the average depth during the first 24 or 36 hours, which might help further explain the higher dielectric readings. In other words, this misfit is due to the presence of excess moisture contents at the surface, which causes the measured dielectric readings to rise, whereas the CRIM values remain dependent on the calculated average moisture contents for the entire depth of the samples. The general trends that show in Figures B-17 through B-24 in Appendix B are summarized in Figures 39 and 40.

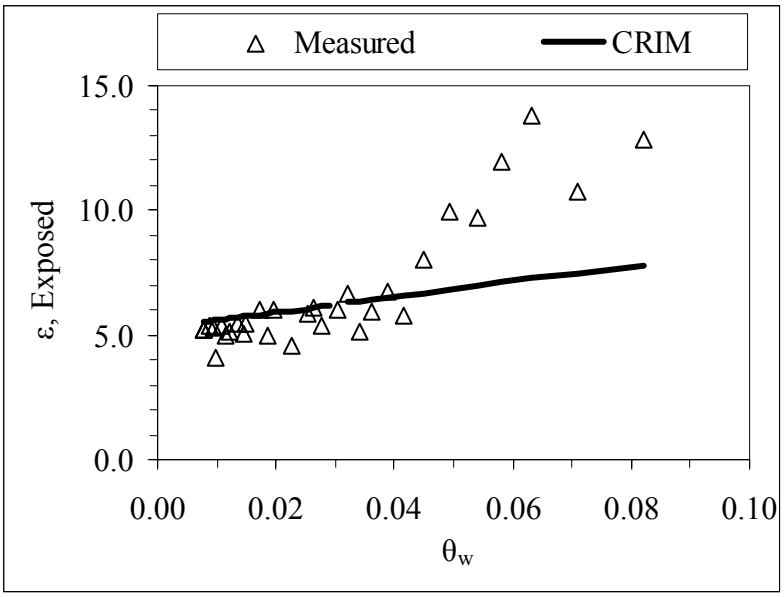

Figure 37 – Dependence of Dielectric Value on Free Moisture Content [w_0=0.44] (Exposed)

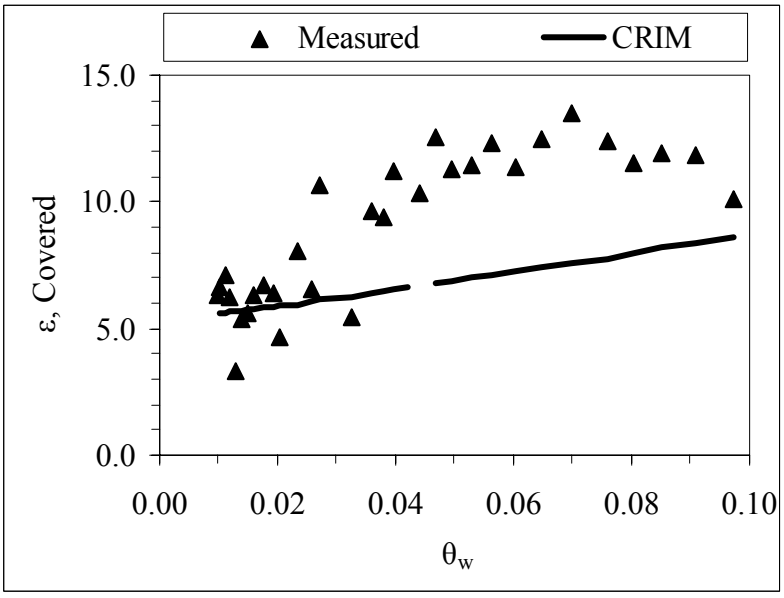

Figure 38 – Dependence of Dielectric Value on Free Moisture Content [w_0=0.44] (Covered)

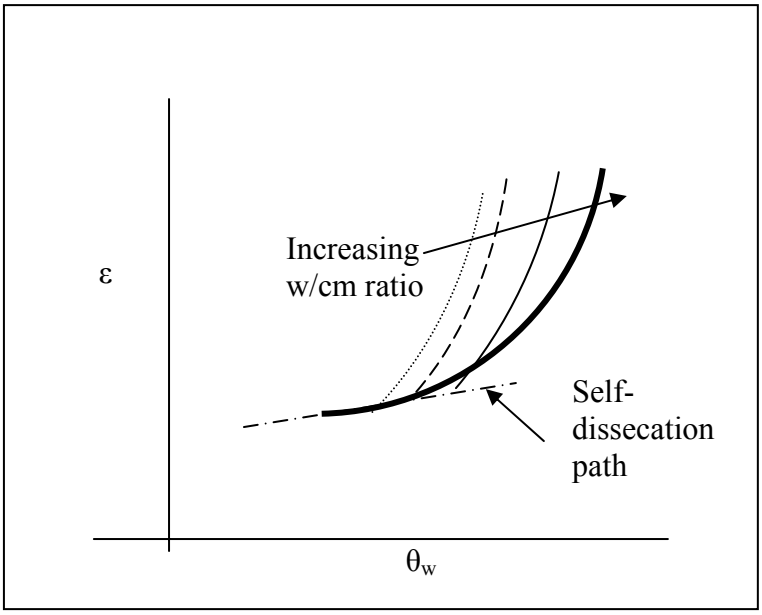

Figure 39 – Conceptual Dependence of Dielectric Value on Volumetric Content of Free (Capillary) Moisture (Exposed)

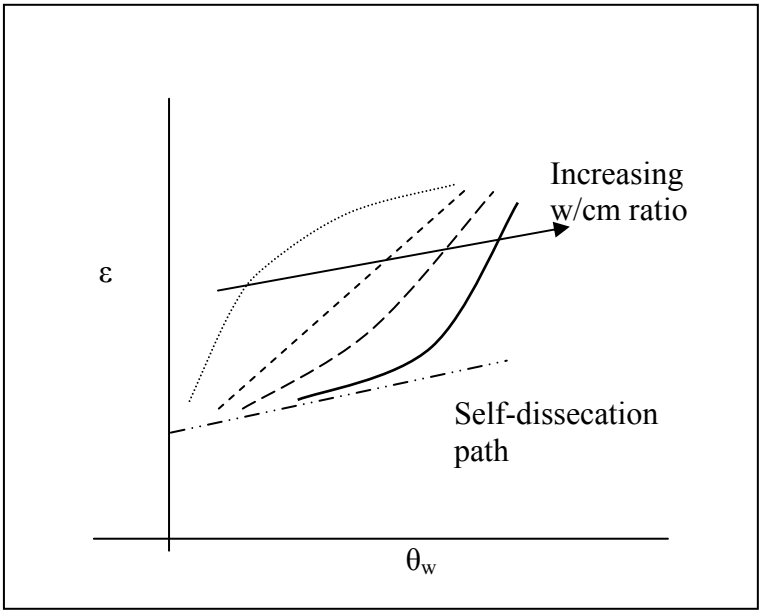

Figure 40 – Conceptual Dependence of Dielectric Value on Volumetric Content of Free (Capillary) Moisture (Covered)

The difference between the model and the actual measurements due to excess surface moisture can provide clues for the actual volumetric quantities of moisture and porosity. The difference between the measured and the predicted CRIM value can be expressed in the form:

$$\Delta\varepsilon^{0.5} = \varepsilon^{0.5} - \varepsilon_{CRIM}{}^{0.5} \tag{54}$$

where:

$\Delta\varepsilon^{0.5}$ = Powered difference between measured and predicted dielectric value of concrete

$\varepsilon^{0.5}$ = Powered measured dielectric value of concrete

$\varepsilon_{CRIM}{}^{0.5}$ = Powered CRIM approximation

The difference then becomes:

$$\begin{aligned}\Delta\varepsilon^{0.5} = &\left(\theta'_p\,\varepsilon_p^{0.5} + \theta'_w\,\varepsilon_w^{0.5} + \theta_{HCP}\varepsilon_{HCP}^{0.5} + \theta_c\varepsilon_c^{0.5} + \theta_s\varepsilon_s^{0.5}\right)\\ &-\left(\theta_p\varepsilon_p^{0.5} + \theta_w\varepsilon_w^{0.5} + \theta_{HCP}\varepsilon_{HCP}^{0.5} + \theta_c\varepsilon_c^{0.5} + \theta_s\varepsilon_s^{0.5}\right)\end{aligned} \tag{55}$$

If it is assumed that the volumetric proportions of aggregate and hydrated cement products should be the same whether predicted or measured, then the difference simplifies to:

$$\Delta\varepsilon^{0.5} = \left(\theta'_p\,\varepsilon_p^{0.5} + \theta'_w\,\varepsilon_w^{0.5}\right) - \left(\theta_p\varepsilon_p^{0.5} + \theta_w\varepsilon_w^{0.5}\right) \tag{56}$$

or,

$$\Delta\varepsilon^{0.5} = \varepsilon_p^{0.5}\left(\theta'_p - \theta_p\right) - \varepsilon_w^{0.5}\left(\theta'_w - \theta_w\right) \tag{57}$$

where:

θ'_p = Real volumetric proportion of porosity

θ'_w = Real volumetric proportion of free moisture

Therefore, the difference between the measured and predicted dielectric values can be expressed simply as:

$$\Delta\varepsilon^{0.5} = \varepsilon_p^{0.5}\Delta\theta_p - \varepsilon_w^{0.5}\Delta\theta_w \tag{58}$$

where:

$\Delta\theta_p$ = Actual difference in volumetric content of porosity

$\Delta\theta_w$ = Actual difference in volumetric content of free moisture

Alternatively, the difference may be corrected by using a statistical correction factor as obtained in Figures 41 and 42, for the lack of a time-dependent, fundamental moisture volumetric distribution gradient with depth. The rest of these graphical fits can be found in Figures B-25 through B-32 in Appendix B, and the statistical analysis for these fits are available in Appendix C.

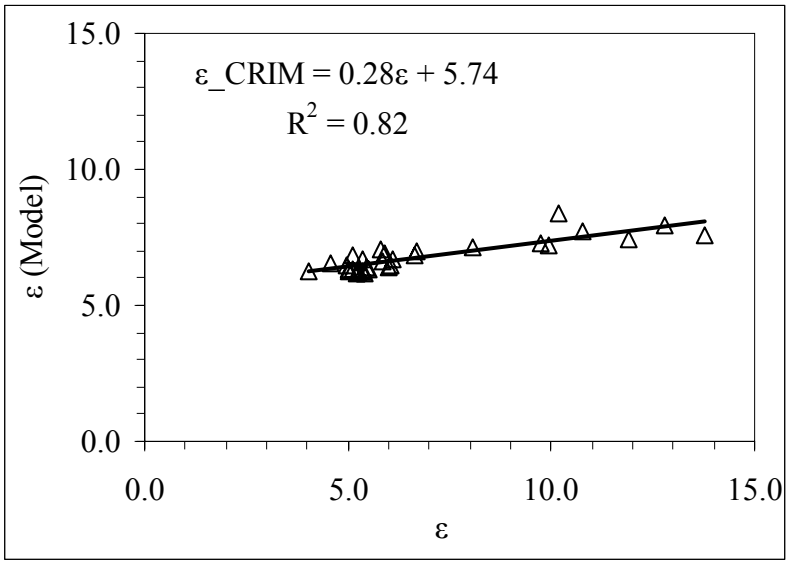

Figure 41 – Determination of Correction Factor for CRIM (Exposed) [w_0=0.44]

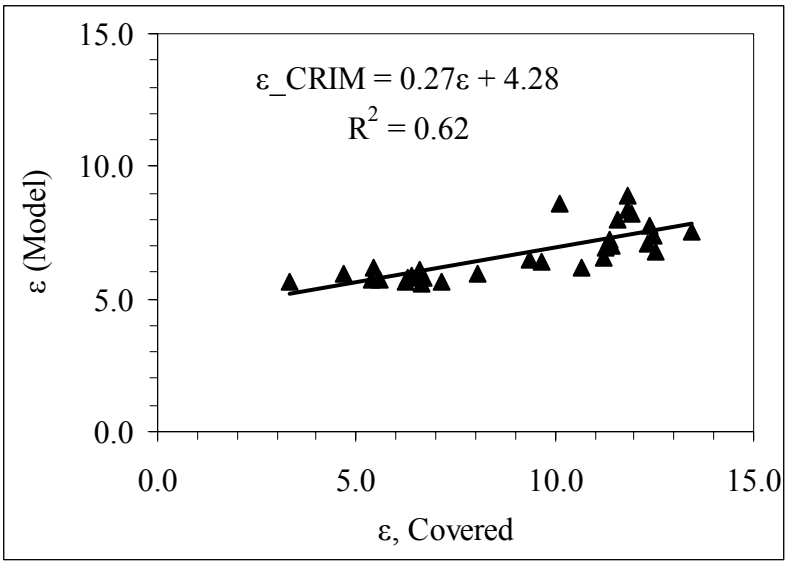

Figure 42 – Determination of Correction Factor for CRIM (Covered) [w_0=0.44]

CHAPTER VI
SUMMARY AND RECOMMENDATIONS

Moisture availability and loss is recognized in concrete research, but lacks effective action in concrete construction. The fundamental assessment of moisture loss is not commonly performed on-site, and cannot be easily quantified, for there is not a practical, direct way to measure it. The same can be said for strength and hydration properties, for which it is necessary to use invasive and destructive testing. Therefore, indirect measurements of moisture loss through surface dielectric testing show promise in the detection of moisture content and degree of hydration. Previous research show successful use of surface electromagnetic measurements on soil-aggregate systems for the assessment of moisture content, but there has not existed a fully established testing program put in place for the use of concrete dielectric constant measurements as indicators of capillary moisture content. In addition, surface dielectric measurements have its own limitations, yet the penetration capabilities of the dielectric probe used in this study did not diminish its sensitivity. This sensitivity was used as an advantage, because it is within the surface layers of concrete that surface distresses like spalling occur, and changes between actual surface concrete properties and predicted average-depth concrete properties could be differentiated.

To satisfy the objectives set forth at the beginning of this study, it was necessary to choose a convenient approach that would allow the detection of fundamental properties through the use of a non-invasive surface probe. The basic structure of the investigation revolved around three main ideas. The first one corresponds to a simple mass conservation principle, for any mass loss observed corresponds to the loss of the free (capillary) moisture content. The second main idea is based on the fact that the dielectric constant of water is higher than any other component in concrete, and that high dielectric values must correspond to high volumetric free moisture content. The third main idea is the concept that the dielectric value of any composite material is just the

addition of the individual dielectric contributions from each of the components, with their volumetric proportions controlling the proportionality of those contributions.

The three most important testing practices involved destructive strength testing, the determination of mass loss, and the direct surface measurement of the dielectric constant of the material. The results from these three tests suggested that there is clear evidence of how dielectric measurements are strongly affected by free moisture availability, which in turn is affected by hydration. The link between these relationships identified potentially reliable, non-destructive tools through which curing and hydration characteristics can be assessed quantitatively. It was important, however, to prevent as many unintended effects from uncontrollable factors. For that matter, the basic, "worst case" constants such as the environment and mixture proportioning were strictly controlled.

Strength testing allowed for a relatively good regression and approximation of the degree of hydration history, and showed clear sensitivity to exposure levels. Relative humidity measurements kept at a controlled environment showed near steady-state trends that were sensitive to the different water-cementitious ratios, but the response to exposure levels is unknown, since relative humidity was not measured under covered conditions.

Moisture loss showed high sensitivity to hydration at or around the setting time, and the dielectric value showed significant sensitivity to curing "quality" (exposure level). The ultimate moisture loss is not likely to be higher than 30 percent of the net water used from mixture design, even under the most extreme climatic conditions. However, the losses were more pronounced for the higher water-cement ratios. The higher the degree of severity of this loss, the more it restricts the ultimate amount of non-evaporable water fraction essential to hydration. The degree of precision in the approximation of the non-

evaporable and free moisture contents depends on the volumetric relationships and initial assumptions used.

The dielectric constant history is unreliable and highly variable before setting, and cannot be used in the analysis. Between one and three days from casting, the decreasing trend appears, but the variability remains high. After the third day from casting, the variability drops, giving an indication of stabilized hydration and moisture conditions in concrete. Statistically, however, the dielectric measurements are sensitive to the difference in "curing quality" (exposure level) of concrete within the same batch, even soon after setting time.

Dependences between parameters were also analyzed. Relative humidity turned out to be very sensitive to the free (capillary) moisture content and hence to the dielectric value of concrete. Relative humidity can become an indicator of self-dissecation, whereas the free (capillary) moisture content on its own cannot. However, relative humidity trends and the asymptotic model show that this is possible only when compared against either free moisture content or dielectric constant, and only when ambient conditions are kept constant. Besides, it was seen from the relative humidity-free moisture relationship that Parrot's investigation does not apply to hardening concrete because: 1) his study deals with concrete that has already hardened and cured underwater (where porosity and microstructure are already defined), and 2) his sorption/desorption isotherms are mostly functions of permeability (porosity, microstructure connectivity), and of the bonding state of capillary moisture.

Free moisture shows a clear dependence with the degree of hydration and its approximation is limited by the volumetric model used. In this study, the volumetric free moisture content is a linear relationship sensitive to mix design parameters, degree of hydration, and curing quality.

Dielectric value measurements show a clear dependence on water-cementitious ratios and on curing quality when compared against volumetric moisture content. Excess surface moisture and self-dissecation greatly influence these measurements with self-dissecation being more pronounced for low water cement ratios. These influences cause the composite dielectric model to deviate from the real dielectric value, yet the difference in dielectric value readings can help quantify the actual moisture content of the surface concrete layer. In other words, CRIM works, but lacks fit during early concrete ages (less than 1 day) due to excess surface moisture, time during which the dielectric value of concrete is much higher than the calculated average moisture content. The dielectric constant of self-dissecated concrete is always well approximated by CRIM.

In general, the results suggest that dielectric constant measurements can be used as a quick, non-invasive and non-destructive tool to predict free (capillary) moisture content and to approximate the degree of hydration. Dielectric constant measurements may be used as a tool to approximate ranges of free moisture content changes and self-dissecation kick-off points, ranges of differences between surface and average moisture content, and ranges of hydration variation. In order to jump from the approximation of the degree of hydration to the approximation of the time-dependent compressive strength, it would be necessary to obtain ultimate strength values determined from short strength test programs.

Although the results show extensive evidence for the potential of dielectric measurement as a quantitative assessment tool, at this point only a framework can be proposed due to the basic level and limited database from which these test results are obtained. To this regard, it may be feasible to establish threshold values for the volumetric free moisture content from dielectric readings. The free moisture content model as a function of hydration along with the dielectric constant history may be used to detect a major change in the dielectric loss rates, which indicates self-dissecation. At this point curing

procedures can be put in place to prevent further moisture loss. Therefore, self-dissecation detection is the key factor in the timing of curing compound application.

The investigation for surface dielectric measurements can offer an unlimited potential for curing quality assessment. Yet an expanded database is needed. The proposed models are recommended to be refined, tested and expanded to include the water-cement ratio as a variable, with a corresponding sensitivity analysis. The variation of type and content of cement, aggregate gradation, concrete surface roughness, pozzolans and liquid admixtures needs to be characterized and compared against the baseline results presented in this study in the near future.

REFERENCES

1. Al-Qadi, I. L., Hazim, O. A., Su, W., and Riad, S. M. (1995). "Dielectric Properties of Portland Cement Concrete at Low Radio Frequencies." *ASCE Journal of Materials in Civil Engineering*, 7(3), 192-198.

2. Anderson, J. C. (1964). *Dielectrics*, Reinhold Publishing Corporation, New York.

3. Breugel, K. van (1991). *Simulation of Hydration and Formation of Structure in Cement-Based Materials*, Delft University of Technology, Netherlands.

4. Cano-Barrita, P.F. De J., Balcom, B. J., Bremmer, T. W., MacMillan, M. B., and Langley, W. S. (2004). "Moisture Distribution in Drying Ordinary and High Performance Concrete Cured in a Simulated Hot Dry Climate." Materials and Structures, 37(272), 522-531.

5. Çengel, Y. A. and Turner, R. H. (2001). *Fundamentals of Thermal-Fliud Sciences*, McGraw-Hill, New York.

6. Frolov, G. V., and Ivanovskii, G. A. (1984). "A Quasibalancing Dielectric Water-Content Meter for Powdery Building Materials." *Measurement Techniques*, 27(3), 468-470.

7. Guthrie, S., and Scullion, T. (2000). "Using Dielectric Measurements to Predict Cold Weather Performance of Unstabilized Aggregate Base Materials." *Proc., Annual Meeting of the Transportation Research Board*, TRB, Washington, D.C.

8. Hashin, Z. (1982). "Theory of Composite Materials." *Proc., IUTAM Symposium on Mechanics of Composite Materials*, Pergamon, Blacksburg, VA.

9. Jang, S. H., Mukhopadhay, A., and Zollinger, D. G. (2005). "Hydration Modulation Measures to Mitigate the Negative Effect of Paving Concrete in Hot Weather", *Proc., International Conference on Concrete Pavements,* ISCP, Colorado Springs, CO.

10. Janoo, V., Korhonen, C., and Hovan, M. (1999). "Measurement of Water Content in Portland Cement Concrete." *ASCE Journal of Transportation Engineering*, 125(3), 245-249.

11. Khalaf, F. M. and Wilson, J. G. (1999). "Electrical Properties of Freshly Mixed Concrete." *ASCE Journal of Materials in Civil Engineering*, 11(3), 242-248.

12. Khan, A. A., Cook, W. D., and Mitchell, D. (1995). "Early Age Compressive Stress-Strain Properties of Low-, Medium, and High-Strength Concretes." *ACI Materials Journal*, 92(6), 617-624.

13. Klemunes Jr., J. (1998). *Determining Soil Volumetric Content Using Time Domain Reflectometry*, Federal Highway Administration, McLean, VA

14. Li, Z., Wei, X., and Li, W. (2003). "Preliminary Interpretation of Portland Cement Hydration Process Using Resistivity Measurements." *ACI Materials Journal*, 100(3), 253-257.

15. Mamlouk, M. S. and Zaniewski, J. P. (1999). *Materials for Civil and Construction Engineers*, Addison-Wesley, Menlo Park, CA.

16. Mindess, S., Young, J. F., and Darwin, D. (2003). *Concrete*, 2nd Ed., Prentice Hall, Upper Saddle River, NJ.

17. Neville, A.M. (1995). *Properties of Concrete,* 4th Ed., Longman Group Limited, London, England.

18. Parrot, L. J. (1991). "Factors Influencing Relative Humidity in Concrete." *Magazine of Concrete Research*, 43(154), 45-52.

19. Parrot, L. J. (1992). "Variations of Water Absorption Rate and Porosity with Depth from an Exposed Concrete Surface: Effects of Exposure Conditions and Cement Type." *Cement and Concrete Research*, 22, 1077-1088.

20. Powers, T.C. (1947). "A Discussion of Cement Hydration in Relation to the Curing of Concrete." *PCA Bulletin*, 25, 178-188.

21. Rhim, H. C., and Büyüköztürk, O. (1998). "Electromagnetic Properties of Concrete at Microwave Frequency Range." *ACI Materials Journal*, 95(3), 262-271.

22. Roadscanners Group (2005). "Adek Percometer v.6." *Roadscanners*, <http://www.roadscanners.com> (July 1, 2005).

23. Scullion, T. and Saarenketo, T. (1996). "Using Suction and Dielectric Measurements as Performance Indicators for Aggregate Base Materials." *Transportation Research Record*, 1577, 37-44.

24. Somayaji, S. (2001). *Civil Engineering Materials*, 2nd Ed., Prentice Hall, Upper Saddle River, NJ.

25. Taylor, H. F. W. (1997). *Cement Chemistry*, 2nd Ed., Thomas Telford, London, England.

26. TransTech Systems, Inc. (2003). "Effect of Water and Temperature on Hot Mix Asphalt Density Measurement using Electromagnetic Sensing." *TransTech Technical Notes*, Number 0301

27. Van Beek, A., and Hilshorst, M. A. (1999). "Dielectric Measurements to Characterize the Microstructural Changes of Young Concrete." *Heron*, 44(1), 3-17.

28. Wang, L. (2000). *Process and Prediction of Moisture and Temperature Distributions and History in Hardening Concrete*, Ph.D. Dissertation, Texas A&M University, College Station.

29. Xian-Yu, J., Nan-guo, J., and Zong-jin, L. (2002). "Study on the Electrical Properties of Young Concrete." *Journal of Zhejiang University: Science*, 3(2), 174-180.

30. Zoughi, R., Gray, S. D., and Nowak, P. S. (1995). "Microwave Nondestructive Estimation of Cement Paste Compressive Strength." *ACI Materials Journal*, 92(1), 64-69.

APPENDIX A

VISUAL BASE DATA

UNIT WEIGHT, AIR CONTENT AND SLUMP

Table A-1. Fresh Concrete Properties

Treatment	Slump	Unit Weight	Fresh Air Content
0.32	0.0 cm (0.0 in)	2449 kg/m^3 (153 lb/ft^3)	4.89%
0.36	0.0 cm (0.0 in)	2460 kg/m^3 (153 lb/ft^3)	3.38%
0.40	2.5 cm (1.0 in)	2461 kg/m^3 (153 lb/ft^3)	2.65%
0.44	5.0 cm (2. 0 in)	2459 kg/m^3 (153 lb/ft^3)	1.21%

SETTING TIME DETERMINATION

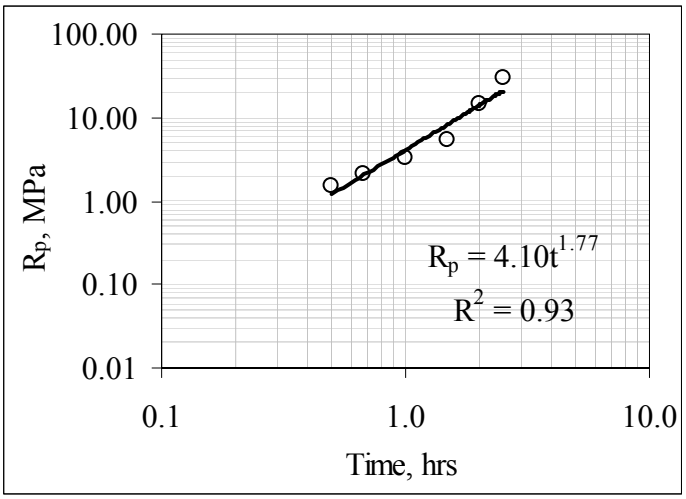

Figure A-1. Setting Time Determination [w_0=0.32]

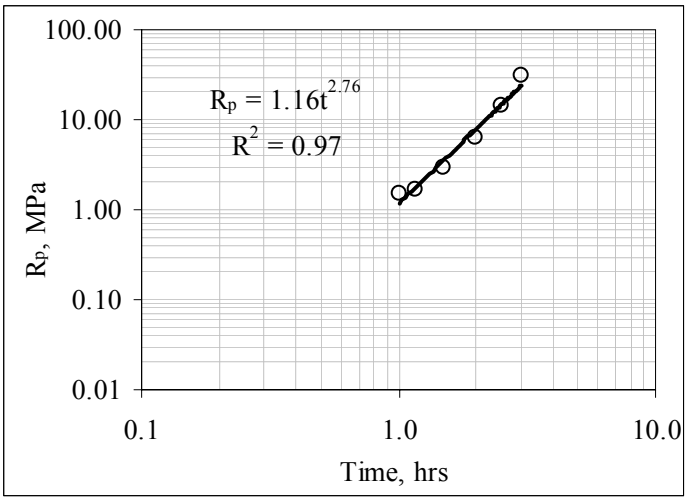

Figure A-2. Setting Time Determination [w_0=0.36]

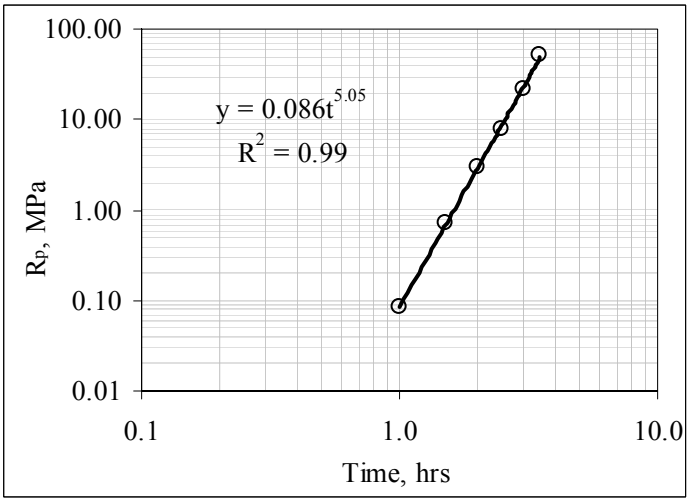

Figure A-3. Setting Time Determination [w_0=0.40]

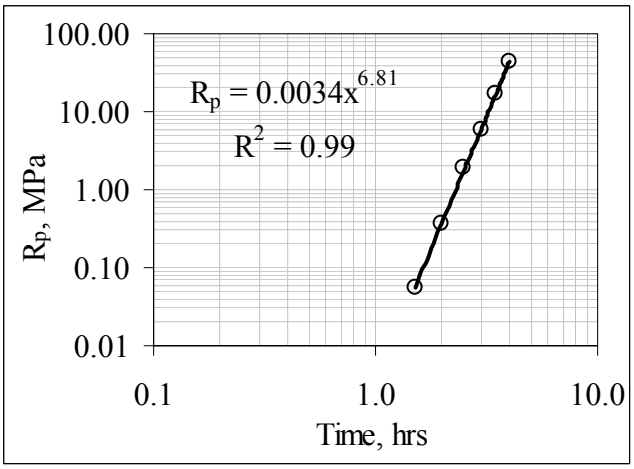

Figure A-4. Setting Time Determination [w_0=0.44]

STRENGTH AND ADIABATIC HEAT MEASUREMENTS

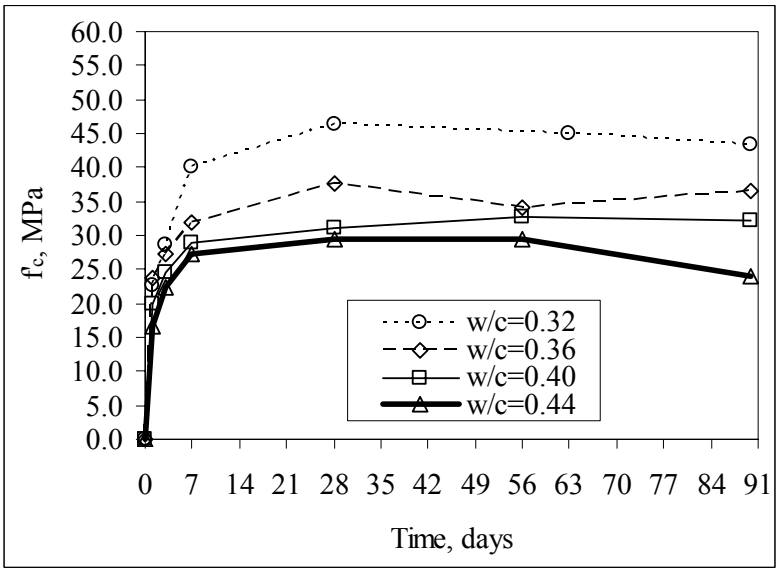

Figure A-5. Compressive Strength (Exposed) [All treatments]

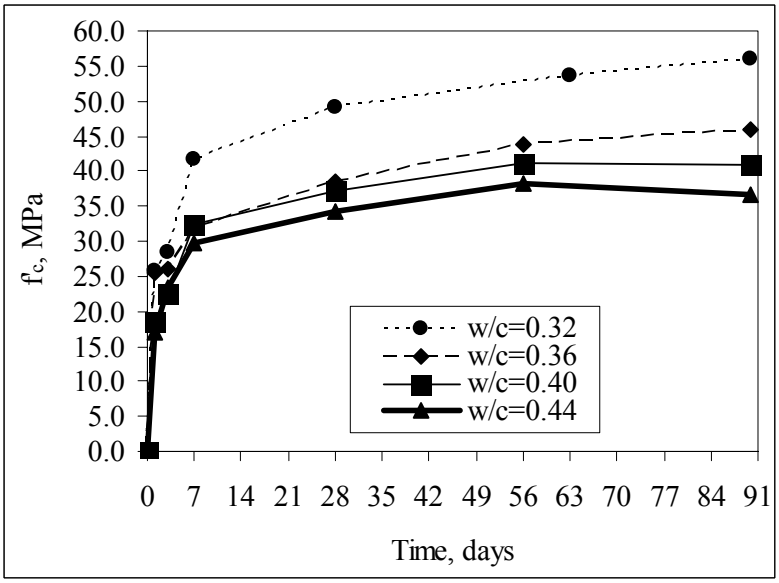

Figure A-6. Compressive Strength (Covered) [All treatments]

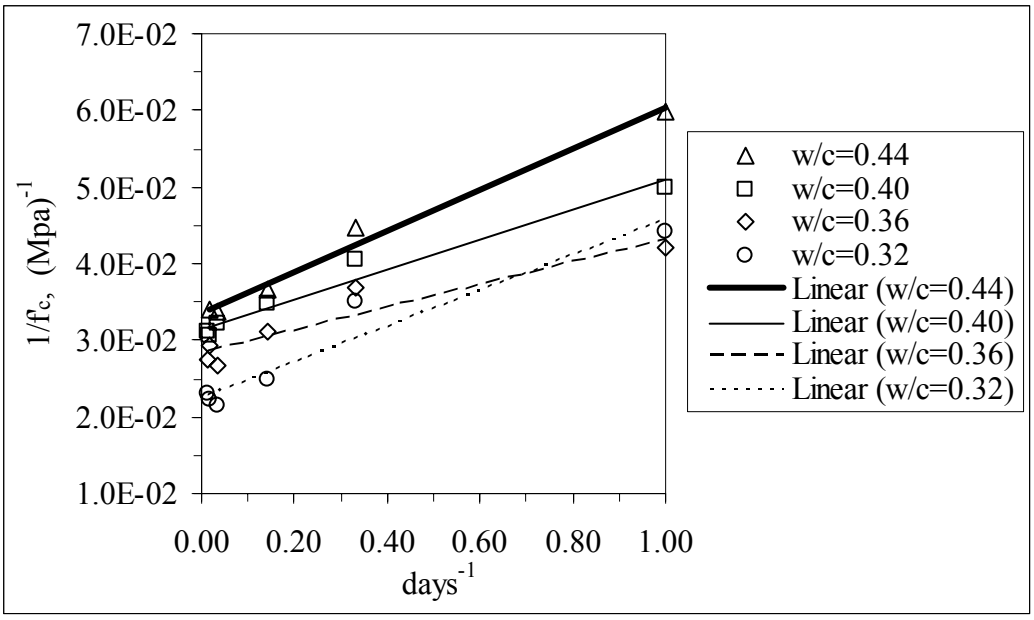

Figure A-7. Compressive Strength Linearization (Exposed) [All treatments]

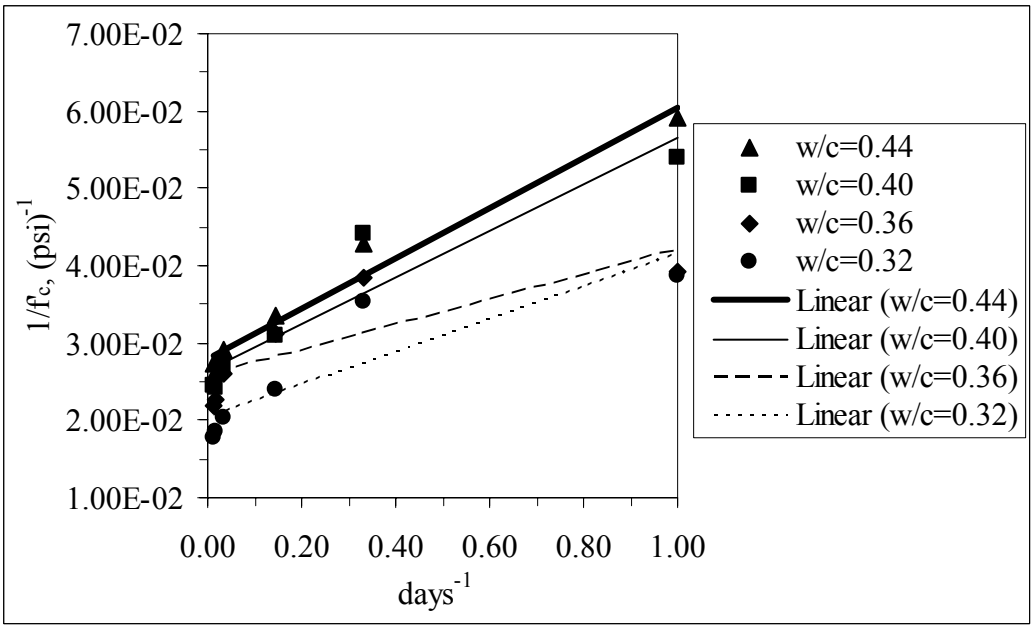

Figure A-8. Compressive Strength Linearization (Covered) [All treatments]

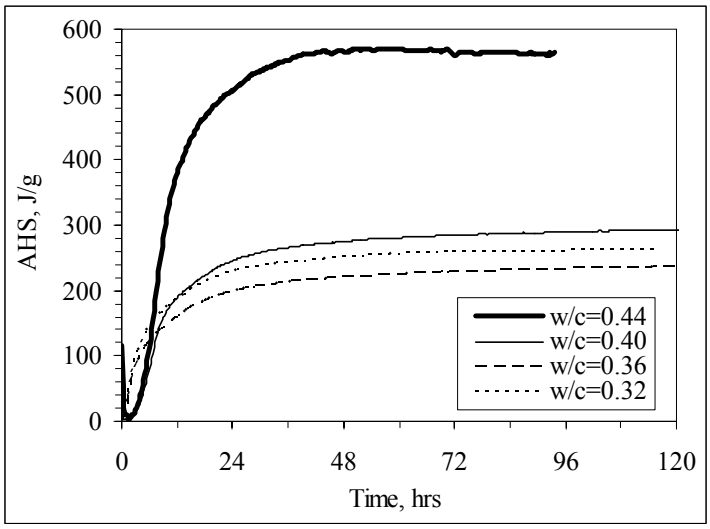

Figure A-9. Adiabatic Heat Signature History [All treatments]

DEGREE OF HYDRATION

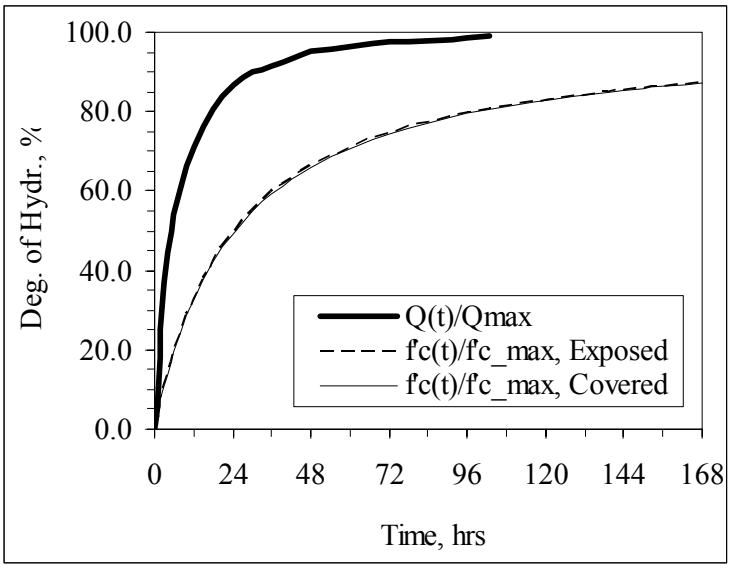

Figure A-10. Calculated Degree of Hydration [w_0=0.32]

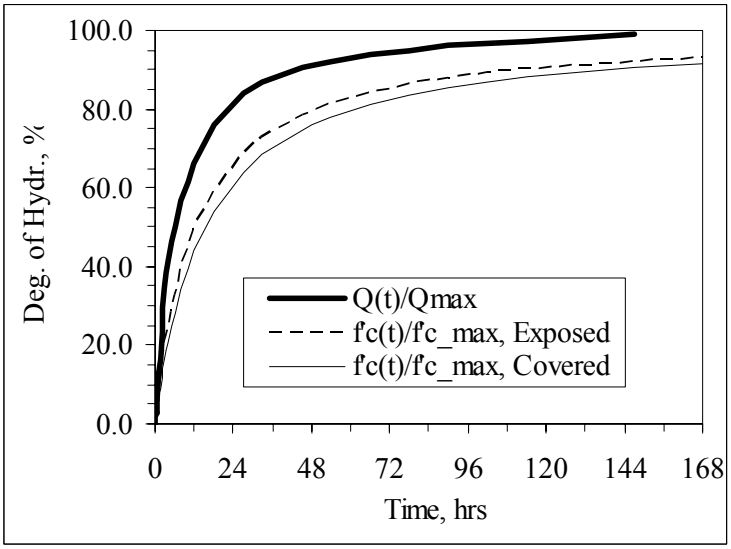

Figure A-11. Calculated Degree of Hydration [w_0=0.36]

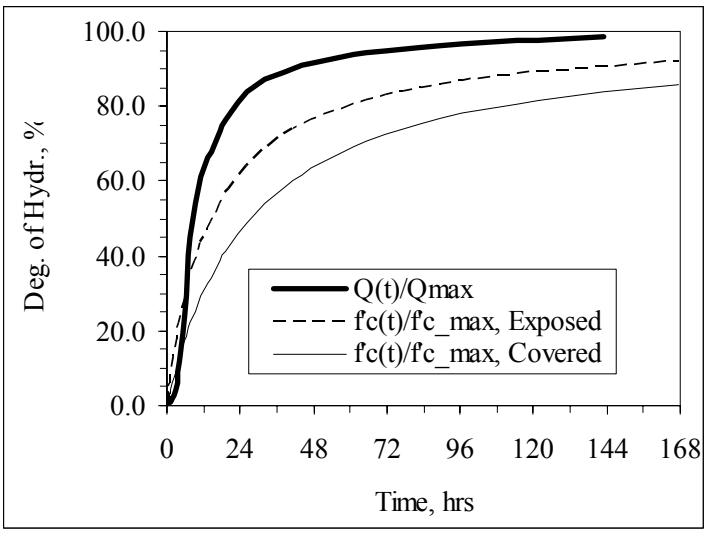

Figure A-12. Calculated Degree of Hydration [w_0=0.40]

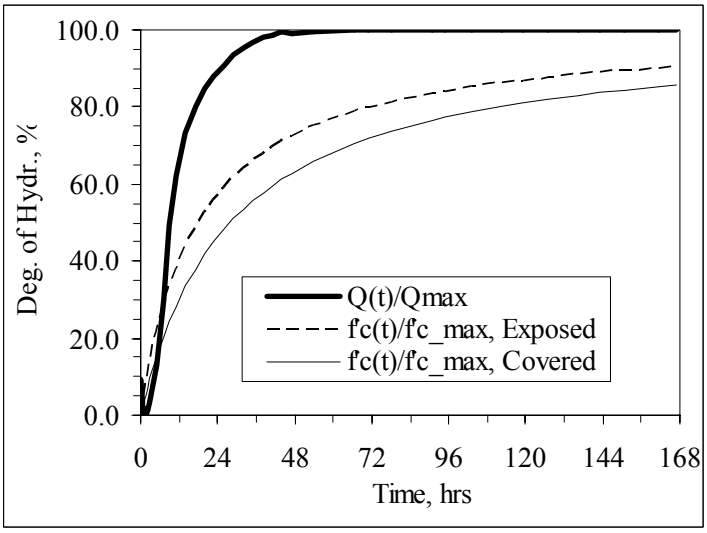

Figure A-13. Calculated Degree of Hydration [w_0=0.44]

DIELECTRIC CONSTANT HISTORY

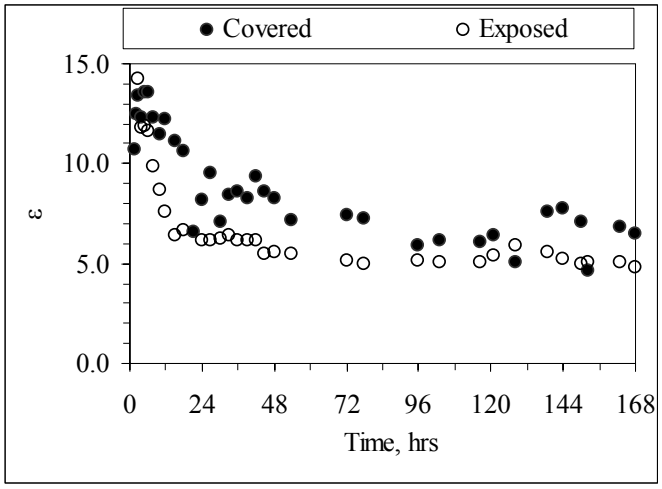

Figure A-14. Dielectric Constant History [w_0=0.32]

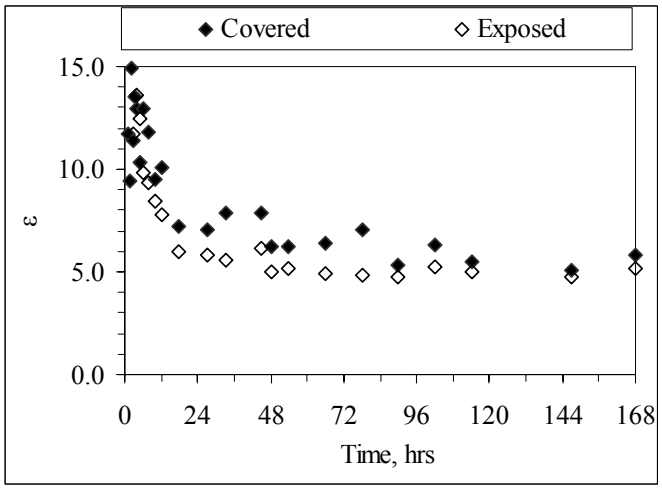

Figure A-15. Dielectric Constant History [w_0=0.36]

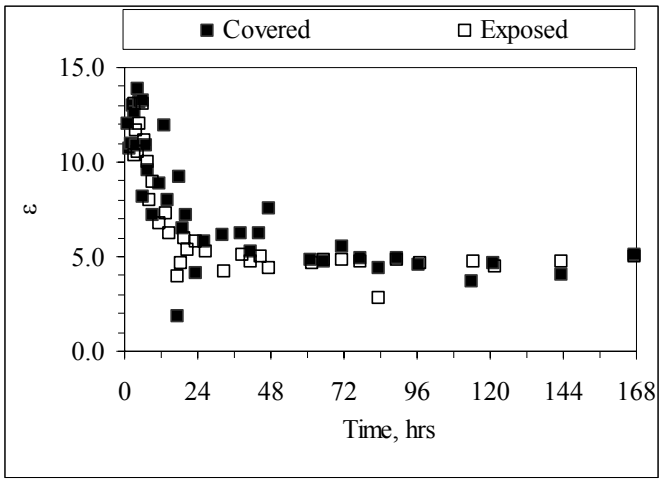

Figure A-16. Dielectric Constant History [w_0=0.40]

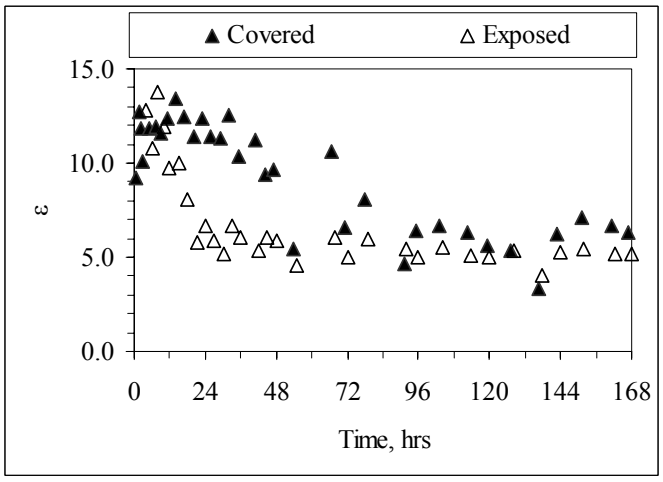

Figure A-17. Dielectric Constant History [w_0=0.44]

RELATIVE HUMIDITY

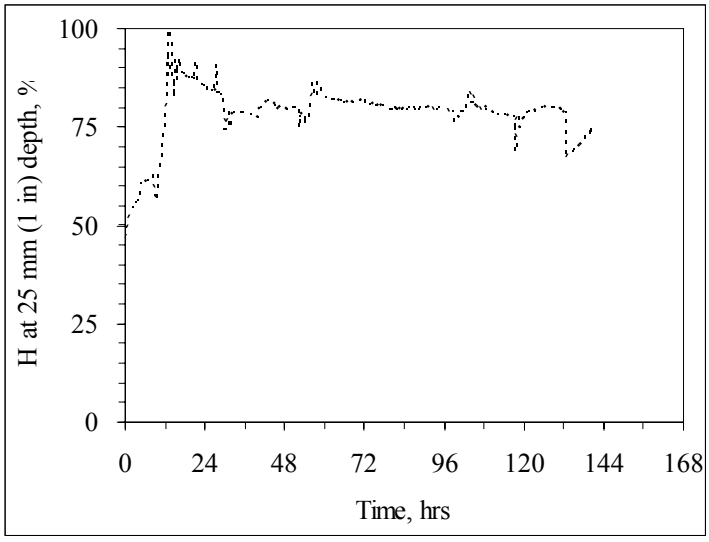

Figure A-18. Relative Humidity Measurements [w_0=0.32]

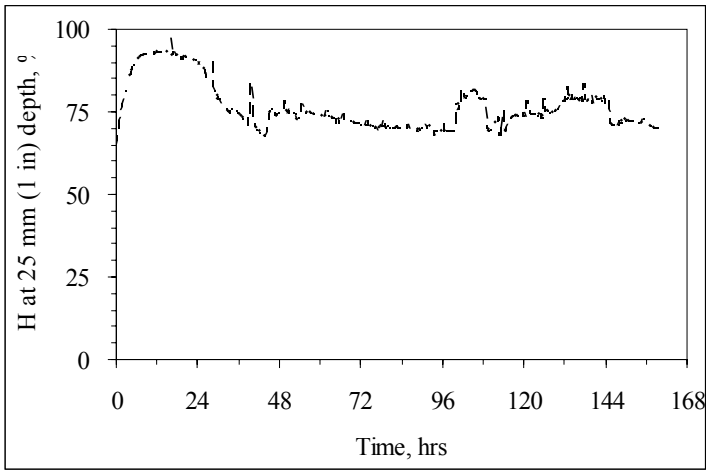

Figure A-19. Relative Humidity Measurements [w_0=0.36]

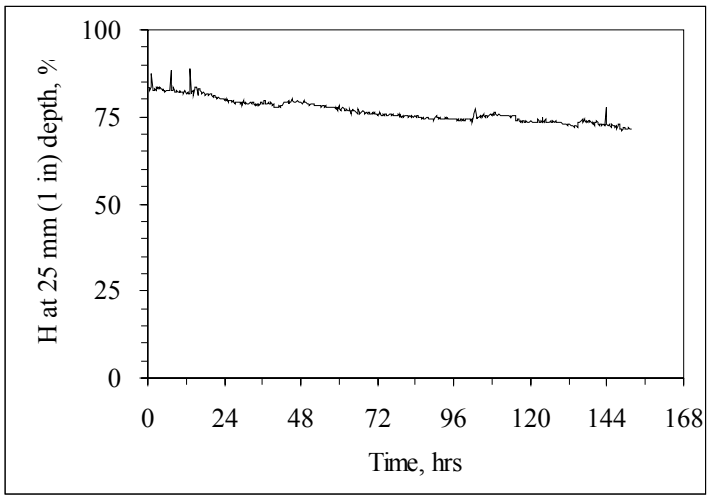

Figure A-20. Relative Humidity Measurements [w_0=0.40]

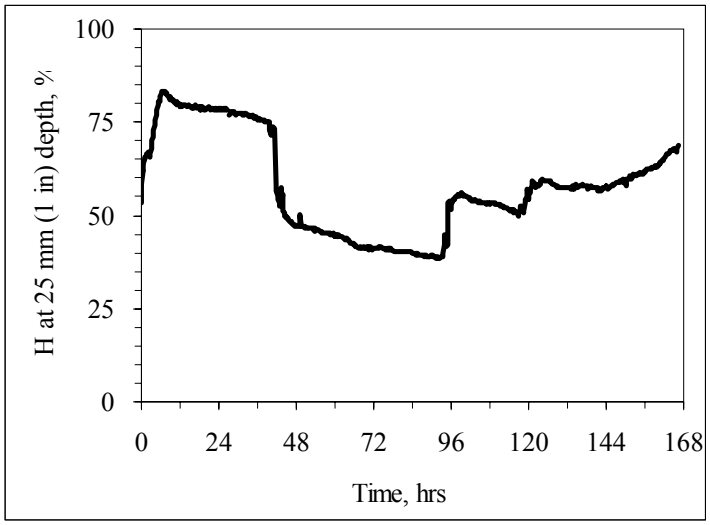

Figure A-21. Relative Humidity Measurements [w_0=0.44]

MOISTURE LOSS

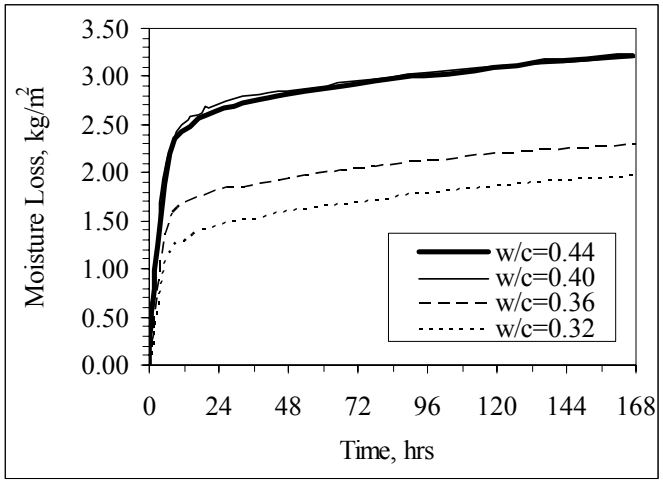

Figure A-22. Moisture Mass Loss per Area [All treatments]

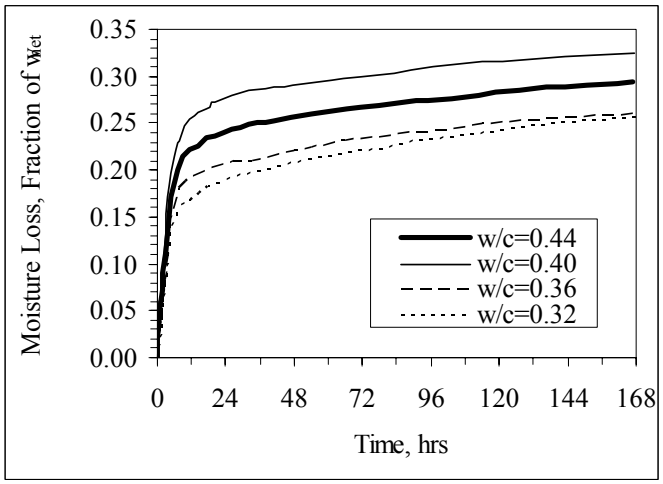

Figure A-23. Moisture Mass Loss per Net Water [All treatments]

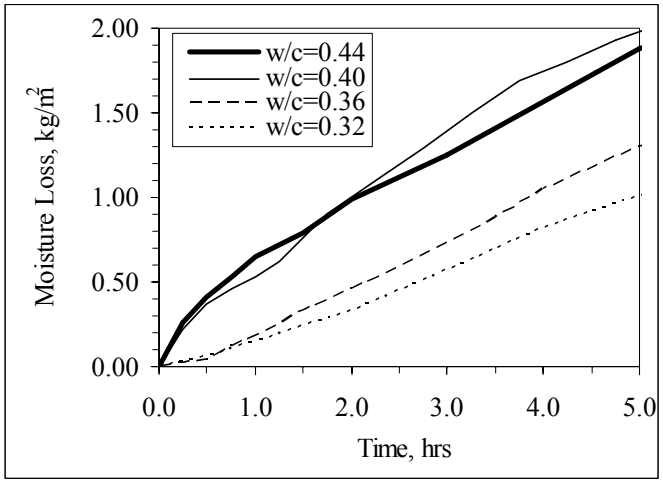

Figure A-24. Early Moisture Mass Loss per Area [All treatments]

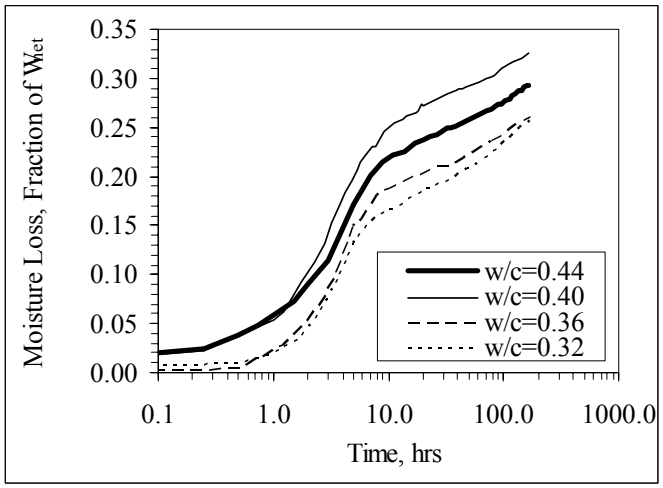

Figure A-25. Detail of Moisture Mass Loss per Net Water [All treatments]

MOISTURE FRACTION HISTORY

EXPOSED LEVEL

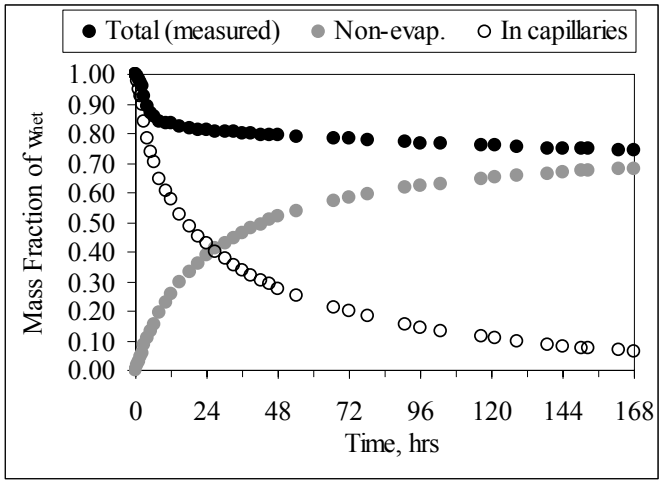

Figure A-26. Approximated Moisture Fraction Change (Exposed) [w_0=0.32]

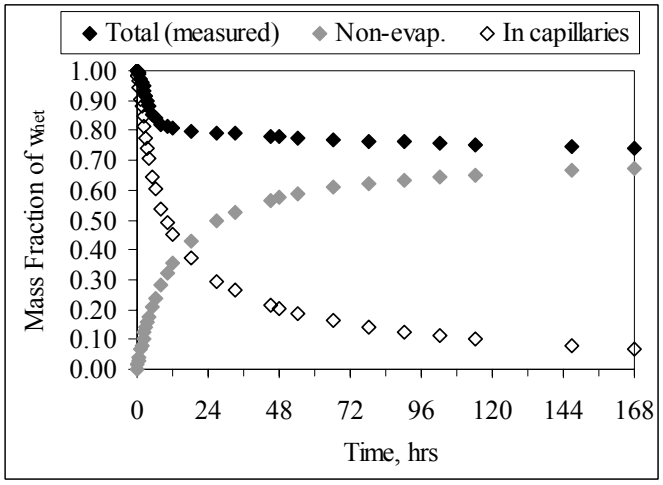

Figure A-27. Approximated Moisture Fraction Change (Exposed) [w_0=0.36]

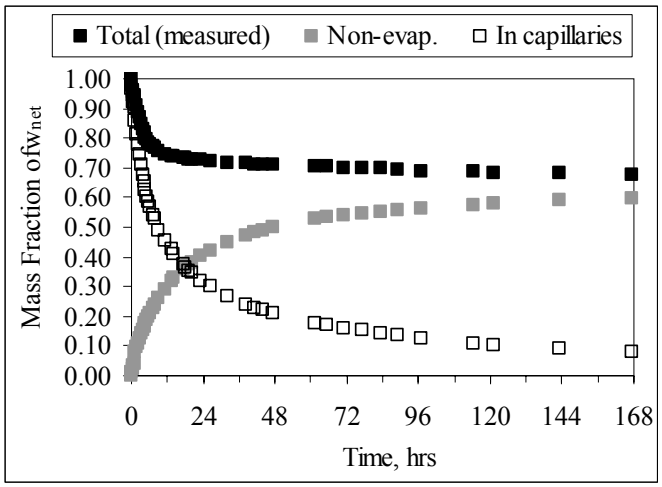

Figure A-28. Approximated Moisture Fraction Change (Exposed) [w_0=0.40]

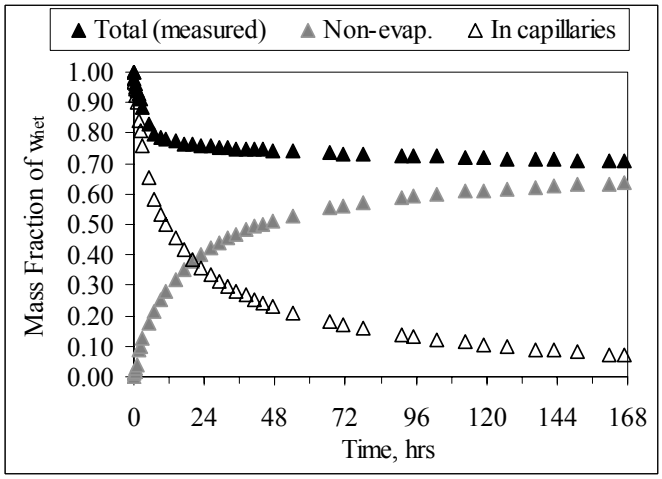

Figure A-29. Approximated Moisture Fraction Change (Exposed) [w_0=0.44]

COVERED LEVEL

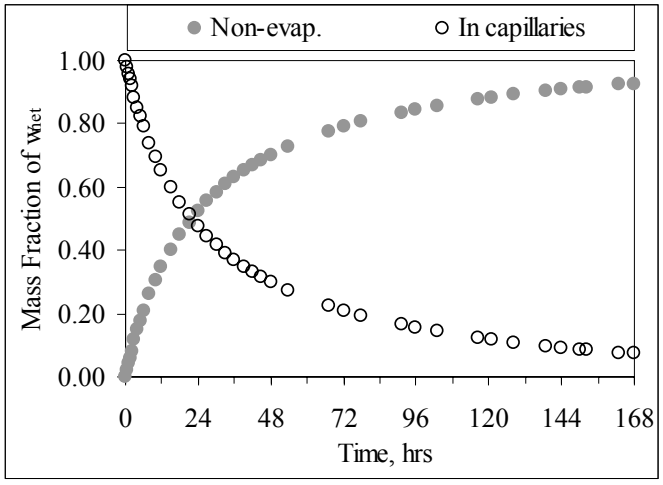

Figure A-30. Approximated Moisture Fraction Change (Covered) [w_0=0.32]

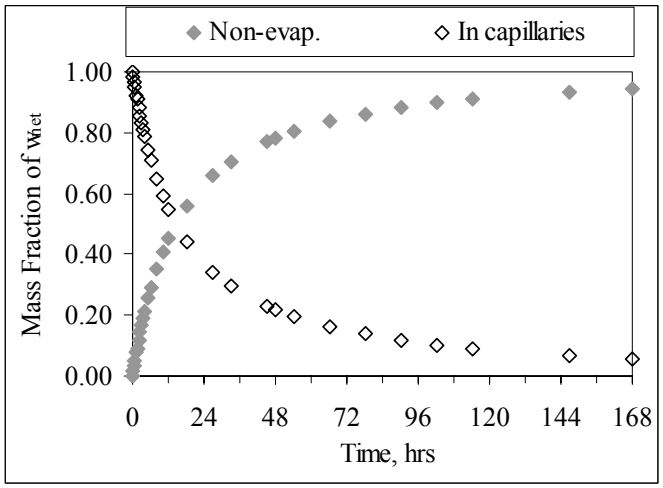

Figure A-31. Approximated Moisture Fraction Change (Covered) [w_0=0.36]

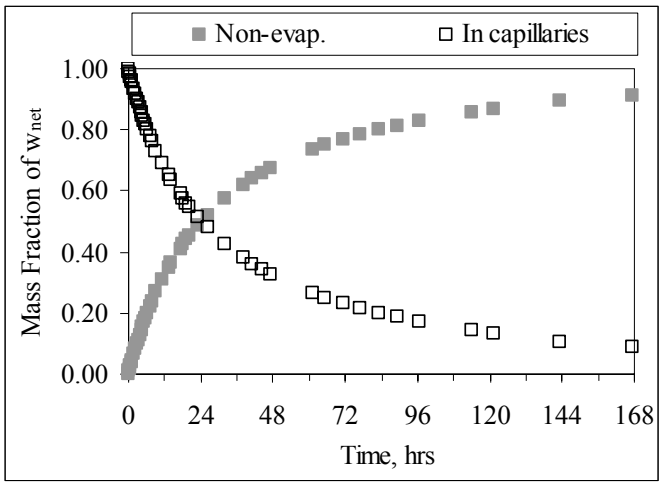

Figure A-32. Approximated Moisture Fraction Change (Covered) [w_0=0.40]

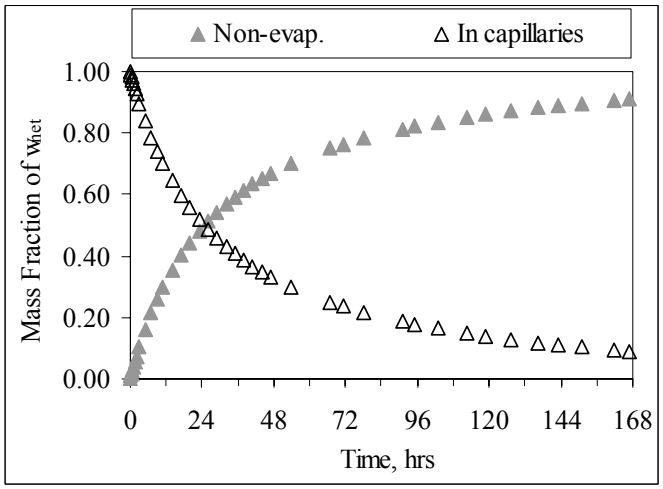

Figure A-33. Approximated Moisture Fraction Change (Covered) [w_0=0.44]

FREE AND NON-EVAPORABLE MOISTURE

EXPOSED LEVEL

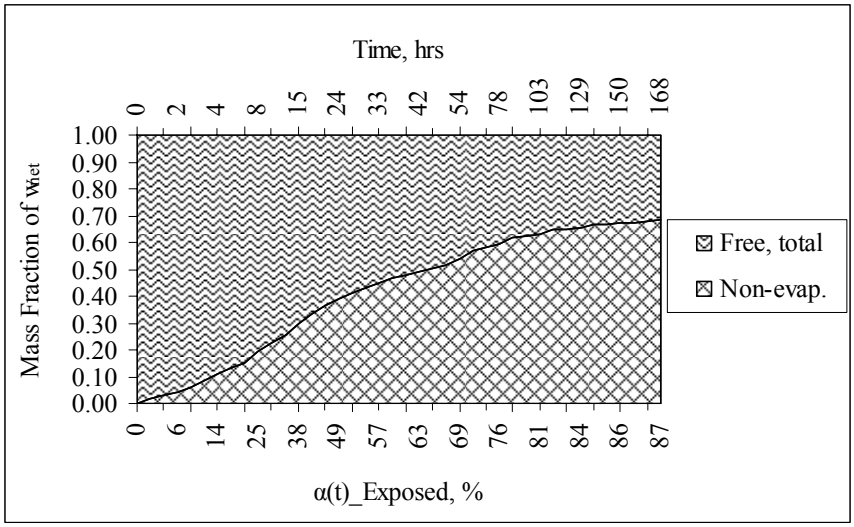

Figure A-34. Approximated Total Moisture Fractioning (Exposed) [w_0=0.32]

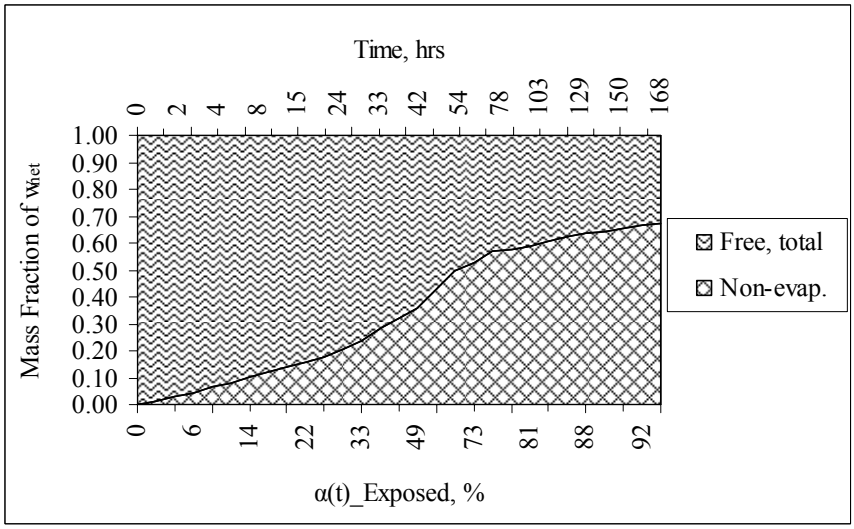

Figure A-35. Approximated Total Moisture Fractioning (Exposed) [w_0=0.36]

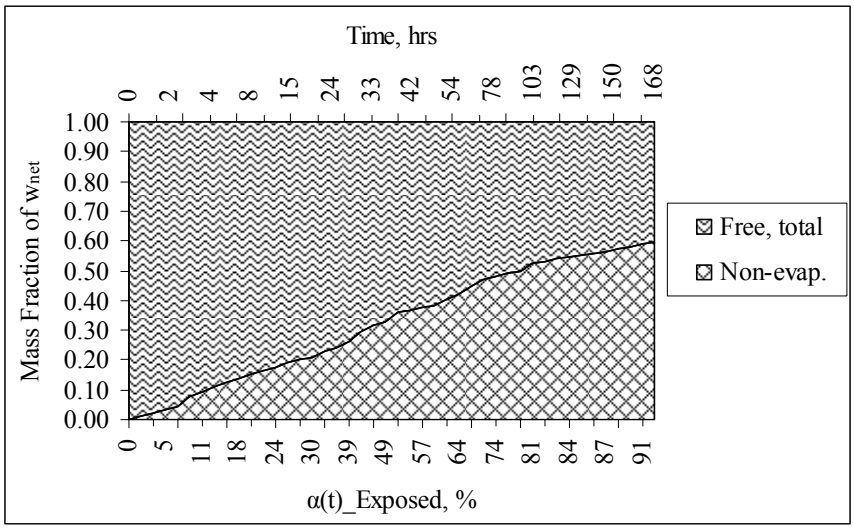

Figure A-36. Approximated Total Moisture Fractioning (Exposed) [w_0=0.40]

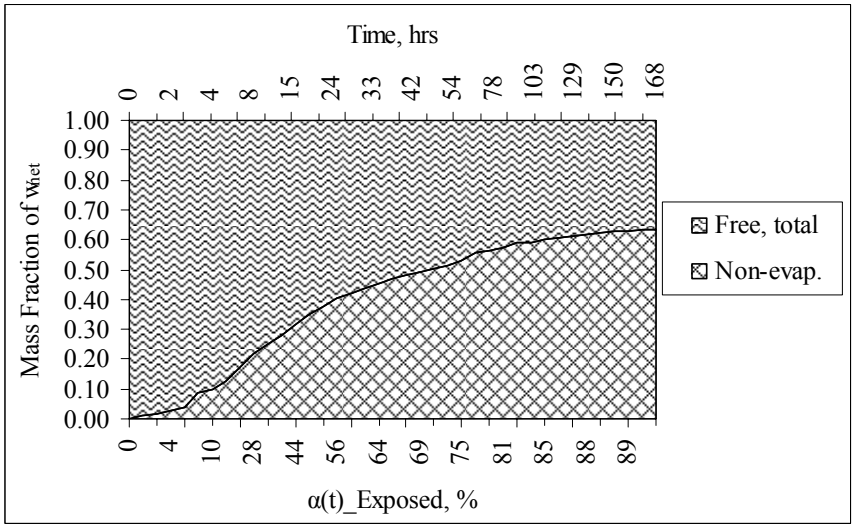

Figure A-37. Approximated Total Moisture Fractioning (Exposed) [w_0=0.44]

COVERED LEVEL

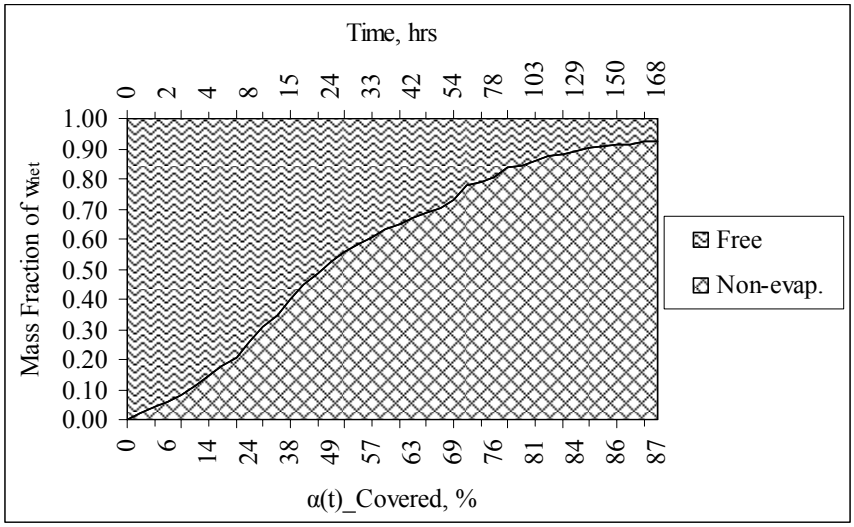

Figure A-38. Approximated Total Moisture Fractioning (Covered) [w_0=0.32]

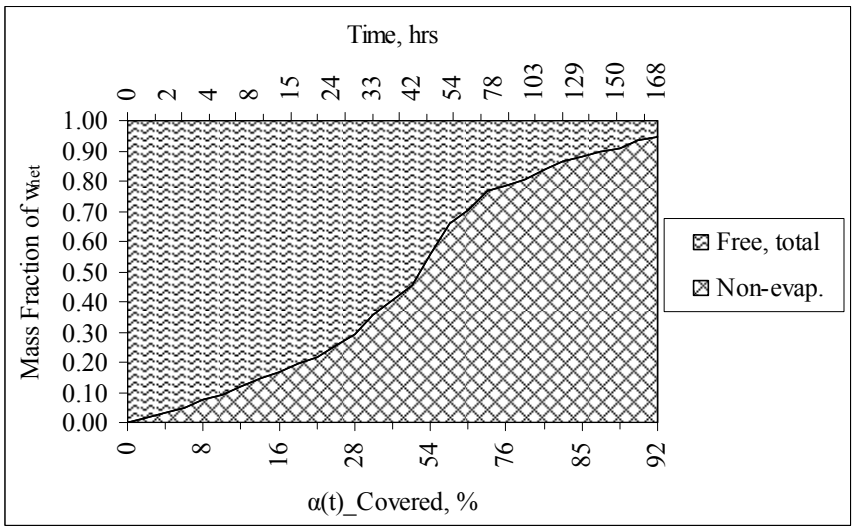

Figure A-39. Approximated Total Moisture Fractioning (Covered) [w_0=0.36]

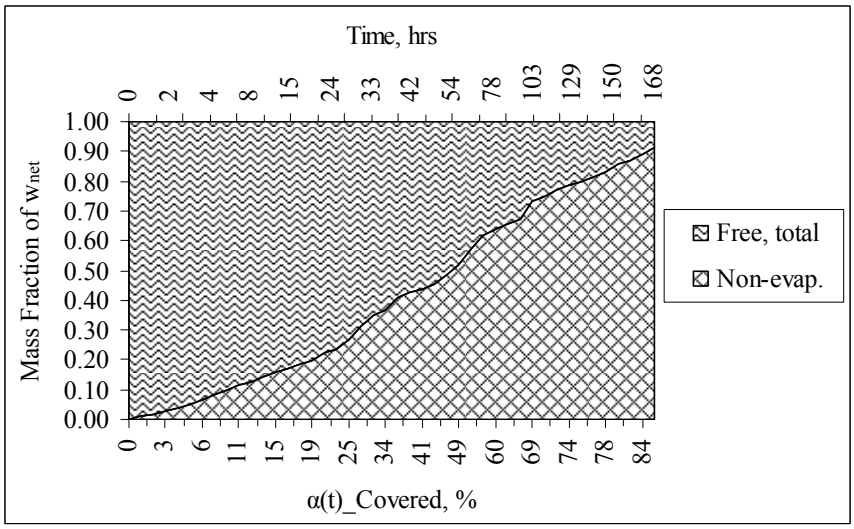

Figure A-40. Approximated Total Moisture Fractioning (Covered) [w_0=0.40]

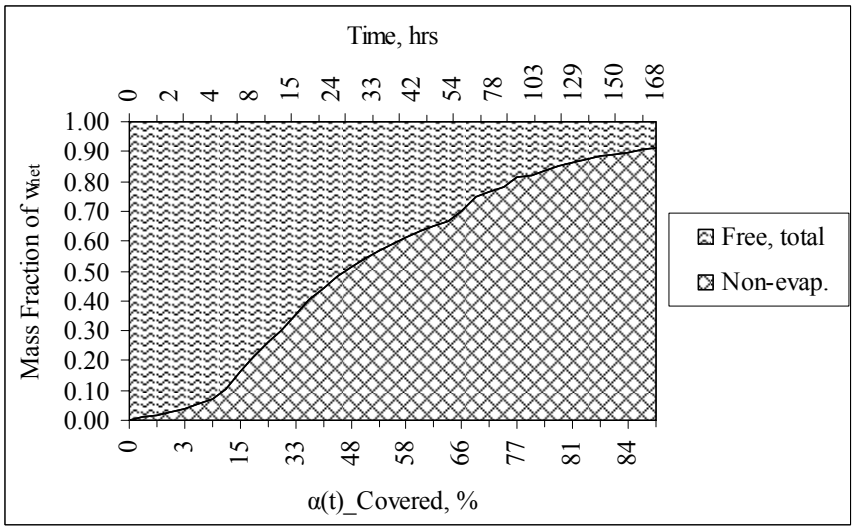

Figure A-41. Approximated Total Moisture Fractioning (Covered) [w_0=0.44]

VOLUMETRIC DIAGRAM

EXPOSED LEVEL

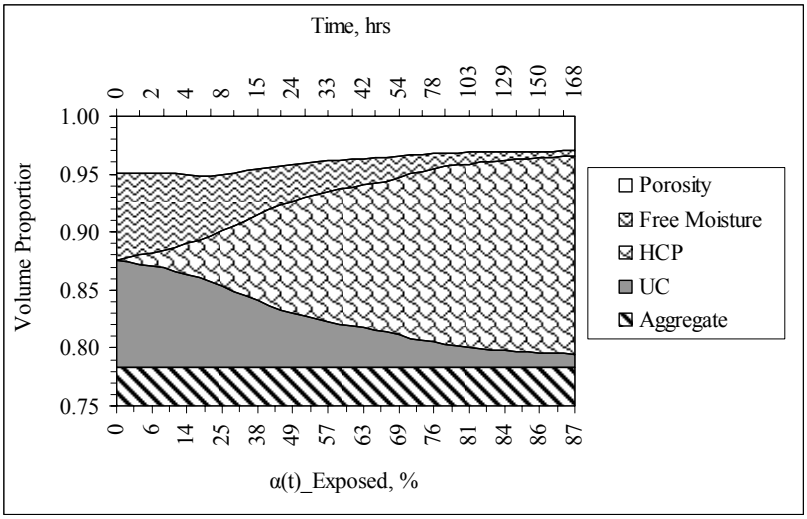

Figure A-42. Approximated Volumetric Proportions (Exposed) [w_0=0.32]

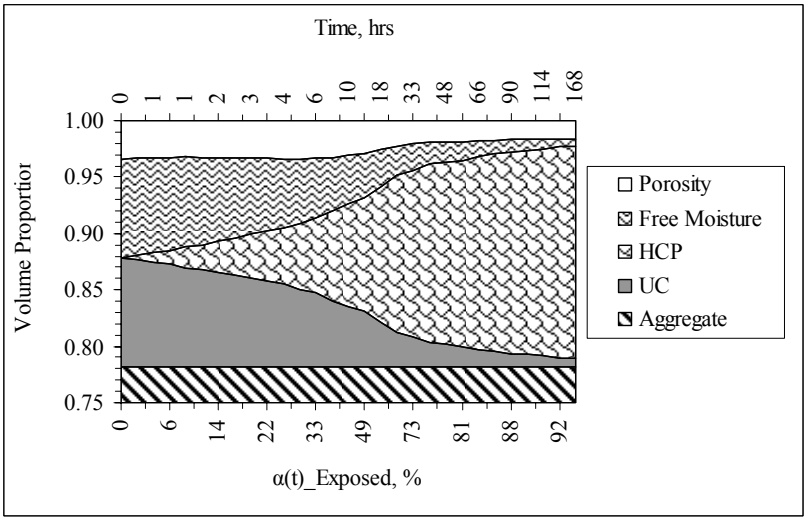

Figure A-43. Approximated Volumetric Proportions (Exposed) [w_0=0.36]

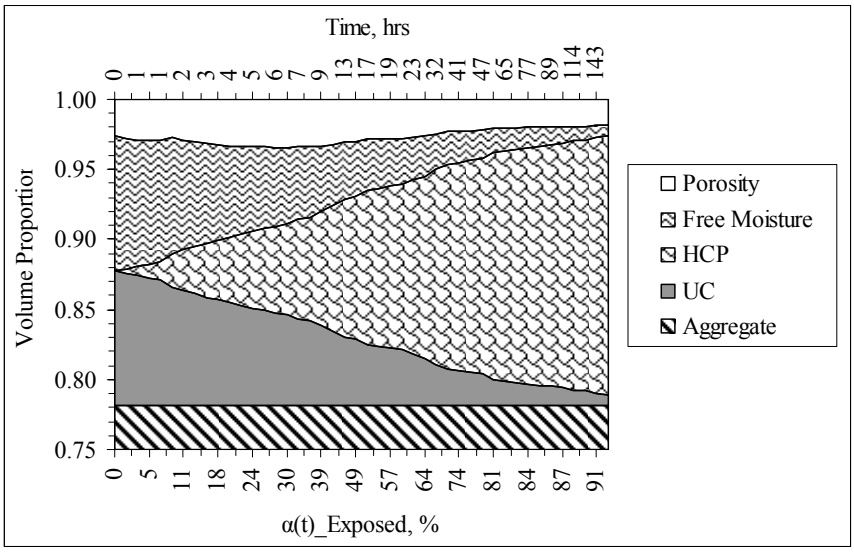

Figure A-44. Approximated Volumetric Proportions (Exposed) [w_0=0.40]

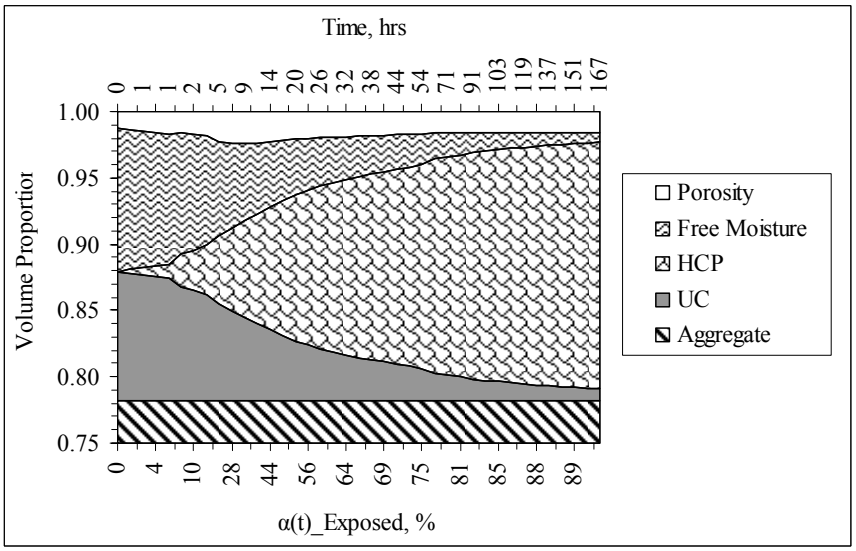

Figure A-45. Approximated Volumetric Proportions (Exposed) [w_0=0.44]

COVERED LEVEL

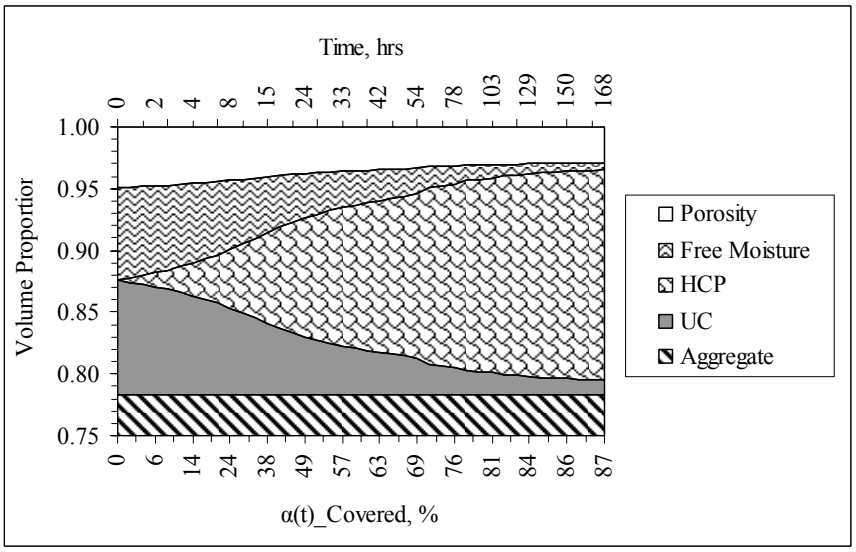

Figure A-46. Approximated Volumetric Proportions (Covered) [w_0=0.32]

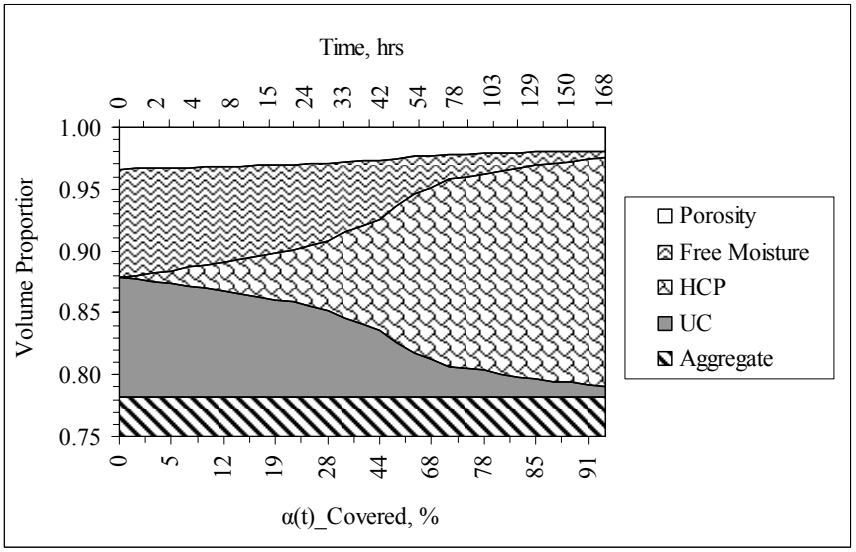

Figure A-47. Approximated Volumetric Proportions (Covered) [w_0=0.36]

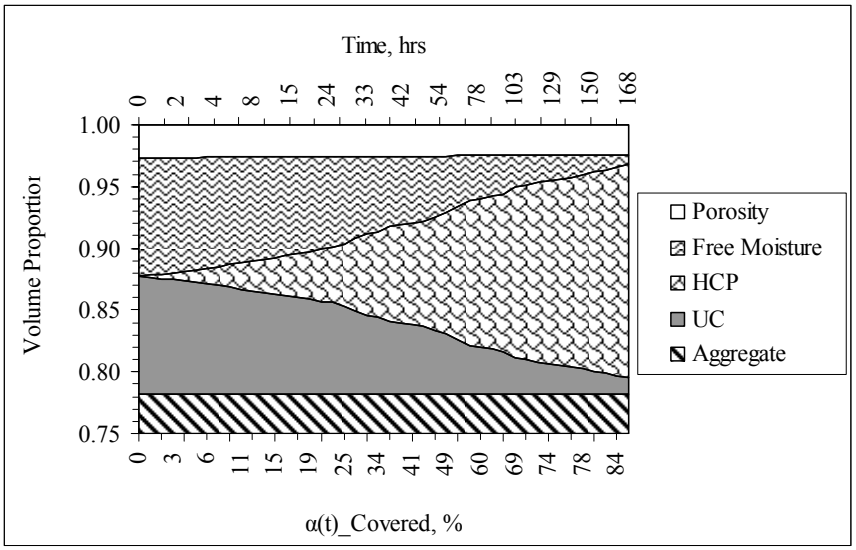

Figure A-48. Approximated Volumetric Proportions (Covered) [w_0=0.40]

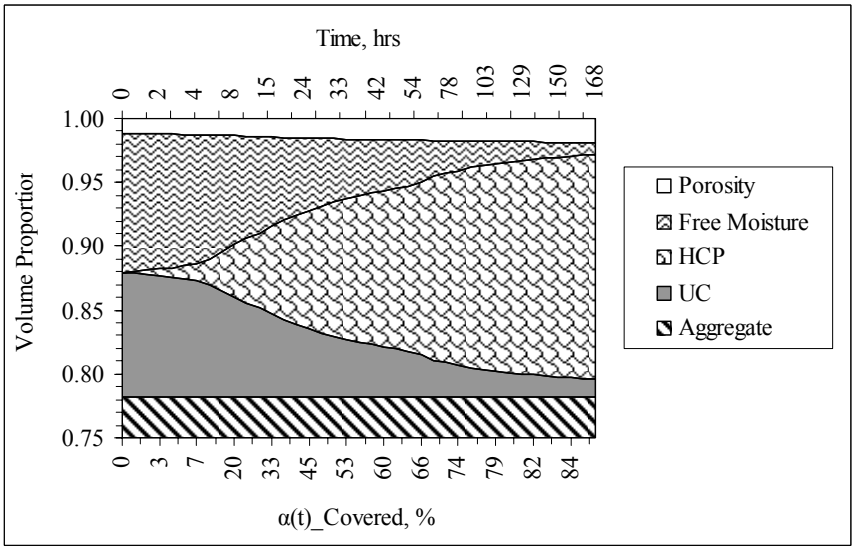

Figure A-49. Approximated Volumetric Proportions (Covered) [w_0=0.44]

APPENDIX B

MAIN ANALYSIS

FREE MOISTURE VS. H

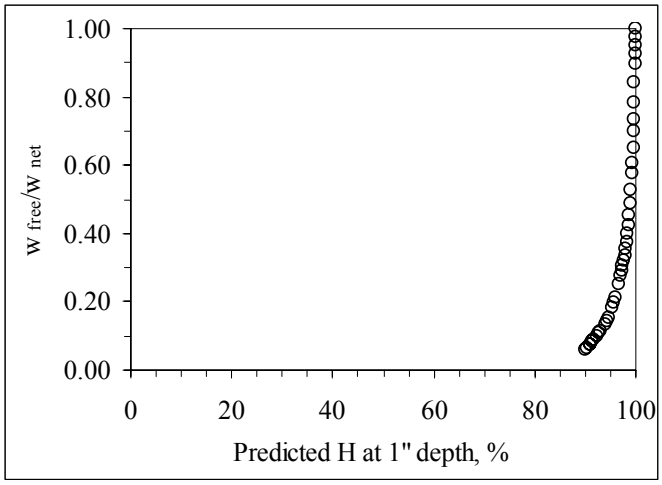

Figure B-1. Free Moisture Sensitivity to Relative Humidity Changes [w_0=0.32]

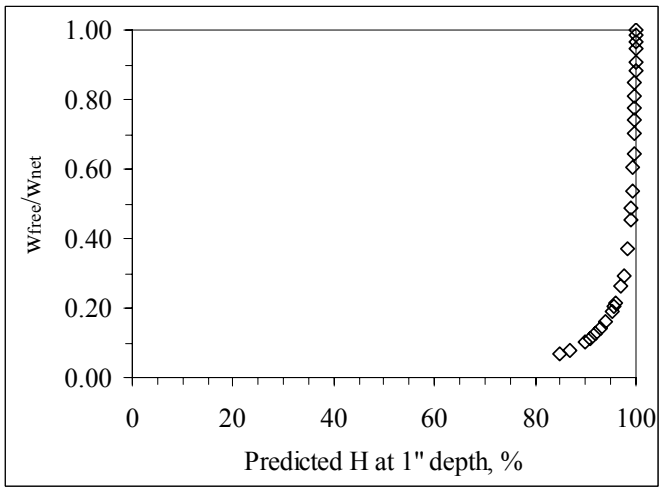

Figure B-2. Free Moisture Sensitivity to Relative Humidity Changes [w_0=0.36]

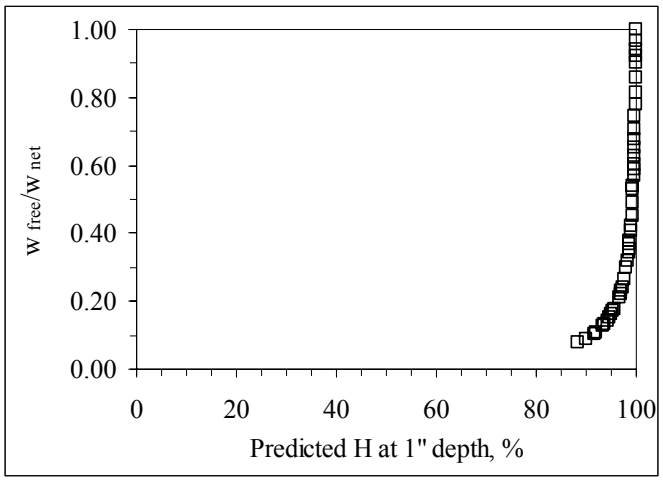

Figure B-3. Free Moisture Sensitivity to Relative Humidity Changes [w_0=0.40]

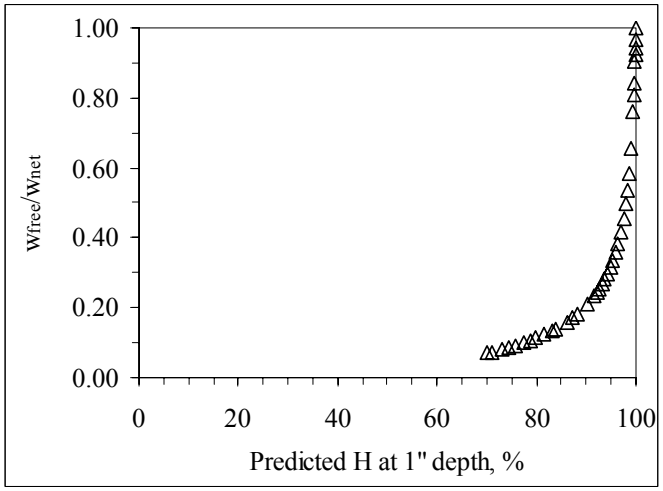

Figure B-4. Free Moisture Sensitivity to Relative Humidity Changes [w_0=0.44]

DIELECTRIC VALUE VS. H

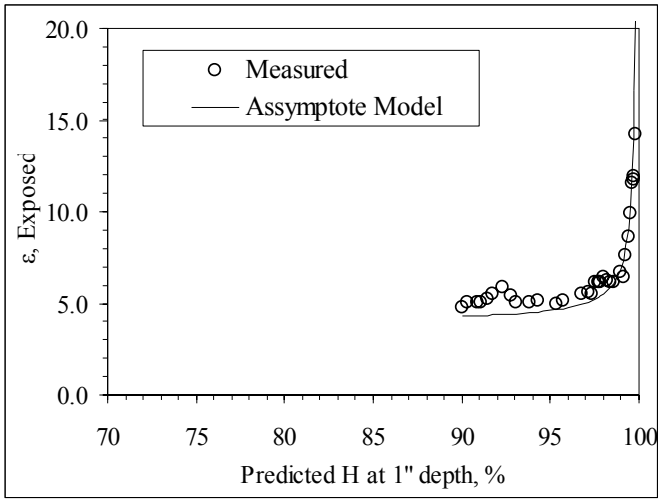

Figure B-5. Dielectric Constant Sensitivity to Relative Humidity [w_0=0.32]

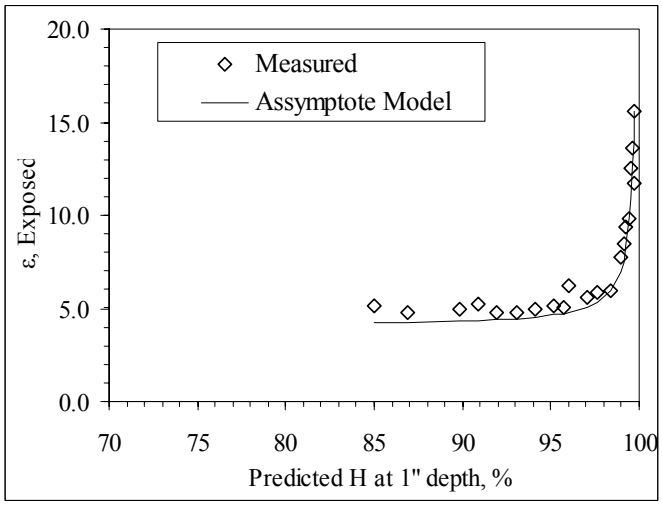

Figure B-6. Dielectric Constant Sensitivity to Relative Humidity [w_0=0.36]

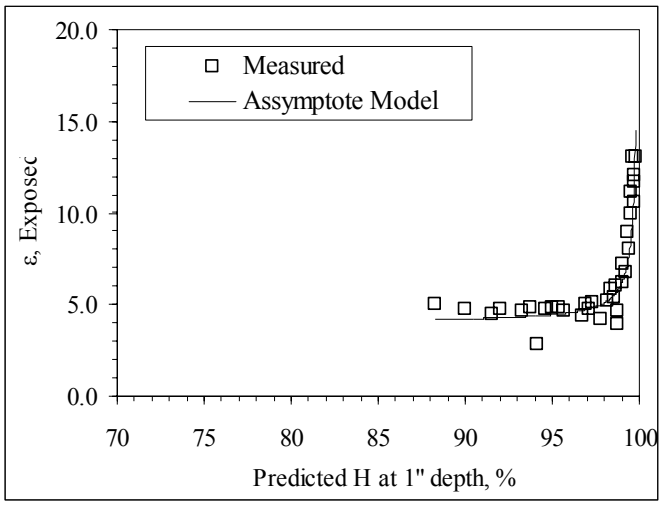

Figure B-7. Dielectric Constant Sensitivity to Relative Humidity [w_0=0.40]

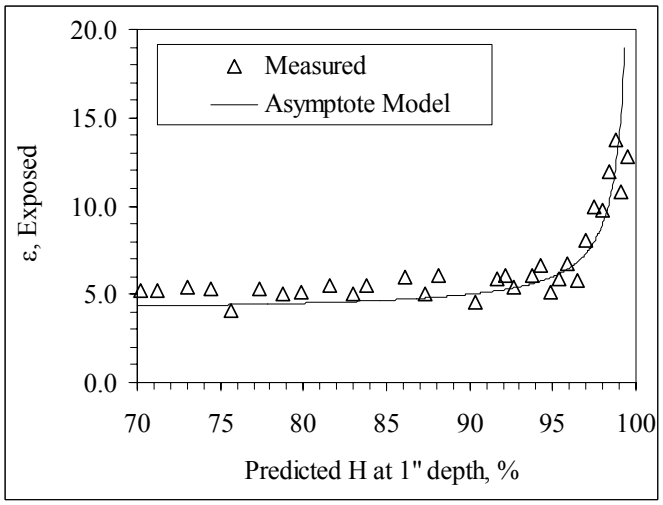

Figure B-8. Dielectric Constant Sensitivity to Relative Humidity [w_0=0.44]

DIELECTRIC VALUE VS. DEGREE OF HYDRATION

EXPOSED LEVEL

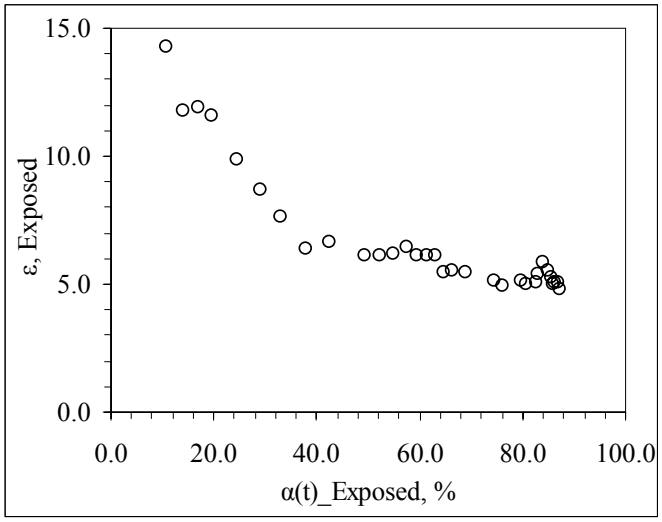

Figure B-9. Dielectric Constant Sensitivity to Degree of Hydration (Exposed) [w_0=0.32]

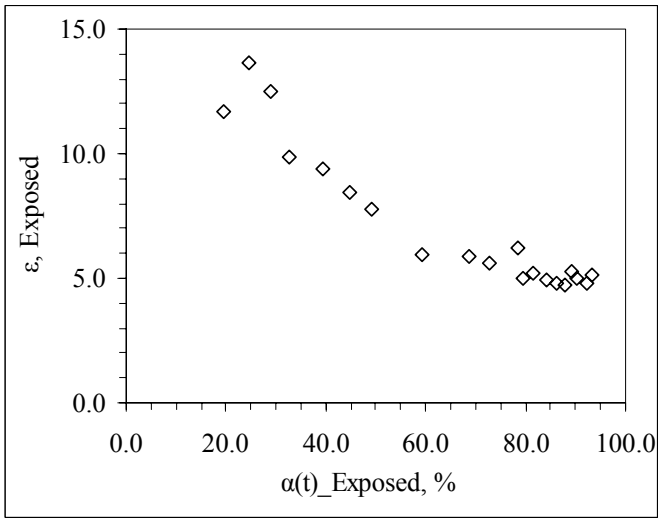

Figure B-10. Dielectric Constant Sensitivity to Degree of Hydration (Exposed) [w_0=0.36]

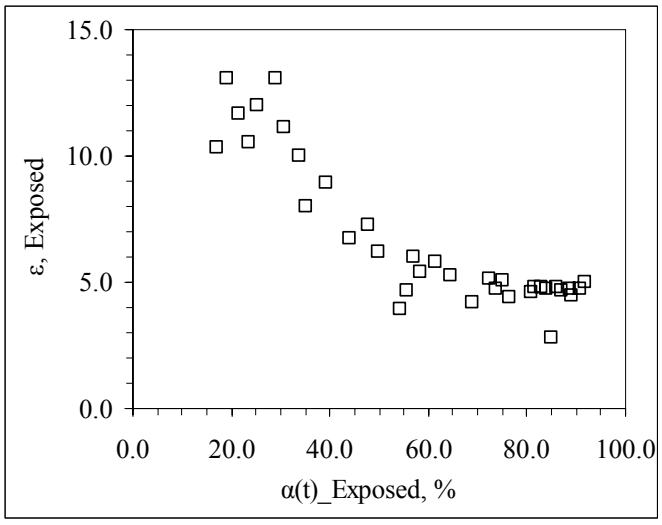

Figure B-11. Dielectric Constant Sensitivity to Degree of Hydration (Exposed) [w_0=0.40]

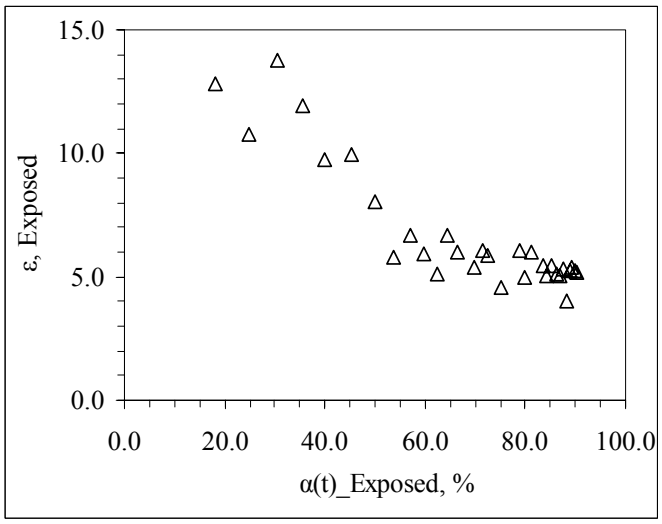

Figure B-12. Dielectric Constant Sensitivity to Degree of Hydration (Exposed) [w_0=0.44]

COVERED LEVEL

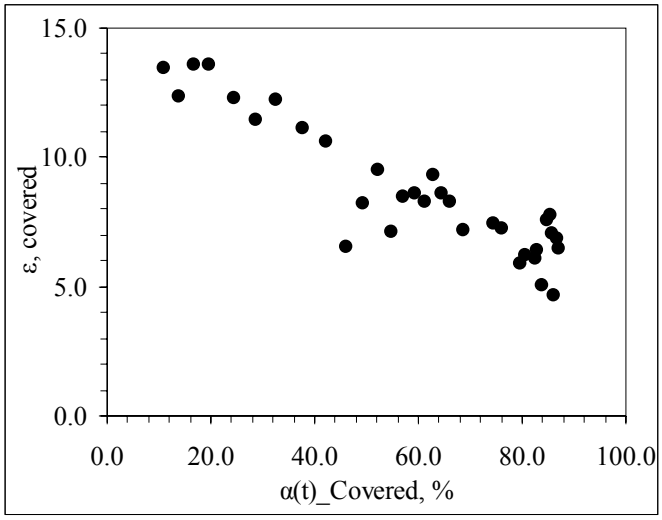

Figure B-13. Dielectric Constant Sensitivity to Degree of Hydration (Covered) [w_0=0.32]

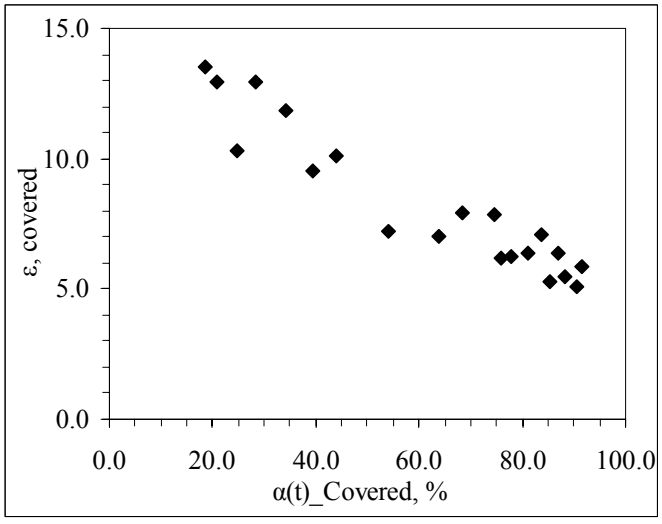

Figure B-14. Dielectric Constant Sensitivity to Degree of Hydration (Covered) [w_0=0.36]

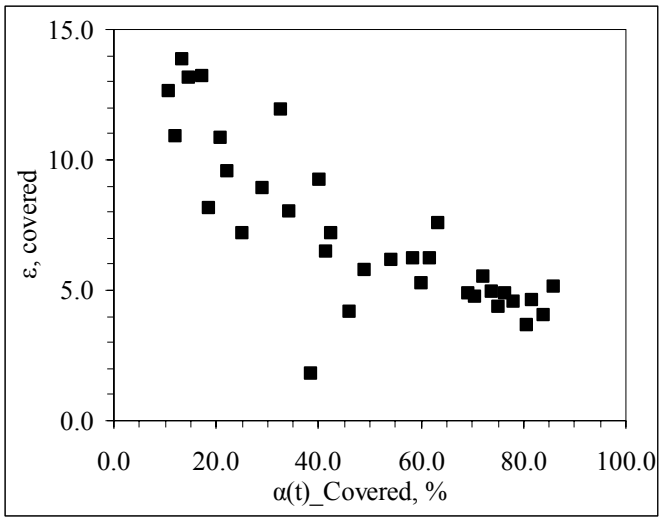

Figure B-15. Dielectric Constant Sensitivity to Degree of Hydration (Covered) [w_0=0.40]

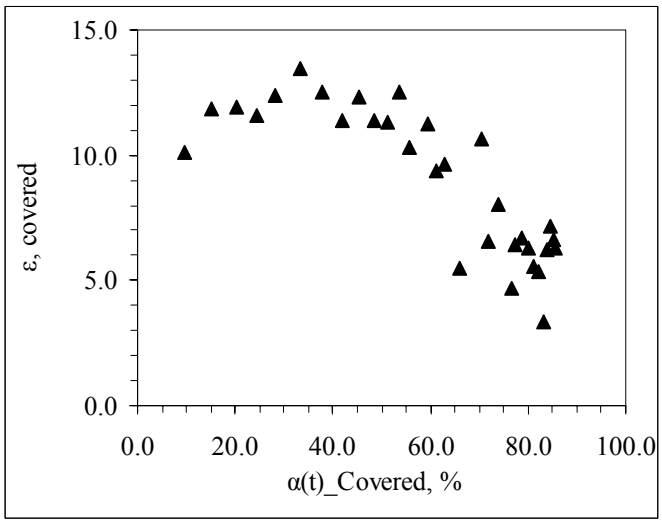

Figure B-16. Dielectric Constant Sensitivity to Degree of Hydration (Covered) [w_0=0.44]

DIELECTRIC VALUE VS. FREE MOISTURE AND CRIM APPROXIMATION

EXPOSED LEVEL

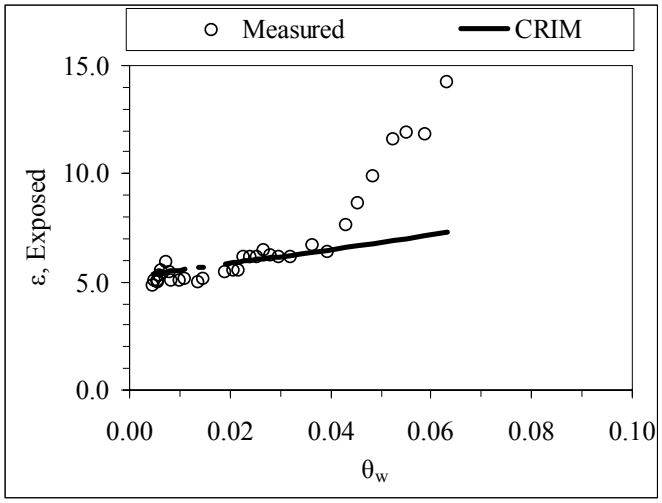

Figure B-17. Dielectric Constant, Free Moisture and CRIM Fit (Exposed) [w_0=0.32]

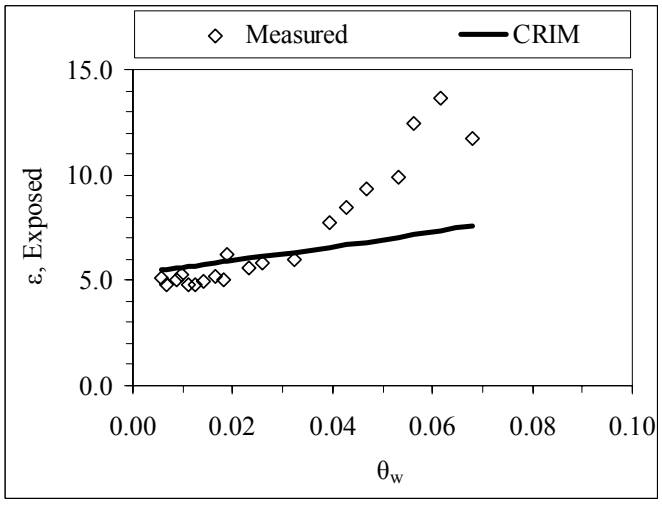

Figure B-18. Dielectric Constant, Free Moisture and CRIM Fit (Exposed) [w_0=0.36]

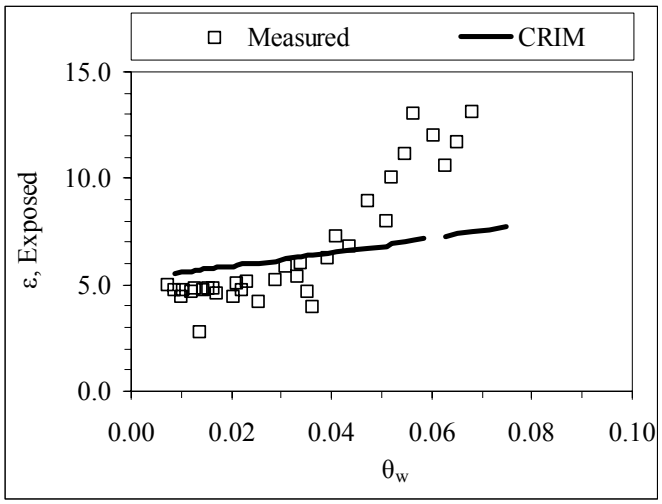

Figure B-19. Dielectric Constant, Free Moisture and CRIM Fit (Exposed) [w_0=0.40]

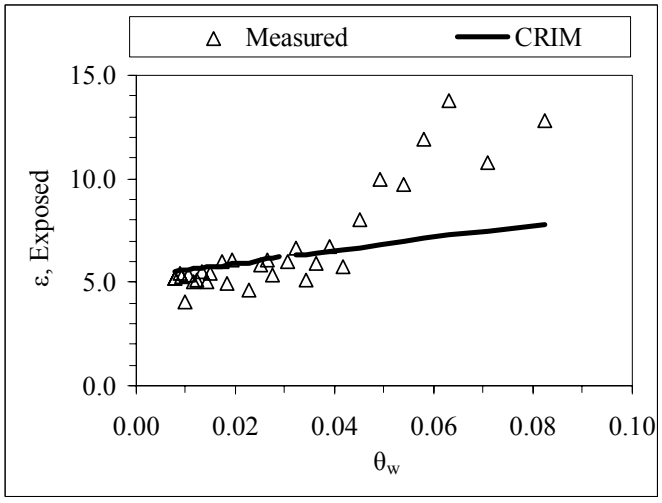

Figure B-20. Dielectric Constant, Free Moisture and CRIM Fit (Exposed) [w_0=0.44]

COVERED LEVEL

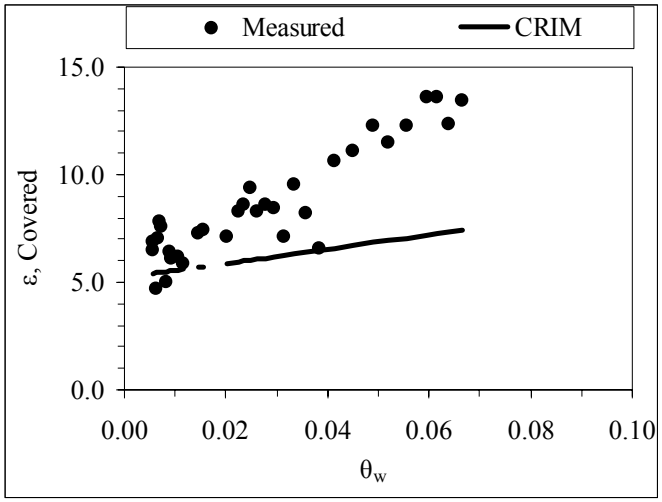

Figure B-21. Dielectric Constant, Free Moisture and CRIM Fit (Covered) [w_0=0.32]

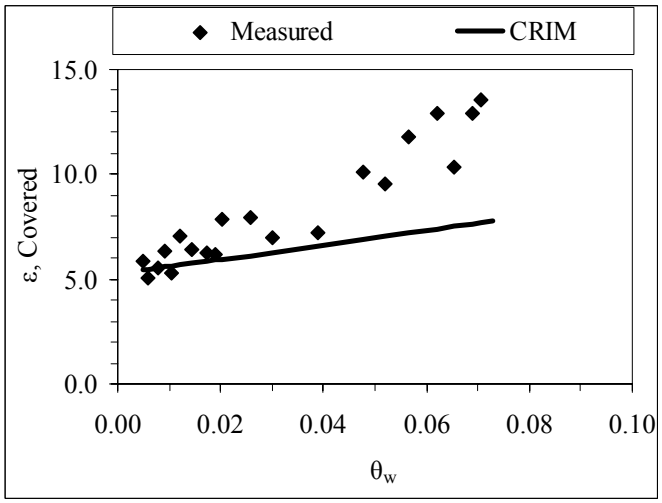

Figure B-22. Dielectric Constant, Free Moisture and CRIM Fit (Covered) [w_0=0.36]

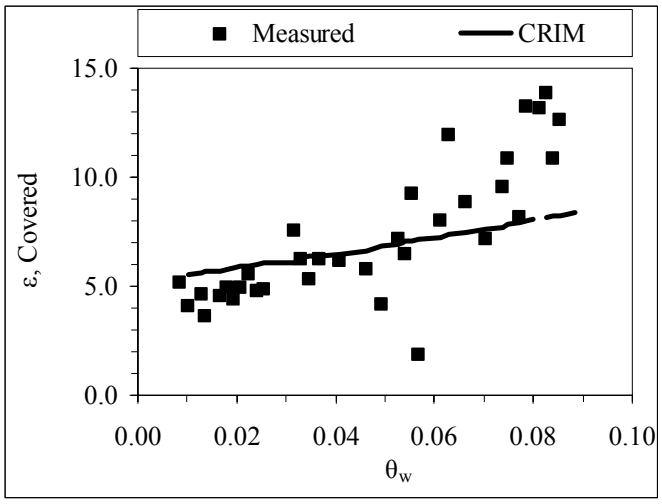

Figure B-23. Dielectric Constant, Free Moisture and CRIM Fit (Covered) [w_0=0.40]

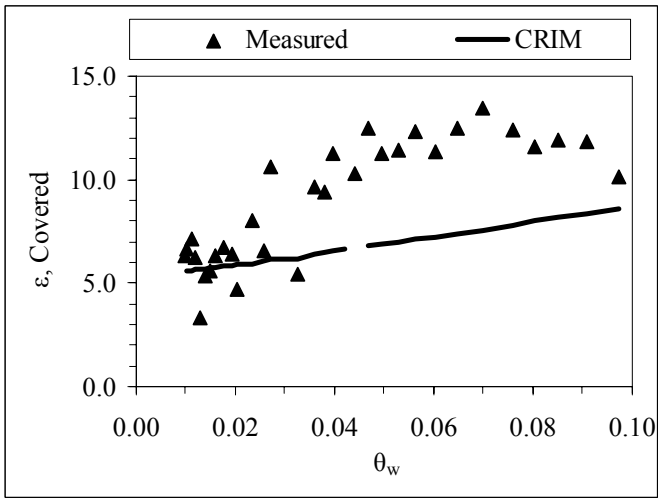

Figure B-24. Dielectric Constant, Free Moisture and CRIM Fit (Covered) [w_0=0.44]

CRIM CALIBRATION

EXPOSED LEVEL

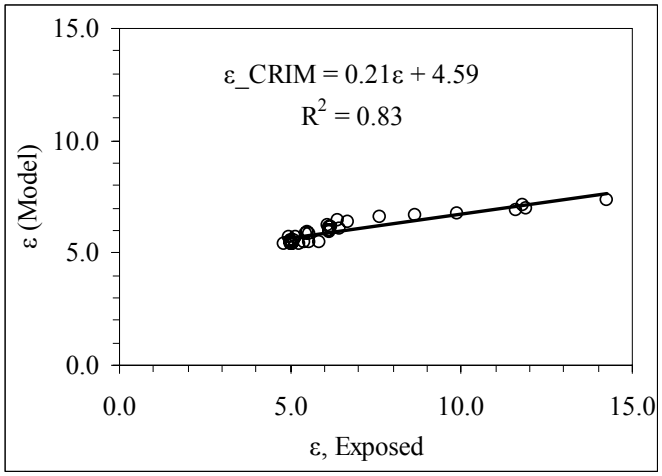

Figure B-25. CRIM Statistical Calibration (Exposed) [w_0=0.32]

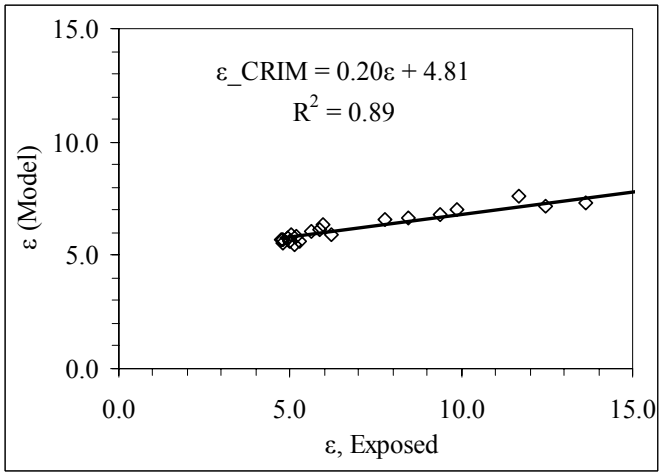

Figure B-26. CRIM Statistical Calibration (Exposed) [w_0=0.36]

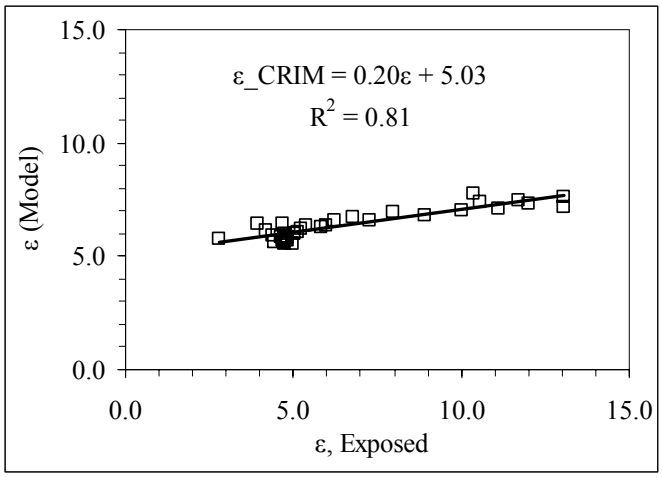

Figure B-27. CRIM Statistical Calibration (Exposed) [w_0=0.40]

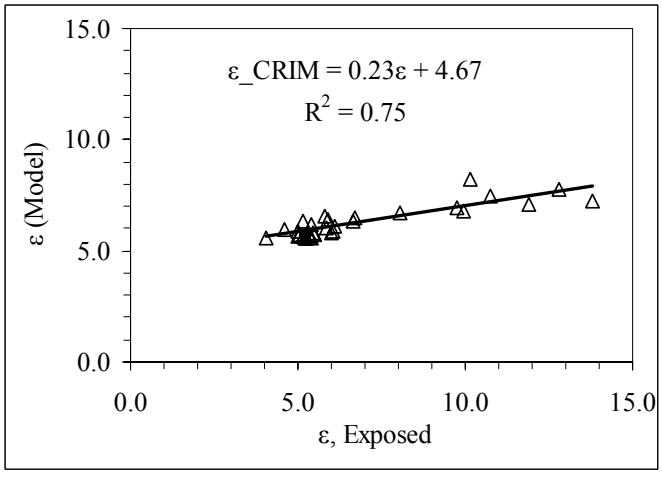

Figure B-28. CRIM Statistical Calibration (Exposed) [w_0=0.44]

COVERED LEVEL

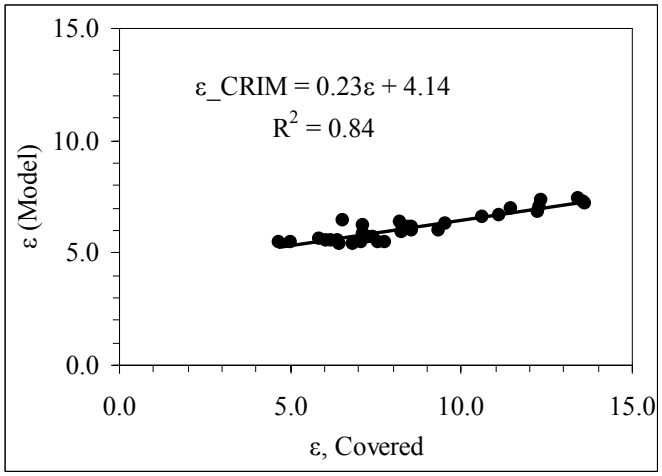

Figure B-29. CRIM Statistical Calibration (Covered) [w_0=0.32]

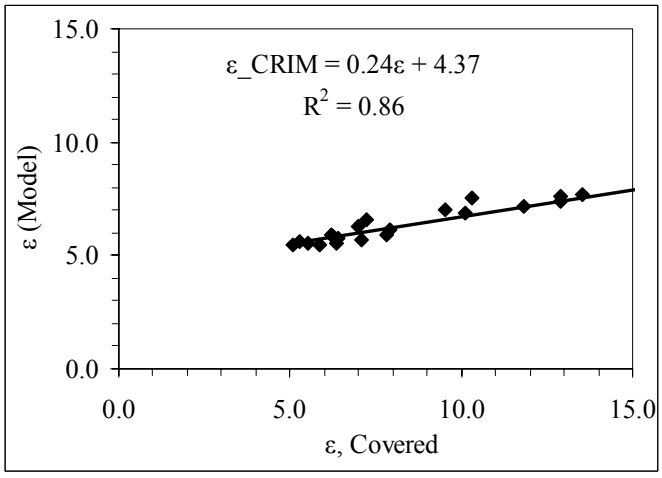

Figure B-30. CRIM Statistical Calibration (Covered) [w_0=0.36]

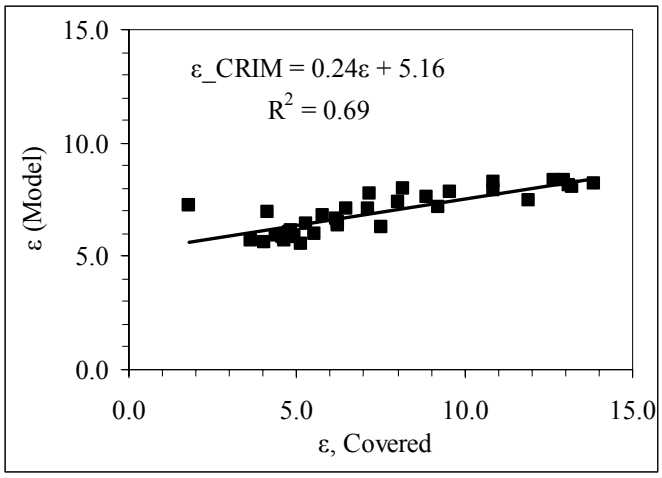

Figure B-31. CRIM Statistical Calibration (Covered) [w_0=0.40]

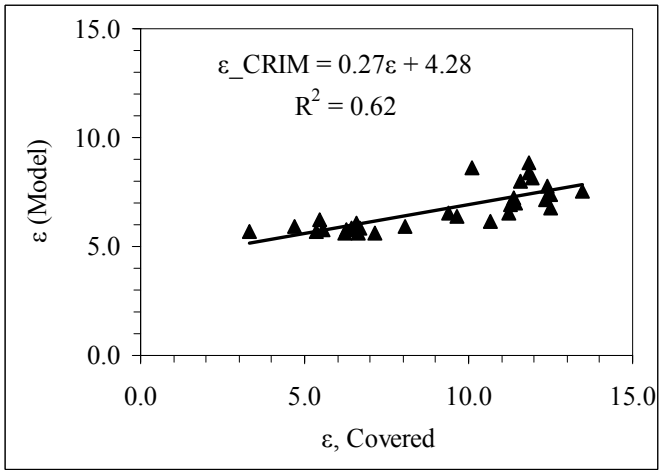

Figure B-32. CRIM Statistical Calibration (Covered) [w_0=0.44]

APPENDIX C

STATISTICAL ANALYSIS

EFFECT OF EXPOSURE ON DIELECTRIC VALUE

0.32 TREATMENT

Table C-1. Paired T-Test and Confidence Interval: DC0.32[cov], DC0.32[exp]

Parameter	N	Mean	Std. Dev	SE Mean
DC0.32[cov]	32	8.711	2.576	0.455
DC0.32[exp]	32	6.746	2.452	0.433
Difference	32	1.965	1.326	0.234

95% CI for mean difference: (1.486, 2.443)

T-Test of mean difference, $H_0 = 0$ (vs $H_a = 0$): T-Value = 8.38, P-Value = 0.000

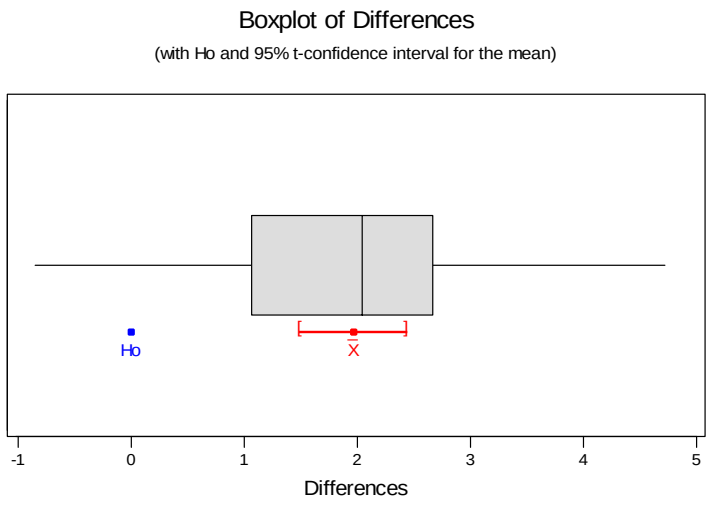

Figure C-1. Boxplot of Differences in Dielectric Constant between Covered and Exposed Measurements [w_0=0.32]

0.36 TREATMENT

Table C-2. Paired T-Test and Confidence Interval: DC0.36[cov], DC0.36[exp]

Parameter	N	Mean	Std. Dev	SE Mean
DC0.36[cov]	21	8.681	3.336	0.728
DC0.36[exp]	21	7.492	3.337	0.728
Difference	21	1.190	1.670	0.364

95% CI for mean difference: (0.429, 1.950)

T-Test of mean difference, $H_0 = 0$ (vs $H_a = 0$): T-Value = 3.26, P-Value = 0.004

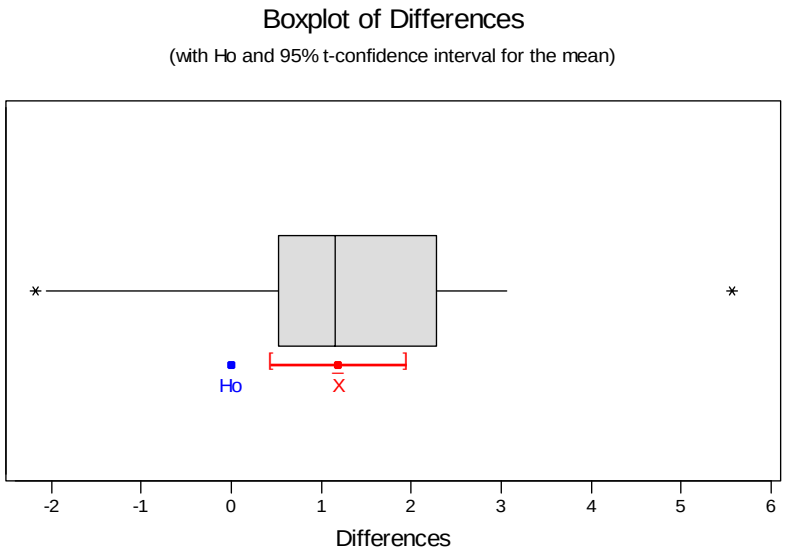

Figure C-2. Boxplot of Differences in Dielectric Constant between Covered and Exposed Measurements [w_0=0.36]

0.40 TREATMENT

Table C-3. Paired T-Test and Confidence Interval: DC0.40[cov], DC0.40[exp]

Parameter	N	Mean	Std. Dev	SE Mean
DC0.40[cov]	34	7.225	3.156	0.541
DC0.40[exp]	34	6.570	2.901	0.497
Difference	34	0.654	1.706	0.293

95% CI for mean difference: (0.059, 1.250)

T-Test of mean difference, $H_0 = 0$ (vs $H_a = 0$): T-Value = 2.24, P-Value = 0.032

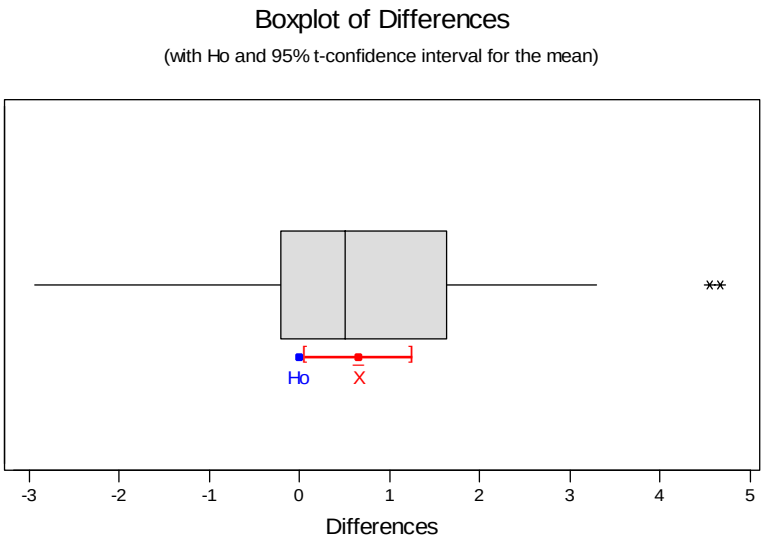

Figure C-3. Boxplot of Differences in Dielectric Constant between Covered and Exposed Measurements [w_0=0.40]

0.44 TREATMENT

Table C-4. Paired T-Test and Confidence Interval: DC0.44[cov], DC0.44[exp]

Parameter	N	Mean	Std. Dev	SE Mean
DC0.44[cov]	31	8.992	2.925	0.525
DC0.44[exp]	31	6.733	2.559	0.460
Difference	31	2.259	2.443	0.439

95% CI for mean difference: (1.363, 3.155)

T-Test of mean difference, $H_0 = 0$ (vs $H_a = 0$): T-Value = 5.15, P-Value = 0.000

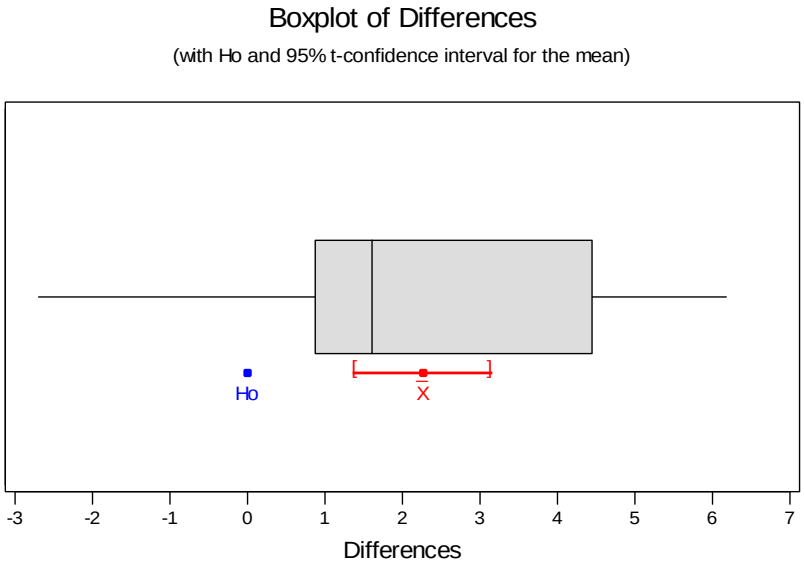

Figure C-4. Boxplot of Differences in Dielectric Constant between Covered and Exposed Measurements [w_0=0.44]

REGRESSION STATISTICS AND ANOVA FOR ASYMPTOTE MODEL

0.32 TREATMENT

Table C-5. Analysis of Variance: DC0.32(H_asymptote) versus DC0.32[exp]

Source	DF	SSE	MSE	F-Statistic	P-Value
Regression	1	467.815	467.815	646.84	0.000
Error	30	21.697	0.723		
Total	31	489.511			

Regression Equation: DC0.32(H_asymptote) = - 3.897 + 1.585 DC0.32[exp]

S = 0.850427, R^2 = 95.6%, R^2(adj) = 95.4%

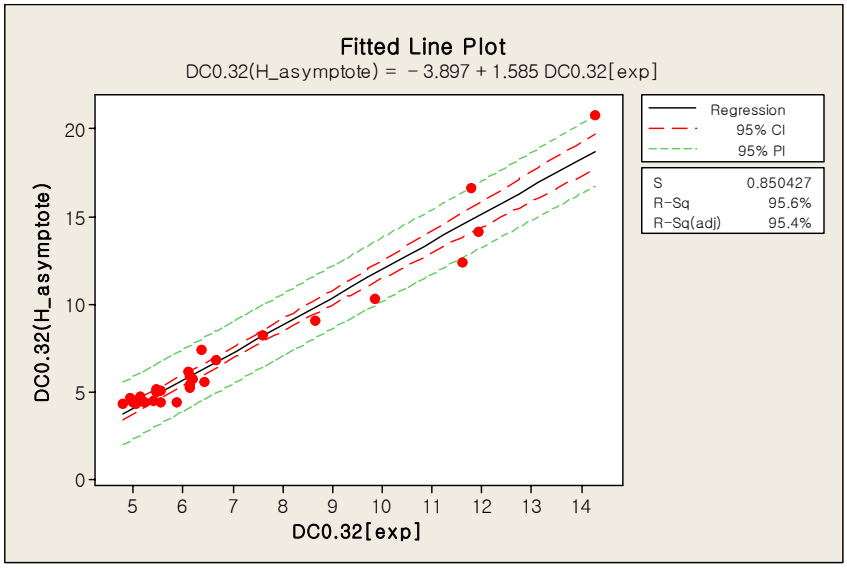

Figure C-5. Regression Fit for Asymptote Model [w_0=0.32]

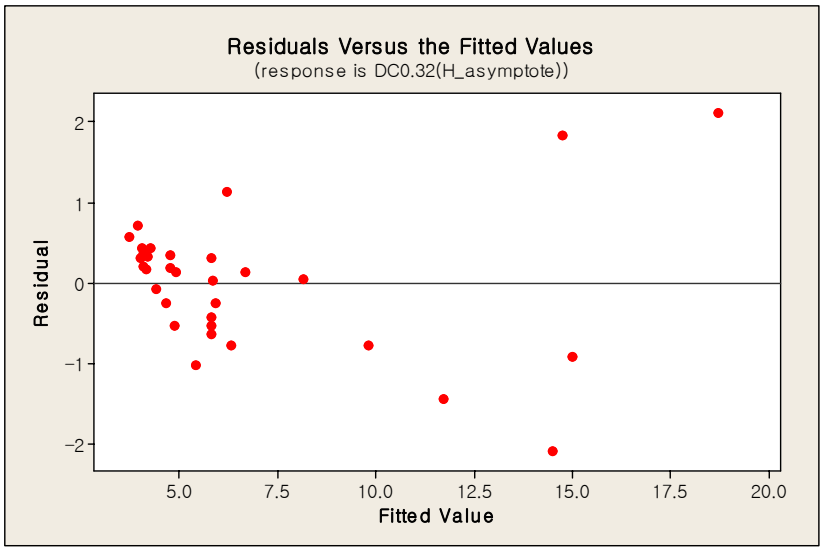

Figure C-6. Residual Plot for Asymptote Model [w_0=0.32]

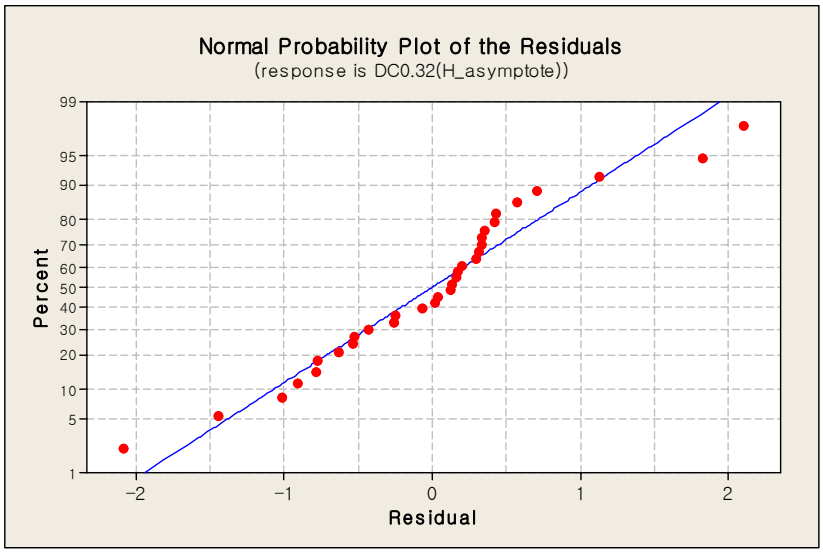

Figure C-7. Normal Probability Plot for Asymptote Model Residuals [w_0=0.32]

0.36 TREATMENT

Table C-6. Analysis of Variance: DC0.36(H_asymptote) versus DC0.36[exp]

Source	DF	SSE	MSE	F-Statistic	P-Value
Regression	1	227.559	227.559	179.01	0.000
Error	19	24.153	1.271		
Total	20	251.711			

Regression equation: DC0.36(H_asymptote) = - 0.5986 + 1.011 DC0.36[exp]

S = 1.12747, R^2 = 90.4%, R^2(adj) = 89.9%

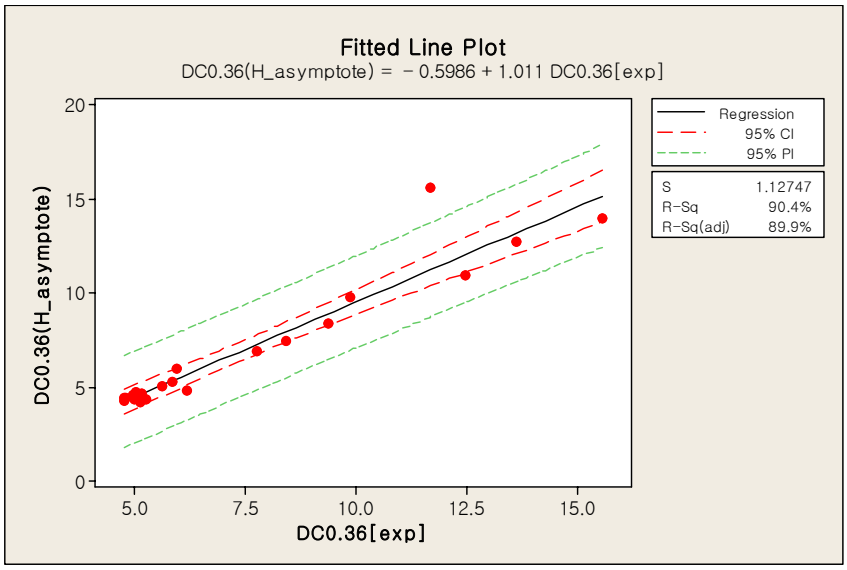

Figure C-8. Regression Fit for Asymptote Model [w_0=0.36]

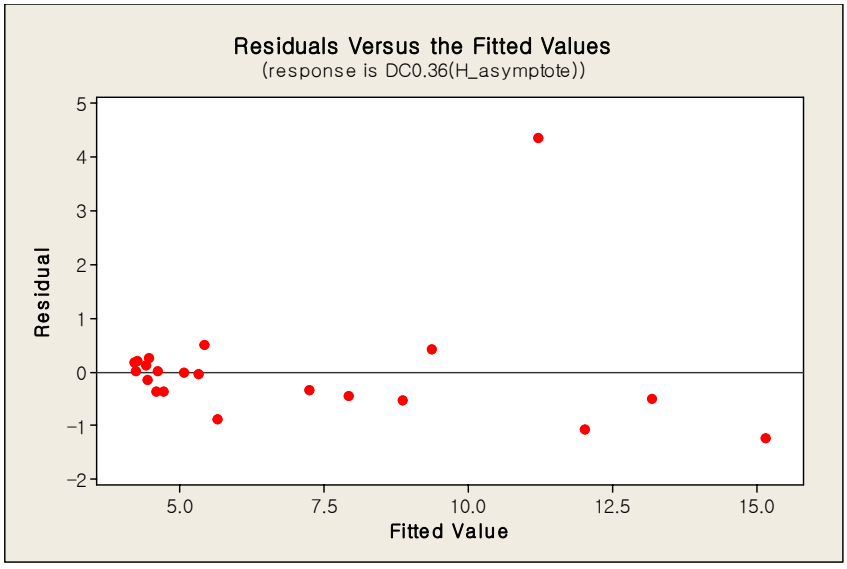

Figure C-9. Residual Plot for Asymptote Model [w_0=0.36]

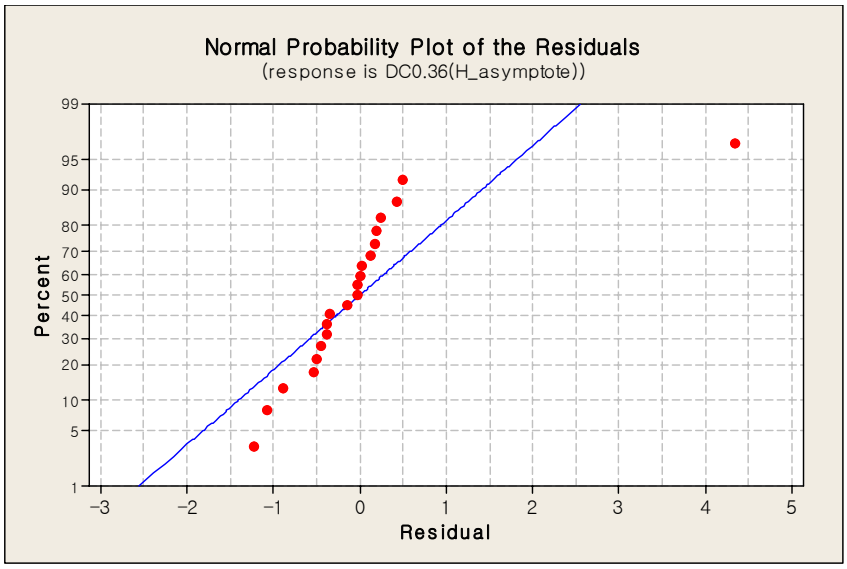

Figure C-10. Normal Probability Plot for Asymptote Model Residuals [w_0=0.36]

0.40 TREATMENT

Table C-7. Analysis of Variance: DC0.40(H_asymptote) versus DC0.40[exp]

Source	DF	SSE	MSE	F-Statistic	P-Value
Regression	1	210.584	210.584	142.73	0.000
Error	33	48.689	1.475		
Total	34	259.273			

Regression equation: DC0.40(H_asymptote) = 0.7884 + 0.8499 DC0.40[exp]

S = 1.21467, R^2 = 81.2%, R^2(adj) = 80.7%

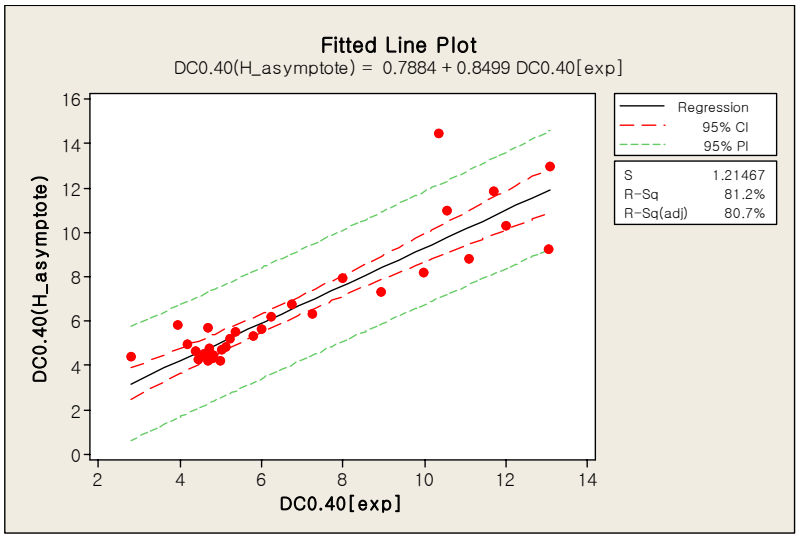

Figure C-11. Regression Fit for Asymptote Model [w_0=0.40]

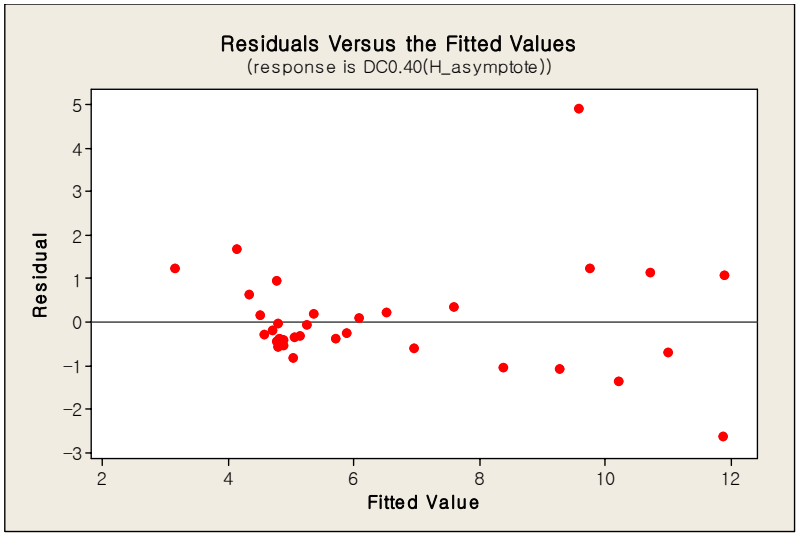

Figure C-12. Residual Plot for Asymptote Model [w_0=0.40]

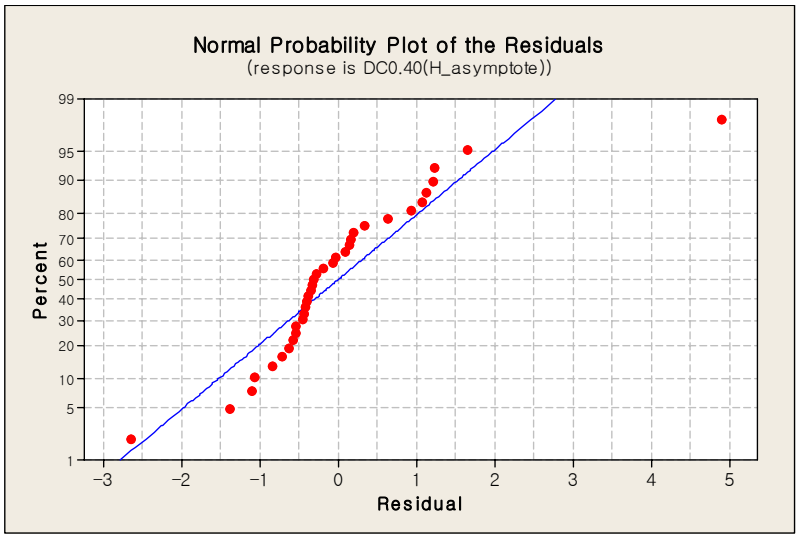

Figure C-13. Normal Probability Plot for Asymptote Model Residuals [w_0=0.40]

0.44 TREATMENT

Table C-8. Analysis of Variance: DC0.44(H_asymptote) versus DC0.44[exp]

Source	DF	SSE	MSE	F-Statistic	P-Value
Regression	1	329.170	329.170	76.61	0.000
Error	29	124.611	4.297		
Total	30	453.781			

Regression equation: DC0.44(H_asymptote) = - 2.090 + 1.294 DC0.44[exp]

S = 2.07290, R^2 = 72.5%, R^2(adj) = 71.6%

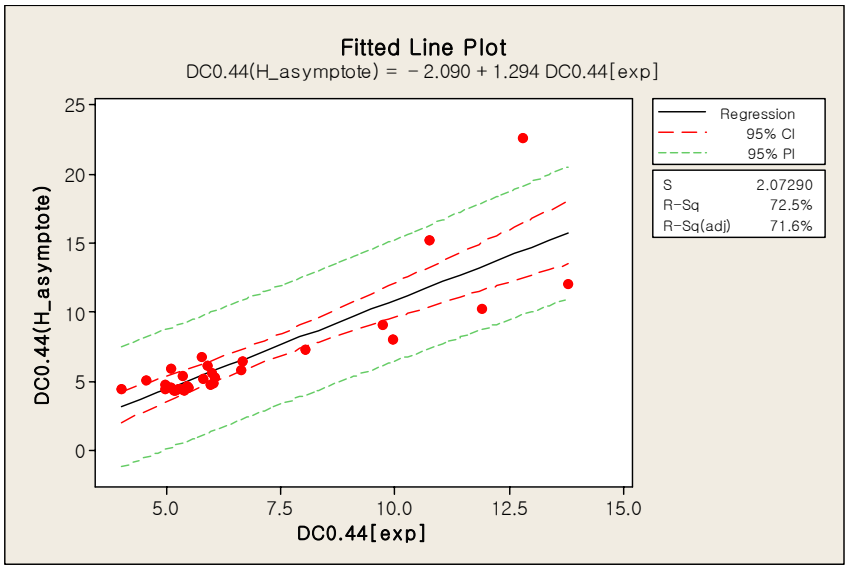

Figure C-14. Regression Fit for Asymptote Model [w_0=0.44]

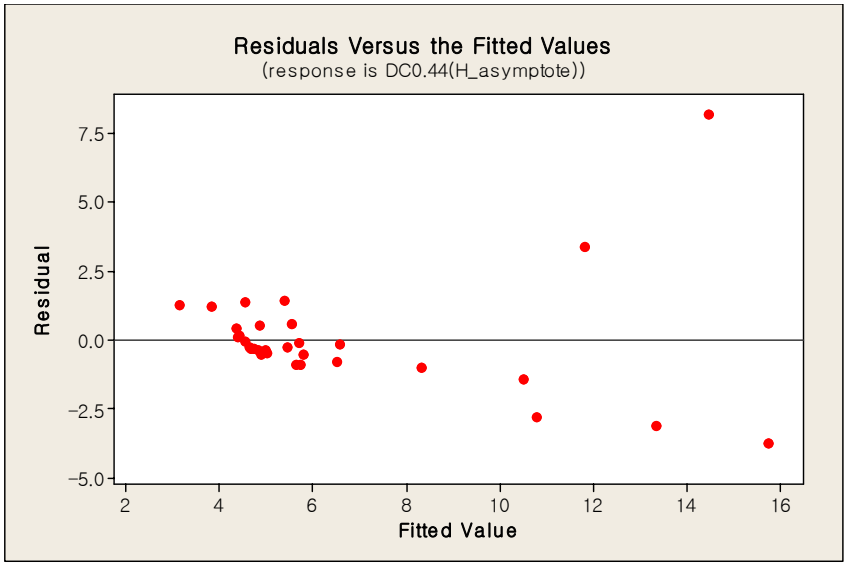

Figure C-15. Residual Plot for Asymptote Model [w_0=0.44]

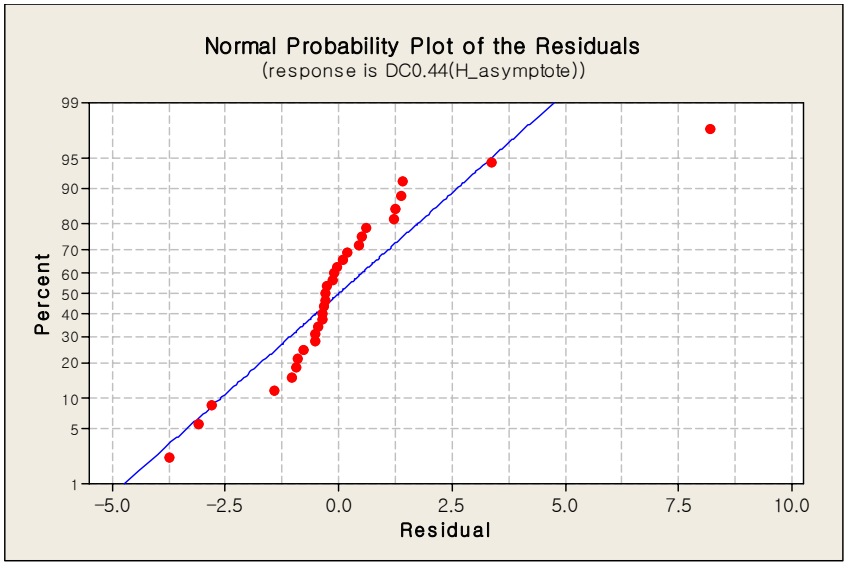

Figure C-16. Normal Probability Plot for Asymptote Model Residuals [w_0=0.44]

ANALYSIS OF VARIANCE FOR CRIM FIT

EXPOSED LEVEL

Table C-9. Regression Analysis: DC0.32model versus DC0.32[exp]

Predictor	Coeff.	SE Coeff.	T-value	P-value
Constant	4.5964	0.1268	36.24	0.000
DC0.32[exp]	0.21278	0.01770	12.02	0.000

Regression equation: DC0.32model = 4.60 + 0.213 DC0.32[exp]

S = 0.2417, R^2 = 82.8%, R^2(adj) = 82.2%

Table C-10. Analysis of Variance: DC0.32model versus DC0.32[exp]

Source	DF	SSE	MSE	F-statistic	P-value
Regression	1	8.4357	8.4357	144.45	0.000
Residual Error	30	1.7520	0.0584		
Total	31	10.1877			

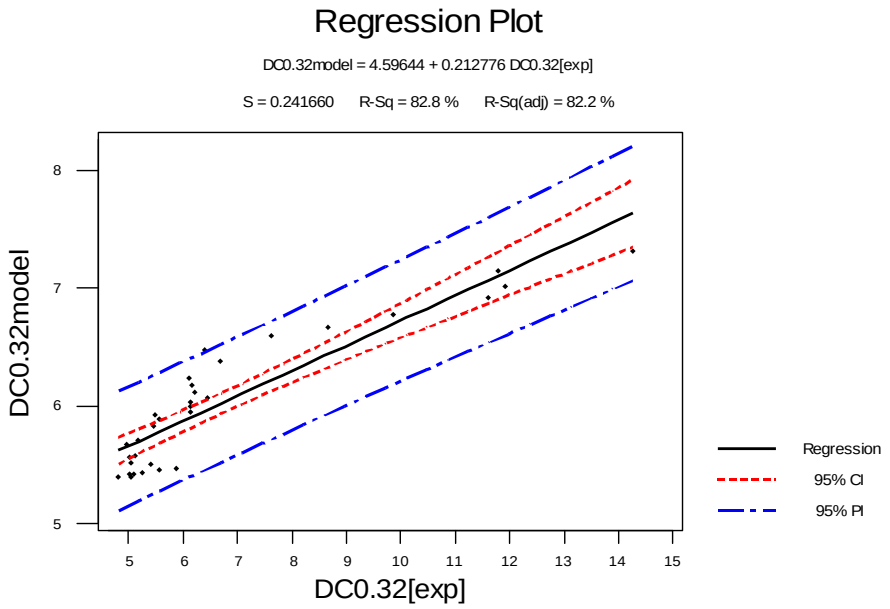

Figure C-17. Regression Plot for CRIM Fit (Exposed) [w_0=0.32]

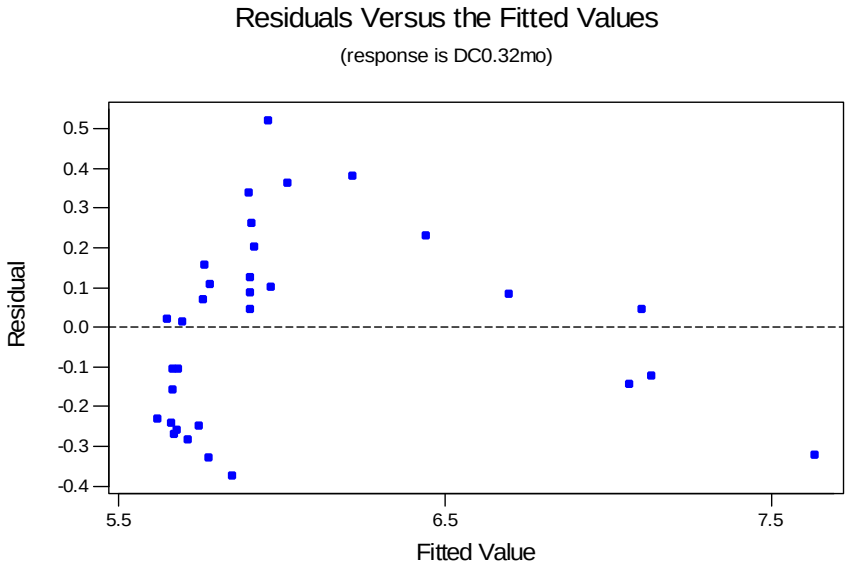

Figure C-18. Residual Plot for CRIM Fit (Exposed) [w_0=0.32]

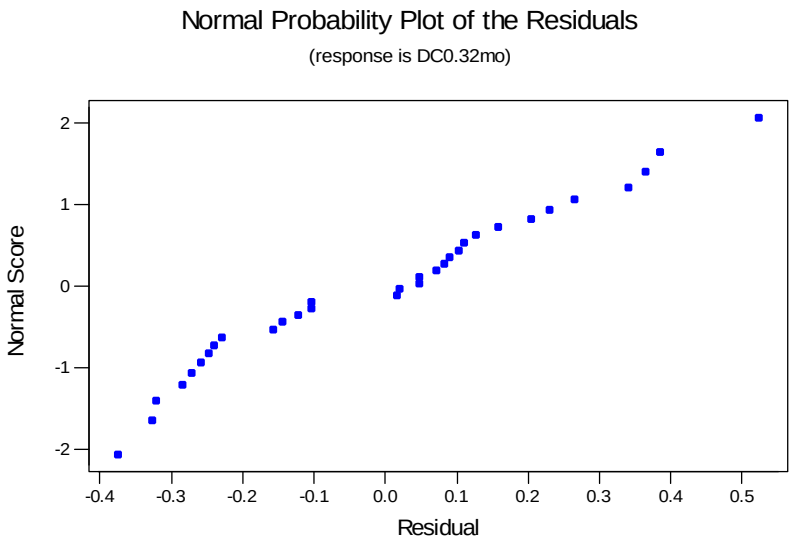

Figure C-19. Normal Probability Plot for CRIM Fit (Exposed) [w_0=0.32]

Table C-11. Regression Analysis: DC0.36model versus DC0.36[exp]

Predictor	Coeff.	SE Coeff	T-value	P-value
Constant	4.8062	0.1306	36.79	0.000
DC0.36[exp]	0.19805	0.01599	12.38	0.000

Regression equation: DC0.36model = 4.81 + 0.198 DC0.36[exp]

S = 0.2387, R^2 = 89.0%, R^2(adj) = 88.4%

Table C-12. Analysis of Variance: DC0.36model versus DC0.36[exp]

Source	DF	SSE	MSE	F-statistic	P-value
Regression	1	8.7362	8.7362	153.38	0.000
Residual Error	19	1.0822	0.0570		
Total	20	9.8184			

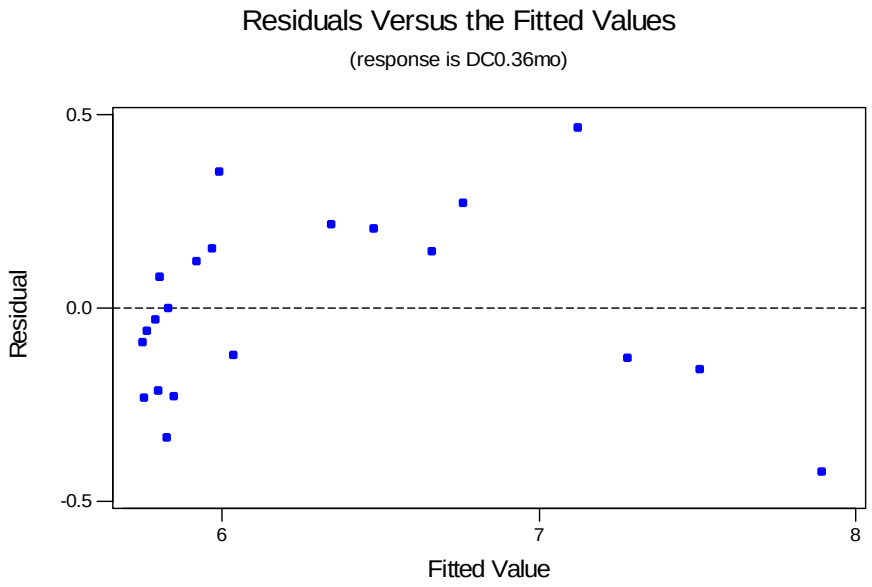

Figure C-20. Residual Plot for CRIM Fit (Exposed) [w_0=0.36]

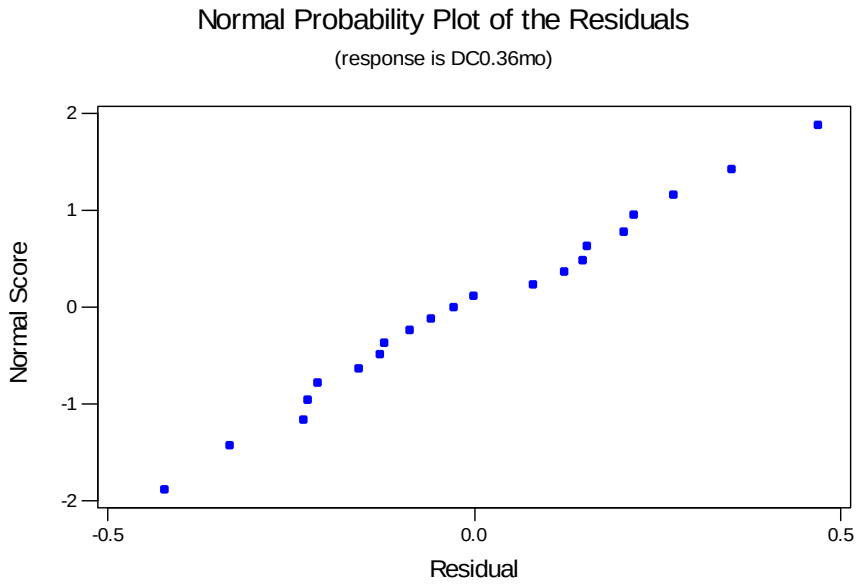

Figure C-21. Normal Probability Plot for CRIM Fit (Exposed) [w_0=0.36]

Table C-13. Regression Analysis: DC0.40model versus DC0.40[exp]

Predictor	Coeff.	SE Coeff	T-value	P-value
Constant	5.0338	0.1243	40.51	0.000
DC0.40[exp]	0.20106	0.01708	11.77	0.000

Regression equation: DC0.40model = 5.03 + 0.201 DC0.40[exp]

S = 0.2917, R^2 = 80.8%, R^2(adj) = 80.2%

Table C-14. Analysis of Variance: DC0.40model versus DC0.40[exp]

Source	DF	SSE	MSE	F-statistic	P-value
Regression	1	11.785	11.785	138.55	0.000
Residual Error	33	2.807	0.085		
Total	34	14.592			

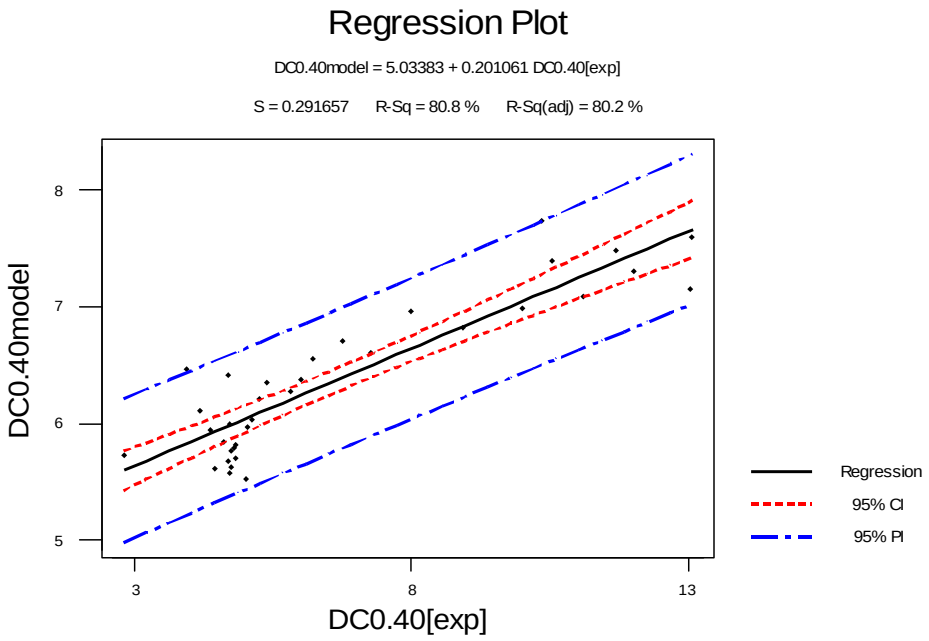

Figure C-22. Regression Plot for CRIM Fit (Exposed) [w_0=0.40]

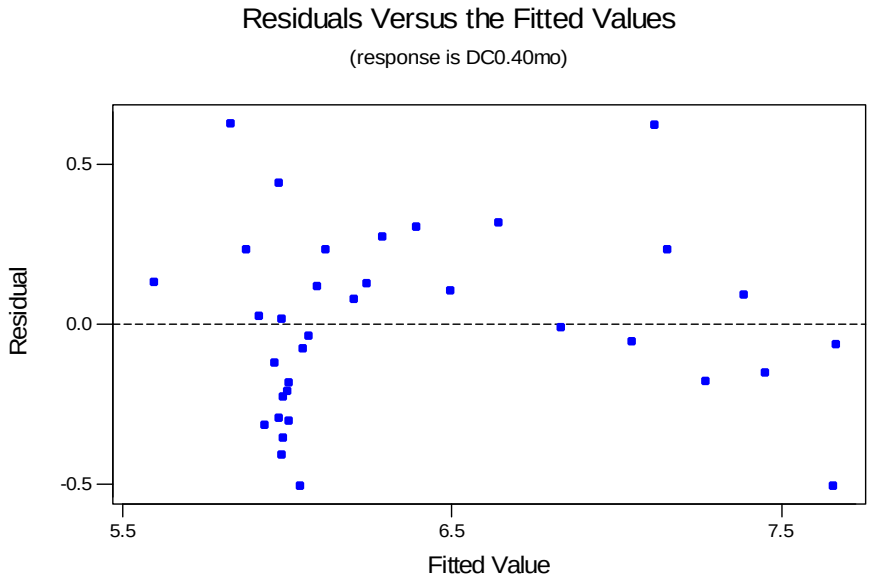

Figure C-23. Residual Plot for CRIM Fit (Exposed) [w_0=0.40]

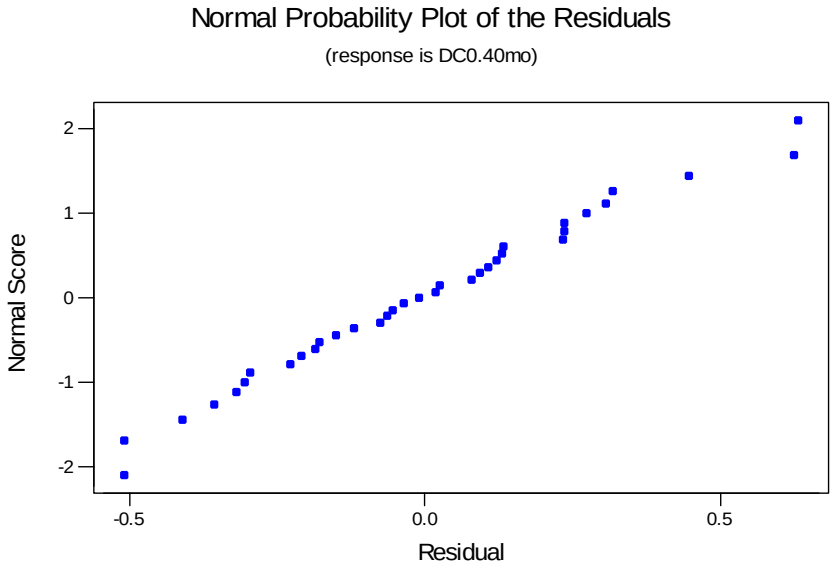

Figure C-24. Normal Probability Plot for CRIM Fit (Exposed) [w_0=0.40]

Table C-15. Regression Analysis: DC0.44model versus DC0.44[exp]

Predictor	Coeff.	SE Coeff	T-value	P-value
Constant	4.6259	0.1624	28.48	0.000
DC0.44[exp]	0.24720	0.02260	10.94	0.000

Regression equation: DC0.44model = 4.63 + 0.247 DC0.44[exp]

S = 0.3167, R^2 = 80.5%, R^2(adj) = 79.8%

Table C-16. Analysis of Variance: DC0.44model versus DC0.44[exp]

Source	DF	SSE	MSE	F-statistic	P-value
Regression	1	12.007	12.007	119.69	0.000
Residual Error	29	2.909	0.100		
Total	30	14.916			

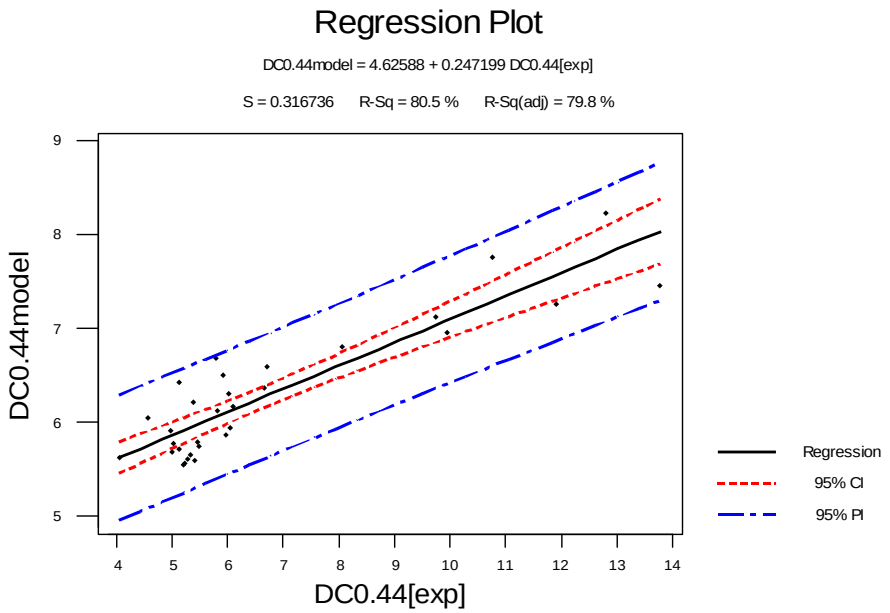

Figure C-25. Regression Plot for CRIM Fit (Exposed) [w_0=0.44]

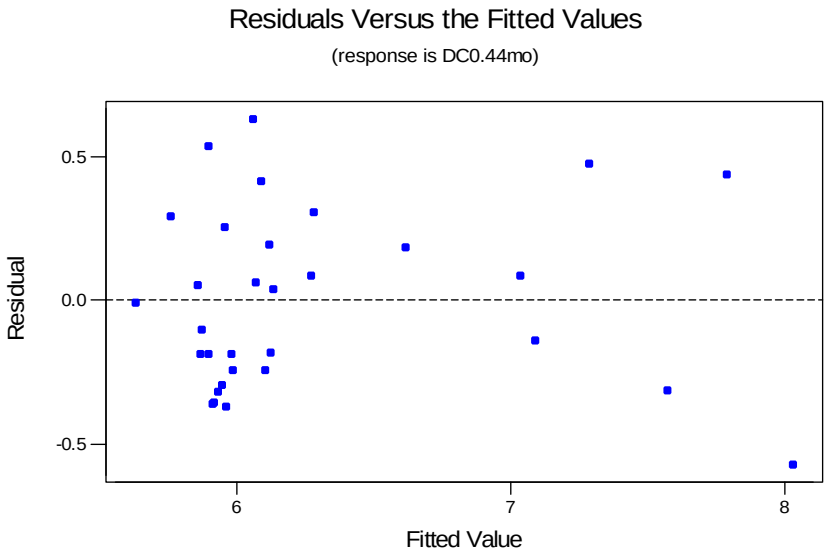

Figure C-26. Residual Plot for CRIM Fit (Exposed) [w_0=0.44]

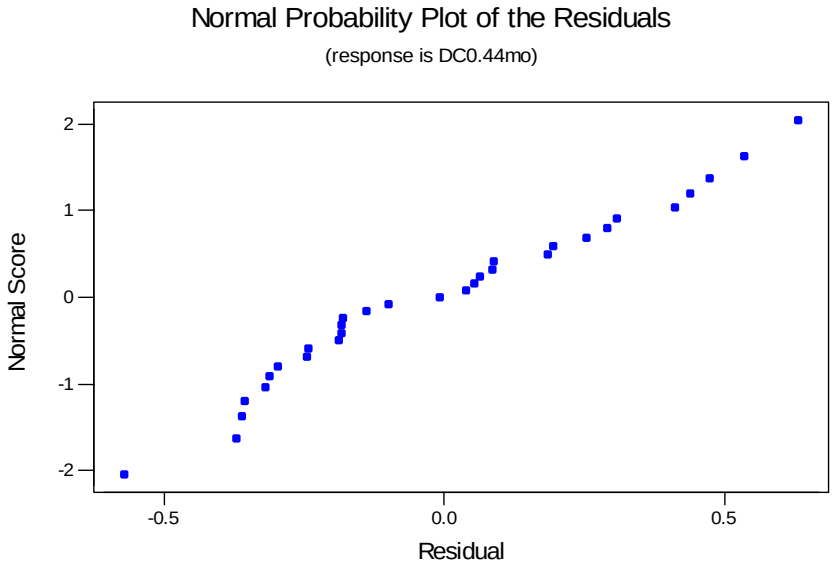

Figure C-27. Normal Probability Plot for CRIM Fit (Exposed) [w_0=0.44]

COVERED LEVEL

Table C-17. Regression Analysis: DC0.32model versus DC0.32[cov]

Predictor	Coeff	SE Coeff	T-value	P-value
Constant	4.1402	0.1639	25.27	0.000
DC0.32[cov]	0.23269	0.01819	12.79	0.000

Regression equation: DC0.32model = 4.14 + 0.233 DC0.32[cov]

S = 0.2638, R^2 = 84.1%, R^2(adj) = 83.6%

Table C-18. Analysis of Variance: DC0.32model versus DC0.32[cov]

Source	DF	SSE	MSE	F-statistic	P-value
Regression	1	11.386	11.386	163.58	0.000
Residual Error	31	2.158	0.070		
Total	32	13.544			

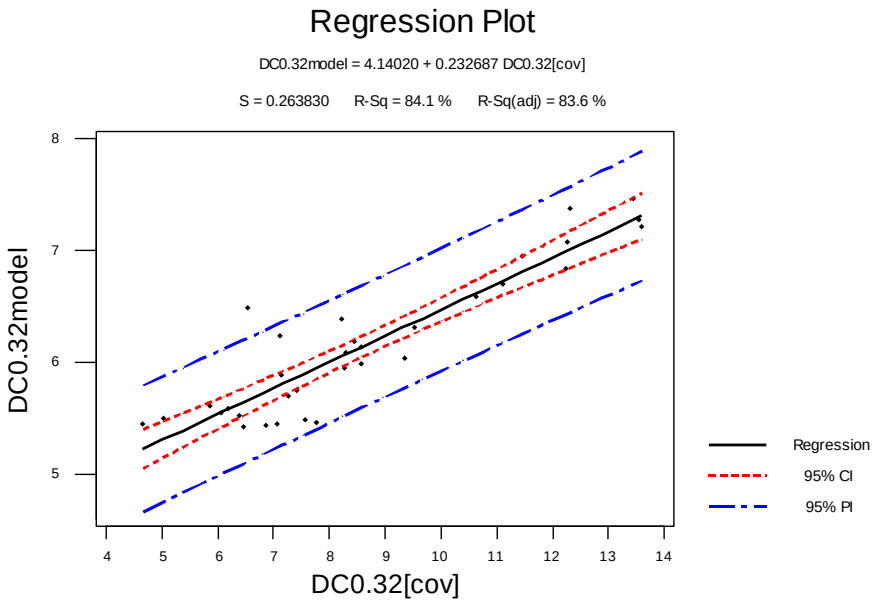

Figure C-28. Regression Plot for CRIM Fit (Covered) [w_0=0.32]

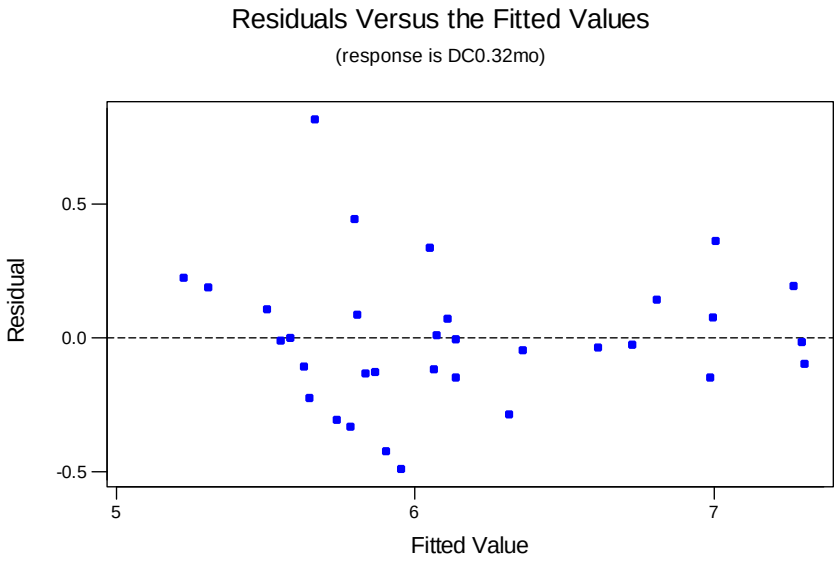

Figure C-29. Residual Plot for CRIM Fit (Covered) [w_0=0.32]

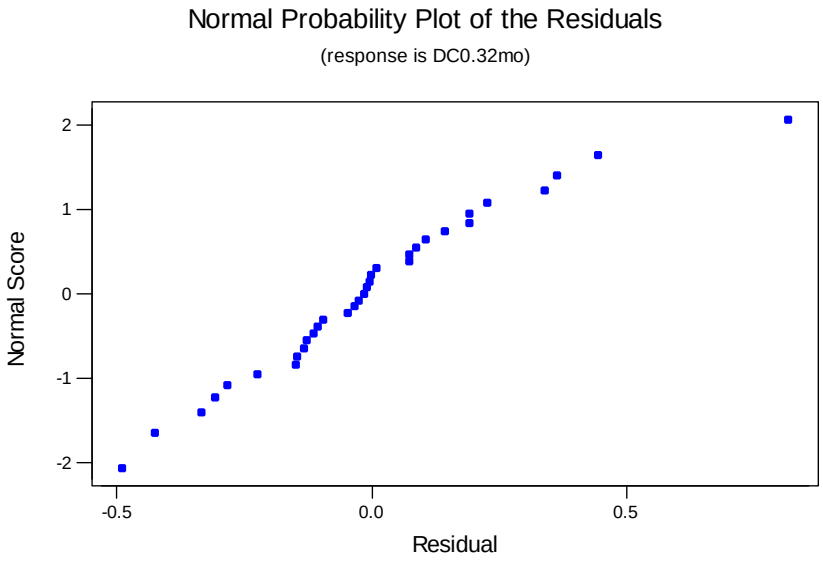

Figure C-30. Normal Probability Plot for CRIM Fit (Covered) [w_0=0.32]

Table C-19. Regression Analysis: DC0.36model versus DC0.36[cov]

Predictor	Coeff	SE Coeff	T-value	P-value
Constant	4.37244	0.1210	20.76	0.000
DC0.36[cov]	0.235800	0.02084	16.09	0.000

Regression equation: DC0.36model = 4.37244 + 0.235800 DC0.36[cov]

S = 0.318522, R^2 = 86.5 %, R^2(adj) = 85.8 %

Table C-20. Analysis of Variance: DC0.36model versus DC0.36[cov]

Source	DF	SSE	MSE	F-statistic	P-value
Regression	1	12.3754	12.3754	121.978	0.000
Error	19	1.9277	0.1015		
Total	20	14.3031			

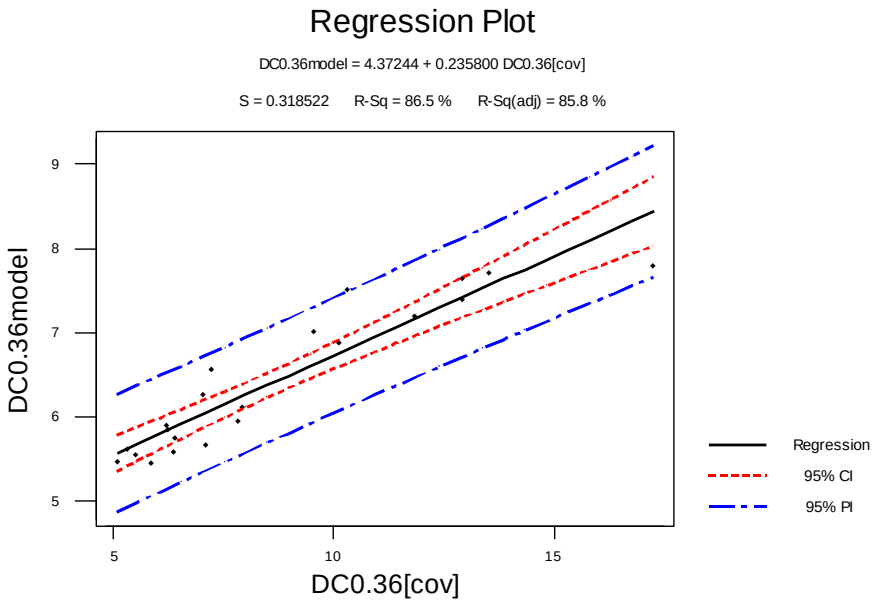

Figure C-31. Regression Plot for CRIM Fit (Covered) [w_0=0.36]

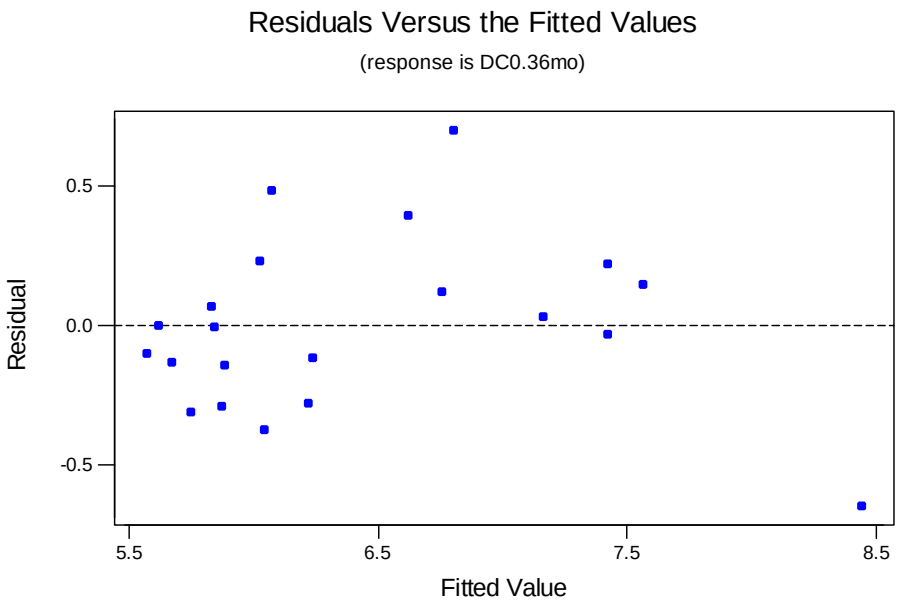

Figure C-32. Residual Plot for CRIM Fit (Covered) [w_0=0.36]

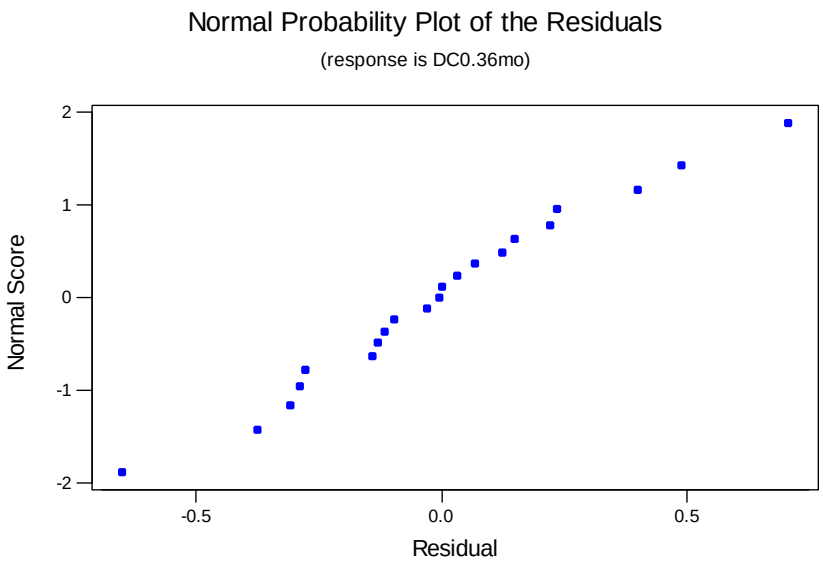

Figure C-33. Normal Probability Plot for CRIM Fit (Covered) [w_0=0.36]

Table C-21. Regression Analysis: DC0.40model versus DC0.40[cov]

Predictor	Coeff	SE Coeff	T-value	P-value
Constant	5.15842	0.1502	19.78	0.000
DC0.40[cov]	0.23722	0.0304	17.10	0.000

Regression equation: DC0.40model = 5.15842 + 0.237220 DC0.40[cov]

S = 0.528649, R^2 = 68.8 %, R^2(adj) = 67.8 %

Table C-22. Analysis of Variance: DC0.40model versus DC0.40[cov]

Source	DF	SSE	MSE	F-statistic	P-value
Regression	1	20.2930	20.2930	72.6126	0.000
Error	33	9.2225	0.2795		
Total	34	29.5156			

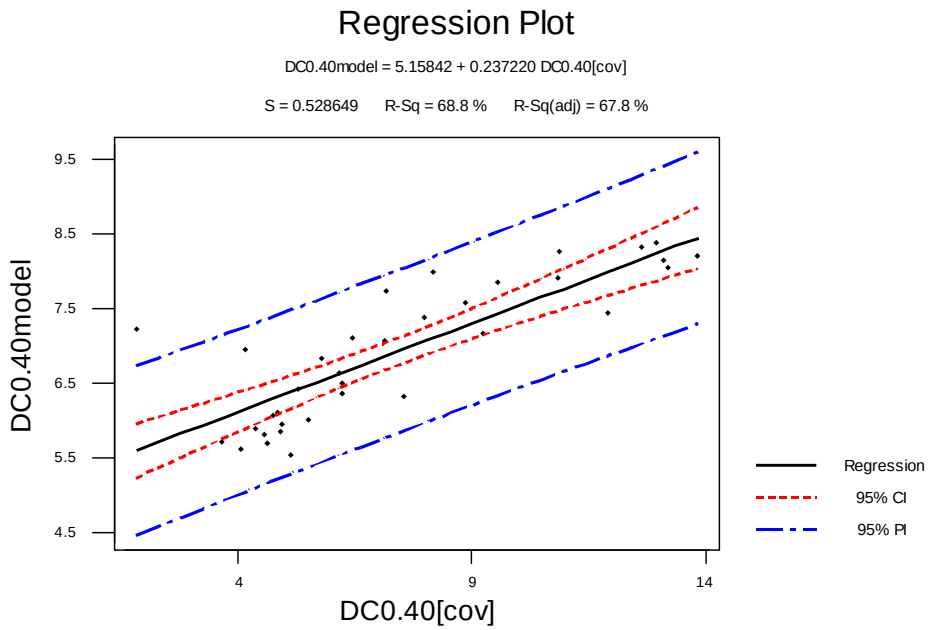

Figure C-34. Regression Plot for CRIM Fit (Covered) [w_0=0.40]

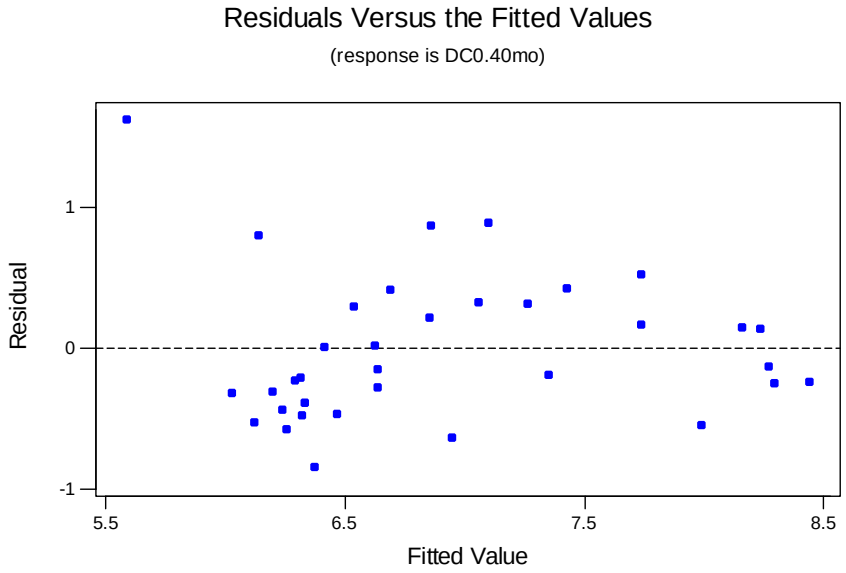

Figure C-35. Residual Plot for CRIM Fit (Covered) [w_0=0.40]

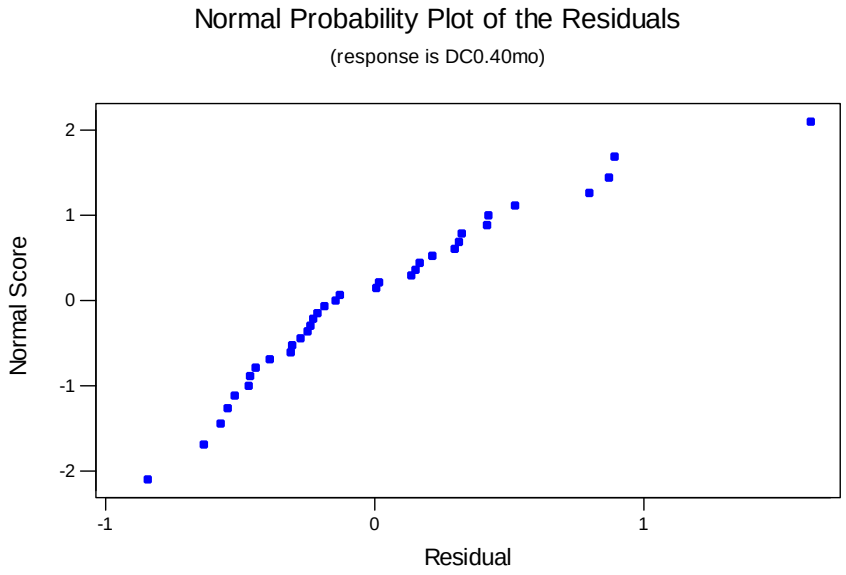

Figure C-36. Normal Probability Plot for CRIM Fit (Covered) [w_0=0.40]

Table C-23. Regression Analysis: DC0.44model versus DC0.44[cov]

Predictor	Coeff	SE Coeff	T-value	P-value
Constant	4.2889	0.3567	12.02	0.000
DC0.44[cov]	0.26817	0.03778	7.10	0.000

Regression equation: DC0.44model = 4.29 + 0.268 DC0.44[cov]

S = 0.6053, R^2 = 63.5%, R^2(adj) = 62.2%

Table C-24. Analysis of Variance: DC0.44model versus DC0.44[cov]

Source	DF	SSE	MSE	F-statistic	P-value
Regression	1	18.456	18.456	50.38	0.000
Residual Error	29	10.625	0.366		
Total	30	29.081			

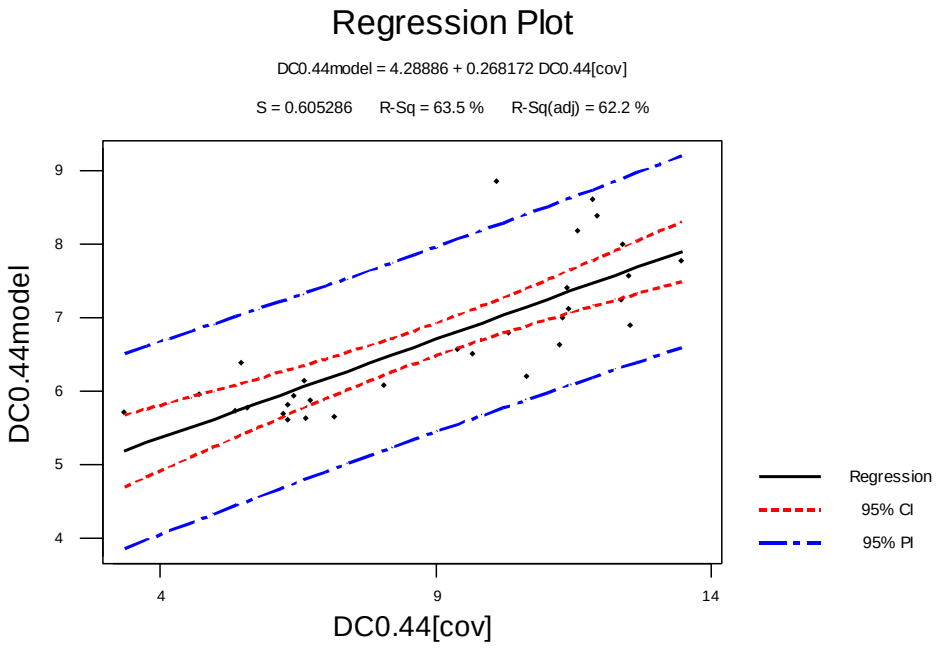

Figure C-37. Regression Plot for CRIM Fit (Covered) [w_0=0.44]

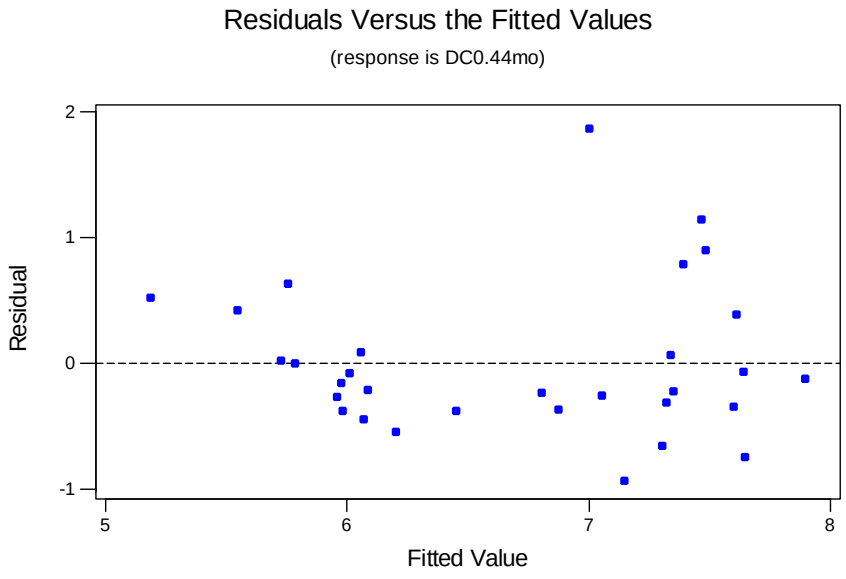

Figure C-38. Residual Plot for CRIM Fit (Covered) [w_0=0.44]

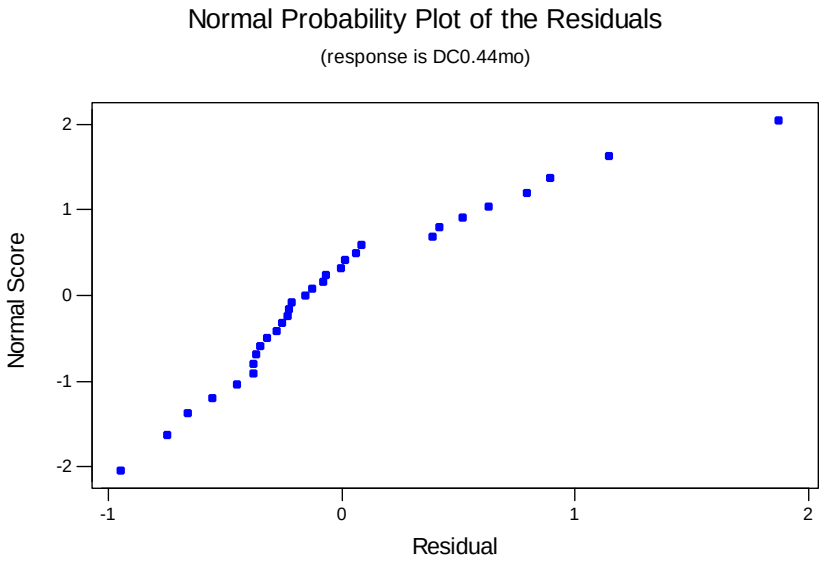

Figure C-39. Normal Probability Plot for CRIM Fit (Covered) [w_0=0.44]

VITA

Ivan Avelar Lezama received his Bachelor of Science in Civil Engineering degree from The University of Texas at El Paso (UTEP) in 2003. His extracurricular involvement at UTEP included the Presidential position for the student chapter of the American Society of Civil Engineers and manager of the chapter's concrete canoe competition project. He continued his graduate studies at Texas A&M University and received his Master of Science in Civil Engineering degree in December 2005.

His research interests focus on Portland cement concrete and include, but are not limited to, the mix design and optimization of the mechanical properties of lightweight high-performance concrete, and the quantitative assessment of curing quality and timing optimization of curing procedures for Portland Cement Concrete, to be exposed in future journal publications.

Mr. Avelar Lezama may be reached within the South Florida Division of APAC Major Projects Group, or at the physical address 7124 Gran Vida, El Paso, TX 79912. His email address is avelivan@yahoo.com.